

# Excitation functions of $^{nat}\text{Zr}+p$ nuclear processes up to 70 MeV: New measurements and compilation

F. Szelecsényi<sup>1\*</sup>, G. F. Steyn<sup>2</sup>, Z. Kovács<sup>1</sup>, C. Vermeulen<sup>3</sup>, K. Nagatsu<sup>4</sup>,  
M. R. Zhang<sup>4</sup> and K. Suzuki<sup>4</sup>

<sup>1</sup>Cyclotron Application Department, Institute for Nuclear Research, Hungarian Academy of Sciences, Bem tér 18/c, Debrecen H-4026, Hungary

<sup>2</sup>iThemba Laboratory for Accelerator Based Sciences, Faure, P.O. Box 722, Somerset West 7129, South Africa

<sup>3</sup>Centre for Radiopharmaceutical Sciences, Paul Scherrer Institute, 5232 Villigen-PSI, Switzerland

<sup>4</sup>Molecular Imaging Center, National Institute of Radiological Sciences, 4-9-1 Anagawa, Inage-ku-Chiba, 263-8555, Japan

**Abstract** Excitation functions for the formation of various radionuclides of Nb, Zr, Y and Sr in proton-induced reactions on natural zirconium were measured up to 66 MeV using the stacked-foil technique. New data are presented for  $^{89m,89g}\text{Nb}$ ,  $^{90(m+g)}\text{Nb}$ ,  $^{91m}\text{Nb}$ ,  $^{92m}\text{Nb}$ ,  $^{95m,95g}\text{Nb}$ ,  $^{96}\text{Nb}$ ,  $^{86}\text{Zr}$ ,  $^{87(m+g)}\text{Zr}$ ,  $^{88}\text{Zr}$ ,  $^{89(0.94m+g)}\text{Zr}$ ,  $^{95}\text{Zr}$ ,  $^{85m,85g}\text{Y}$ ,  $^{86m,86(0.99m+g)}\text{Y}$ ,  $^{87m,87(0.984m+g)}\text{Y}$ ,  $^{88}\text{Y}$ ,  $^{90m}\text{Y}$ ,  $^{91m}\text{Y}$  and  $^{85(0.87m+g)}\text{Sr}$ . The experimental results are compared with the available literature data as well as the evaluated theoretical predictions by means of the TALYS code, up to 70 MeV, as compiled in the TENDL-2013 library. For a number of short-lived radionuclides, i.e.  $^{85m}\text{Y}$ ,  $^{85g}\text{Y}$ ,  $^{86m}\text{Y}$ ,  $^{90m}\text{Y}$ ,  $^{91m}\text{Y}$  and  $^{87(m+g)}\text{Zr}$ , the present experimental cross sections are likely the first to be reported for their formation in  $^{nat}\text{Zr}+p$ .

## 1. Introduction

Excitation functions for  $\text{Zr}+p$  nuclear processes have been investigated by several groups in the past. In recent years, however, there has been a renewed interest in these reactions due to the importance of Zr in several nuclear applications, in particular pertaining to planned new nuclear facilities. Zirconium is, for example, commonly employed as a construction material in nuclear reactors (as a highly corrosion-resistant alloy), a cladding material for nuclear fuel, as a surface coating in specialized fields (both as a metal and in compound form such as ZrN) and as a base material for ceramics. It is expected to be an important structural material in future nuclear energy systems with advanced nuclear fuel cycles, whether based on accelerator driven systems (ADS) or fast reactor (FR) technology (*cf.* Ref. [1] and references therein). In particular for ADS, activation data are required up to higher energies than before. In this regard, for example, a recent study endeavoured to find an optimal set of proton optical potentials specifically for all the individual stable Zr isotopes as well as  $^{nat}\text{Zr}$  [2] in order to predict with better reliability the unmeasured  $\text{Zr}+p$  cross sections using nuclear model calculations.

\*Corresponding author. *E-mail address:* [szele@atomki.hu](mailto:szele@atomki.hu) (F.Szelecsényi)

An ambitious goal is the use of Monte Carlo radiation transport calculations on a geometrically complete model of a nuclear facility followed by quantitative calculations of all the radioactive activation products formed in all the materials in order to predict the build-up of radioactive waste, as well as radiation induced damage, as it develops over the expected operational lifetime of that facility. Reliable quantitative data for  $^{nat}\text{Zr}+p$  are therefore essential.

Excitation-function data for  $\text{Zr}+p$  are also important in the fields of radionuclide production and nuclear wear measurements. Zirconium is a potential target material for the production of some positron emitting medical radionuclides that can be used for immuno-PET scans (labeling different antibodies with blood-clearance half-lives of days to weeks). These radionuclides include  $^{86}\text{Y}$  ( $T_{1/2} = 14.7$  h) and  $^{90}\text{Nb}$  ( $T_{1/2} = 14.6$  h) [3]. Several longer-lived radionuclides produced in Zr-containing surfaces via interactions of light charged particles can be employed to follow the surface loss (wear) of those materials. Among the activation products,  $^{91m}\text{Nb}$  ( $T_{1/2} = 60.86$  d),  $^{92m}\text{Nb}$  ( $T_{1/2} = 10.15$  d),  $^{95g}\text{Nb}$  ( $T_{1/2} = 34.975$  d) and  $^{95}\text{Zr}$  ( $T_{1/2} = 64.02$  d) have suitable decay characteristics for low-energy thin layer activation (TLA) studies (*cf.* Ref. [4]).

In an analysis of the available experimental results for  $^{nat,90,91,92,94,96}\text{Zr}+p$  reactions resulting in the formation of different Nb, Zr, Y and Sr radionuclides, it transpired that the database of the majority of the reactions are not only scanty but also often contradictory. As will become apparent in the discussions below, serious discrepancies persist even in very recent experimental works. To resolve some of these problems and to provide databases for the most important reactions, a project was initiated to systematically re-measure excitation functions for the majority of the  $\text{Zr}+p$  processes. In this regard, we present here new measurements for  $^{nat}\text{Zr}+p$  up to 66 MeV. The experimental results are compared with the available literature data and the evaluated theoretical predictions by means of the TALYS code as compiled in the TENDL-2013 library [5]. As far as we know, in the cases of a number of short-lived radionuclides, namely  $^{85m}\text{Y}$ ,  $^{85g}\text{Y}$ ,  $^{86m}\text{Y}$ ,  $^{90m}\text{Y}$ ,  $^{91m}\text{Y}$  and  $^{87(m+g)}\text{Zr}$ , no previously measured excitation-function data have been published in the literature.

## 2. Experimental

### 2.1 Irradiations

The well-known stacked-foil activation technique was used to measure the excitation functions of radionuclides produced in  $^{nat}\text{Zr}+p$  nuclear reactions from their respective thresholds up to nominally 66 MeV. Five separate irradiations were performed; three at the separated-sector cyclotron facility of iThemba LABS in Faure, South Africa, one at the MGC-20E cyclotron laboratory of ATOMKI in Debrecen, Hungary and one at the AVF-930 isochronous cyclotron facility of the National Institute of Radiological Sciences (NIRS) in Chiba, Japan.

At iThemba LABS, the first stack contained 16  $^{nat}\text{Zr}$  target foils and was irradiated with an average beam current of 80 nA for 3 hours to cover the energy region 66→20 MeV. The second stack was identical to the first one, but targets and other foils from the 9<sup>th</sup> Zr sample were removed before the activation. In the case of the third experiment, the stack was extended with the Zr foils from 9 to 16 (and the appropriate monitor and degrader foils). These stacks were irradiated similarly as the first one, but for shorter periods, of nominally 20

minutes each, in order to assay the relatively short-lived radionuclides (<4 h) in the energy regions 66→45 MeV and 45→20 MeV. All the stacks consisted of high-purity natural Zr foils of 17.9 mg/cm<sup>2</sup> thickness (99.8+%, Goodfellow, UK), 45.9 mg/cm<sup>2</sup> thick Cu monitor foils (99.9%, Goodfellow, UK), 115.9 mg/cm<sup>2</sup> thick Ti monitor/degrader foils (99.99%, Goodfellow, UK), as well as a selection of Al and Cu degrader foils of various thicknesses to obtain well-spaced proton energies across the entire energy region of interest. The bombardments were performed in an accurately calibrated Faraday chamber mounted at the end of an external beamline, details of which can be found in Ref. [6]. The beam was collimated to a spot of 4 mm in diameter. The beam currents and accumulated charges were measured with a Brookhaven Instruments Corporation Model 1000C current integrator connected to a computer, which made it possible to log all values in 1 s intervals during bombardment. The Faraday chamber was evacuated to the same pressure as the beamline, allowing the first foil in each stack to receive the full extracted beam energy, the latter of which was accurately measured using a calibrated 90° bending magnet.

At ATOMKI, the stack contained 21 foils of natural Zr of 17.9 mg/cm<sup>2</sup> thickness (99.8+%, Goodfellow, UK). These target samples were interspersed with Cu degrader foils which also served as monitors. A range of Cu foils with thicknesses of nominally 44.8, 22.4 and 8.96 mg/cm<sup>2</sup> were used to obtain well-spaced proton energies in the region 18→4 MeV. The irradiation time was 2 hours at an average beam current of 60 nA. The beam was collimated to a spot size of 4 mm in diameter. The small stack holder was mounted at the end of an experimental beamline and irradiated in vacuum. The incident beam energy was measured using the two-probe relative phase difference method which has an intrinsic accuracy of better than 3x10<sup>-3</sup> [7].

A single stack consisting of high purity <sup>nat</sup>Zr (thickness: 9.78 mg/cm<sup>2</sup>) foils, supplied by Nilaco, Japan, was activated at NIRS. It was irradiated at the end of an external beamline of the AVF-930 isochronous cyclotron in order to assay the relatively short-lived radionuclides in the energy region 49.4→12.2 MeV. Thin Cu foils (8.96 mg/cm<sup>2</sup>) and Ti foils (of 13.52 and 4.56 mg/cm<sup>2</sup> thickness, respectively) served as monitors while thick Co foils (270 μm) were used as beam degraders. These foils were also purchased from Nilaco. Similar to the iThemba LABS and ATOMKI experiments, the beam was also focused to a spot of 4 mm in diameter. The stack fitted inside a calibrated Faraday chamber which was separated from the beamline vacuum by a 100 μm thick Al entrance window foil. The extracted beam energy was determined by magnetic deflection to be 49.8 MeV, corresponding to an effective incident energy of 49.4 MeV as a result of the small degradation in the window foil. The irradiation lasted for 1 hour while the beam current was kept constant at a value just below 50 nA.

## 2.2 Radionuclide assays

Off-line γ-ray spectra were repeatedly measured for all the activated foils after bombardment. At all three laboratories, accurately calibrated HPGe detectors were used. At iThemba LABS, the detector had a relative efficiency of 15% with a resolution of 1.8 keV FWHM at 1.33 MeV. Canberra Genie 2000 analysis software was used in conjunction with a Canberra DSA 1000 multi-channel analyzer system to determine the photo-peak areas quantitatively. At ATOMKI and NIRS, the detectors had relative efficiencies of 10% and 30%, respectively, with corresponding resolutions of 2.1 keV FWHM and 1.8 keV FWHM at 1.33 MeV. The photo-peak areas were determined using a quantitative analysis software package at NIRS (supplied by Laboratory Equipment Japan) and the FGM program at ATOMKI [8].

## 2.3 Data analysis

The cross sections of the identified activation products were calculated from their characteristic  $\gamma$ -ray emissions using decay data from the NuDat 2.6 database [9] except for the branching ratios of  $^{91m}\text{Nb}$ ,  $^{89g}\text{Nb}$ ,  $^{87g}\text{Zr}$  and  $^{85g}\text{Y}$ , which were taken from Ref. [10]. The decay data used for this purpose are presented in Table 1. The well-known activation formula [11] was employed and corrections were made for decay losses during and after bombardment as well as during counting.

The integrated beam current of each bombardment was measured electronically using calibrated current integrators and was checked independently using appropriate monitor excitation functions. The following three IAEA recommended monitor reactions [12] were used for the above purpose:  $^{nat}\text{Ti}(p,xn)^{48}\text{V}$  (long activation at iThemba LABS and the NIRS experiment),  $^{nat}\text{Cu}(p,xn)^{62}\text{Zn}$  (all stacks at iThemba LABS and NIRS experiment) and  $^{nat}\text{Cu}(p,n)^{65}\text{Zn}$  (long activation at iThemba LABS and ATOMKI experiment). In Figs. 1, 2, and 3 the measured cross sections for  $^{48}\text{V}$ ,  $^{62}\text{Zn}$  and  $^{65}\text{Zn}$ , respectively, are compared with the recommended values. Beam fluxes determined by direct integration agreed well (within 6%) with the monitor reaction results.

The average energy corresponding to each foil in a stack was calculated using the stopping power formula of Anderson and Ziegler [13] and independently checked with the Monte Carlo code SRIM of Ziegler and Biersack [14]. Good agreement was found throughout.

The total uncertainties in the measured cross sections were obtained by summing all the contributing uncertainties in quadrature and are expressed with a  $1\sigma$  (68%) confidence level. These include the uncertainty in beam current integration (3%), counting geometry (1%), detector efficiency (5%), decay corrections (2%), foil thickness (3%) as well as a variable component due to the counting statistics. The uncertainty in energy of each measured data point was estimated from the uncertainty in incident beam energy, the energy region subtended by the foil thickness and straggling as the beam traversed the stack.

## 3. Results and Discussions

### 3.1. General

A literature search for relevant experimental cross sections found 14 studies that reported excitation functions for Zr+p reactions in different energy intervals below 70 MeV [15–28]. All authors measured the activity of their irradiated samples non-destructively, i.e. without prior chemical separations. The majority of the experimental works employed natural Zr foils as targets. Those authors who employed enriched target materials [16,21,24,26,28] reported cross sections only for lower energy regions (<10 MeV) except Levkovskij [21], who presented data up to 30 MeV. These data were converted to natural isotopic composition for comparison with the measurements on natural targets, where appropriate. Takács *et al.* [29] have shown that all cross-section data for proton-induced processes reported by Levkovskij should be decreased by 20% based on the presently accepted value of the monitor reaction

( $^{nat}\text{Mo}(p,X)^{96m}\text{Tc}$ ) used in his original work. These ‘updated’ values of Levkovskij are reproduced in the appropriate figures.

In accordance with Michel *et al.* [22], the measured cross sections will be called ‘independent’ in this work if either the product nuclide is naturally shielded from the decay of its radioactive precursor(s) or if the cross sections of the precursor(s) were determined too. The sum of all independent cross sections of radionuclides decaying to the product will be called ‘cumulative’. The latter type of cross sections is usually measured in cases where the half-lives of all radioactive precursors are short compared to that of the nuclide in question, so that the precursors can completely decay before measuring the target activity. The results below are ordered by decreasing mass number of the residual nuclei.

### 3.2. Formation of Nb radionuclides

There are seven radionuclides of niobium with half-lives between 0.8 h and 200 d that can be produced via proton-induced nuclear reactions on Zr targets. Altogether nine authors reported independent and/or cumulative cross sections for  $^{nat}\text{Zr}+p$  processes, leading to the formation of  $^{97}\text{Nb}$ ,  $^{96}\text{Nb}$ ,  $^{95}\text{Nb}$ ,  $^{92}\text{Nb}$ ,  $^{91}\text{Nb}$ ,  $^{90}\text{Nb}$  and  $^{89}\text{Nb}$  in either metastable or ground states, in different energy regions [15,16,21–26,28]. The present results for  $^{96}\text{Nb}$ ,  $^{95m}\text{Nb}$ ,  $^{95g}\text{Nb}$ ,  $^{92m}\text{Nb}$ ,  $^{91m}\text{Nb}$ ,  $^{90(m+g)}\text{Nb}$ ,  $^{89m}\text{Nb}$  and  $^{89g}\text{Nb}$  are shown in Figs. 4–11, respectively, while the numerical values are presented in Table 2. Although  $^{97}\text{Nb}$  has a half-life of 1.202 h, the experimental conditions did not allow us to measure the rather small cross sections for its formation (via  $^{96}\text{Zr}(p,\gamma)^{97}\text{Nb}$ ). Only one author reported numerical values for this process, below 8 MeV [28].

The available literature values, corrected where necessary, are also reproduced in the appropriate figures. To improve the clarity of figures containing multiple data sets, in the majority of cases the energy and cross-section uncertainties are not shown on the plotted data points with the exception of the present results. In a few figures that contain only sparse data, all data points are presented with uncertainties: Figs. 5, 8, 10 and 11 ( $^{nat}\text{Zr}(p,xn)^{95m}\text{Nb}$ ,  $^{nat}\text{Zr}(p,xn)^{91m}\text{Nb}$ ,  $^{nat}\text{Zr}(p,xn)^{89m}\text{Nb}$  and  $^{nat}\text{Zr}(p,xn)^{89g}\text{Nb}$  reactions, respectively).

#### 3.2.1. The $^{nat}\text{Zr}(p,n)^{96}\text{Nb}$ reaction

Only one reaction populates the ground state of  $^{96}\text{Nb}$  ( $T_{1/2} = 23.35$  h) directly, namely  $^{96}\text{Zr}(p,n)^{96}\text{Nb}$ . This ground state decays to  $^{96}\text{Mo}$ , which is stable. The available literature data [15,16,21–23,25,26] and new results are shown in Fig. 4. Most of the data sets show acceptable agreement with each other. The excitation function reaches a peak maximum of about 14 mb near 8 MeV. The converted data of Skakun *et al.* [25] exhibit a somewhat higher value for the maximum, about 17.8 mb. Beyond 20 MeV, only two groups reported cross sections [22,26]. The data of Uddin *et al.* [26] seem to be systematically higher (20–40%) than the values of Michel *et al.* [22] in this energy region. Some of the data of Michel *et al.* (below 15 MeV) appear to be shifted towards lower energies by 1–2 MeV.

The present measurements provide 31 new cross-section values between 3 and 54 MeV (see Table 2 and Fig. 4). As far as we know, data are presented for the first time beyond 44 MeV. The excitation function based on the present measurements, both in shape and magnitude, is consistent with the previous literature results. The present values also support the data of Michel *et al.* above 20 MeV.

The TENDL-2013 data [5] are mostly in good agreement with the experimental results, especially in the peak region of the excitation function. Between 13 and 24 MeV, however, the TENDL-2013 curve over-predicts the majority of the experimental cross sections. At these energies, the agreement is better with the data of Uddin *et al.* but outside this region the theoretical curve shows better agreement with the values of this work and those of Michel *et al.*

### 3.2.2. The $^{nat}\text{Zr}(p,2n)^{95m}\text{Nb}$ process

Two long-lived states of  $^{95}\text{Nb}$  are populated directly via the  $^{96}\text{Zr}(p,2n)^{95}\text{Nb}$  reaction in the investigated energy region, namely  $^{95m}\text{Nb}$  ( $T_{1/2} = 3.61$  d) and  $^{95g}\text{Nb}$  ( $T_{1/2} = 34.99$  d). The metastable  $^{95m}\text{Nb}$  is also formed via the decay of a precursor, namely  $^{95}\text{Zr}$  ( $T_{1/2} = 64.032$  d). This latter radionuclide is produced via two reactions:  $^{96}\text{Zr}(p,pn)^{95}\text{Zr}$  and  $^{96}\text{Zr}(p,d)^{95}\text{Zr}$ . In addition, at proton energies above 11.64 MeV the formation of  $^{95}\text{Y}$  ( $T_{1/2} = 10.3$  m) via the  $^{96}\text{Zr}(p,2p)^{95}\text{Y}$  reaction will also contribute. The  $^{95}\text{Y}$  decays completely to  $^{95}\text{Zr}$  while the ground state of  $^{95}\text{Zr}$  decays not only to  $^{95m}\text{Nb}$  but to  $^{95g}\text{Nb}$  as well (branching ratios 1.08% and 98.90%, respectively [30] (see also subsection 3.3.1 and Table 1). The  $^{95m}\text{Nb}$  decays to the ground state  $^{95g}\text{Nb}$  (IT: 94.4%) and also feeds  $^{95}\text{Mo}$  ( $\beta^-$ : 5.6%) [9].

Since the threshold energies of the  $^{96}\text{Zr}(p,2n)^{95}\text{Nb}$ ,  $^{96}\text{Zr}(p,pn)^{95}\text{Zr}$  and  $^{96}\text{Zr}(p,d)^{95}\text{Zr}$  reactions are very close to each other (7.59, 7.94 and 5.69 MeV, respectively), the  $^{95m}\text{Nb}$  activity originating from the (p,2n) reaction alone cannot be measured independently without chemical separation. Knowing, however, the respective excitation functions of the  $^{nat}\text{Zr}(p,X)^{95}\text{Zr}$  process and the  $^{96}\text{Zr}(p,2p)^{95}\text{Y}$  reaction, the production cross sections for the  $^{nat}\text{Zr}(p,2n)^{95m}\text{Nb}$  reaction can be derived, in principle, by subtracting the contributions of feeding via  $^{95}\text{Zr}$  and  $^{95}\text{Y}$  decay from the  $^{95m}\text{Nb}$  activity (see Ref. [22] for details). Taking into account, however, the different half-lives of  $^{95}\text{Zr}$  and  $^{95m}\text{Nb}$  ( $T_{\text{Zr-95}}/T_{\text{Nb-95m}} \approx 18$ ) and the small branching ratio for feeding of  $^{95}\text{Zr}$  to  $^{95m}\text{Nb}$ , the contributions of the  $^{96}\text{Zr}(p,pn)^{95}\text{Zr}$  and  $^{96}\text{Zr}(p,d)^{95}\text{Zr}$  reactions are almost negligible. By measuring the  $^{95m}\text{Nb}$  activity after a short cooling period and employing short measurement times, the contributions of the above processes can be decreased further. Thus, by neglecting the contributions from precursor decay, independent cross sections for the  $^{nat}\text{Zr}(p,2n)^{95m}\text{Nb}$  reaction can be derived sufficiently from the measurements but with somewhat higher uncertainties.

The available literature results [21–23] are shown in Fig. 5. According to the papers of Michel *et al.* [22] and Murakami *et al.* [23], they published independent cross sections (i.e. corrected for the decay of  $^{95}\text{Zr}$ ). Due to a lack of experimental details, the assumption is made that the cross sections of Levkovskij [21] have likewise been corrected for precursor decay. The data of Levkovskij and Murakami *et al.* are in acceptable agreement with each other. However, the data of Michel *et al.* show a very large deviation, by more than a factor of 3 in the peak region. While all the authors report the peak maximum at the same energy (near 14 MeV), the respective maxima of about 7.5, 8.5 and 31 mb constitute a large discrepancy.

In the present investigation, the  $^{95m}\text{Nb}$  activities were measured relatively close to EOB using short counting times. These cross sections (14 values, see Table 2 and Fig. 5) are in good agreement with the results of Levkovskij and Murakami *et al.*

The TENDL-2013 data [5] systematically under-predict the excitation function, showing the peak maximum of about 4 mb to be shifted towards a lower energy of close to 12 MeV.

### 3.2.3. The ${}^{\text{nat}}\text{Zr}(p,X){}^{95\text{g}}\text{Nb}$ process

The reactions responsible for the formation of  ${}^{95\text{g}}\text{Nb}$  ( $T_{1/2} = 34.99$  d) are the same as in the case of  ${}^{95\text{m}}\text{Nb}$  (see subsection 3.2.2). In addition, the ground state is also populated by the decay of  ${}^{95\text{m}}\text{Nb}$  ( $T_{1/2} = 3.61$  d) via an isomeric transition (94.4%). Due to this fact and taking into account that the feeding via  ${}^{95}\text{Zr}$  decay is more significant in the case of  ${}^{95\text{g}}\text{Nb}$ , the evaluation of the independent cross sections of the  ${}^{\text{nat}}\text{Zr}(p,2n){}^{95\text{g}}\text{Nb}$  reaction is even more complicated. A reliable method depends on knowledge of the excitation functions of the  ${}^{\text{nat}}\text{Zn}(p,X){}^{95}\text{Zr}$  and  ${}^{\text{nat}}\text{Zn}(p,X){}^{95\text{m}}\text{Nb}$  processes. In this case, one can subtract precursor decay contributions from the measured  ${}^{95\text{g}}\text{Nb}$  activities and calculate the independent cross sections (see also Ref. [22] for details). Similar to the case of  ${}^{95\text{m}}\text{Nb}$ , the above-mentioned scheme requires carefully planned  ${}^{95\text{g}}\text{Nb}$  activity measurements, starting immediately after EOB and using short counting times. In this way, only small fractions of the produced  ${}^{95\text{m}}\text{Nb}$  and  ${}^{95}\text{Zr}$  will have decayed to  ${}^{95\text{g}}\text{Nb}$  at the time of measurement. This leads to increased uncertainties of the measured cross sections.

In spite of the above difficulties, six groups [15,21–23,26,27] published cross sections for the  ${}^{\text{nat}}\text{Zn}(p,X){}^{95\text{g}}\text{Nb}$  process. Figure 6 contains the available literature results. Two authors [22,23] reported independent cross sections after corrections: Michel *et al.* [22] took into account the influence of the longer-lived precursor ( ${}^{95}\text{Zr}$ ) but it is not clear whether this is also the case for the decay of  ${}^{95\text{m}}\text{Nb}$ . Murakami *et al.* [23] corrected their values both for  ${}^{95\text{m}}\text{Nb}$  and  ${}^{95}\text{Zr}$  decay. The detailed experimental conditions of Levkovskij [21] are not described in his original work, but it is assumed that the decays of both precursors were also taken into account. The activity measurements of Uddin *et al.* [26] started 5 hours after EOB and the values were not corrected for the decays of  ${}^{95\text{m}}\text{Nb}$  and  ${}^{95}\text{Zr}$ . According to the paper of Al-Abyad *et al.* [15], the activity measurement started after the complete decay of the  ${}^{95\text{m}}\text{Nb}$ . (Corrections for  ${}^{95}\text{Zr}$  were not mentioned in their work.) Consequently, the cross sections of both the Uddin and Al-Abyad groups are considered to be cumulative for the formation of  ${}^{95(\text{m}+\text{g})}\text{Nb}$ . The data of Visotskij *et al.* [27] are rather dubious since the reported cross sections extend significantly into the energy region below the  ${}^{96}\text{Zr}(p,2n){}^{95\text{g}}\text{Nb}$  reaction threshold.

The majority of the data sets exhibit a prominent peak at about 17 MeV but with a spread of maxima. It ranges from 16 mb (Uddin *et al.*) to 27 mb (Michel *et al.*). Although the results of Al-Abyad *et al.* contain significant precursor contributions, their data nevertheless follow the main trend. Uddin *et al.* reported the lowest values among the research groups. In general, their data are around 20% lower than the average of the others as well as unexpectedly low around 40 MeV. Also noteworthy is that the data of Michel *et al.* are significantly shifted towards lower energies in the region below 20 MeV.

We measured the  ${}^{95\text{g}}\text{Nb}$  activities in the  ${}^{\text{nat}}\text{Zr}$  samples (29 data points) close to EOB by using short counting times and corrected the photo-peak areas for  ${}^{95}\text{Zr}$  and  ${}^{95\text{m}}\text{Nb}$  decay contributions before calculating the cross sections (see Table 2 and Fig. 6). In the peak region, the present results show good agreement with the data of Al-Abyad *et al.*, Levkovskij and Murakami *et al.* Above 25 MeV, the new data support the values of Michel *et al.*

The TENDL-2013 data [5] reproduce the shape of the excitation function well with a maximum value of 28 mb at about 16 MeV. It is evident, however, that there is better agreement with the values of Michel *et al.* than with the other works, especially in the peak region.

### 3.2.4. The $^{nat}\text{Zr}(p,xn)^{92m}\text{Nb}$ process

There are two long-lived states of interest in  $^{92}\text{Nb}$ . The metastable state has a half-life of 10.15 d while the ground state is extremely long-lived ( $3.47 \times 10^7$  y). Both states decay to stable  $^{92}\text{Zr}$ . The ground state will not be further considered in this work. Below 66 MeV, three nuclear reactions form  $^{92m}\text{Nb}$ , namely  $^{92}\text{Zr}(p,n)^{92m}\text{Nb}$ ,  $^{94}\text{Zr}(p,3n)^{92m}\text{Nb}$  and  $^{96}\text{Zr}(p,5n)^{92m}\text{Nb}$ . This radionuclide has no precursors, thus the reported cross sections are for its direct production.

Prior to the present investigation, eight authors [15,16,19,22,23,25–27] presented independent cross sections for the  $^{nat}\text{Zr}(p,xn)^{92m}\text{Nb}$  process, shown in Fig. 7. The low-energy activations by Blaser *et al.* [16], Skakun *et al.* [25] and Vysotskij *et al.* [27] provided data only for the  $^{92}\text{Zr}(p,n)^{92m}\text{Nb}$  reaction below 8 MeV. The results of those studies, which were performed on enriched targets, have been converted to the natural isotopic composition of  $^{92}\text{Zr}$  (17.15%) for purposes of comparison.

The excitation function shows two prominent peaks in the investigated energy region. The first one is located near 11 MeV and the second near 26 MeV. The majority of the experimental results give the maximum of the first peak around 100 mb (80–115 mb). The data of Michel *et al.* [22] seem to be shifted towards lower energies below 24 MeV, by as much as 3 MeV at their lowest-energy measurement. Due to the limited number of the measured data points, it is difficult to accurately determine the peak maximum of Uddin *et al.* [26]. Based on an eye-guide fit, it is estimated to be about 45 mb at 10 MeV.

The various sets of experimental results are very scattered in the region of the second peak. While the energies of the respective maxima [19,22,26] are in reasonably good agreement (around 28 MeV), the corresponding cross-section values range between 16 mb (Uddin *et al.*) and 58 mb (Michel *et al.*). It is surprising to note that two sets of results reported from the same laboratory, within one year, also show a big difference: Khandaker *et al.* [19] published an almost three times higher maximum (around 46 mb) than Uddin *et al.* (16 mb) for the second peak. Even more surprising is that most of the co-authors are common to both studies.

The new cross sections (34 data points, see Table 2 and Fig. 7) cover the whole energy region up to 66 MeV. The results are consistent with the majority of the previous experimental works. In the case of the second peak and higher energies, our measurements are in good agreement with the results of Michel *et al.*

The TENDL-2013 data [5] satisfactorily reproduce the energy positions and the cross-section maxima (110 mb at 11 MeV for the first peak and 64 mb at 25 MeV for the second peak). It should be noted, however, that above 30 MeV the theoretical curve is systematically lower than the experimental data.

### 3.2.5. The $^{nat}\text{Zr}(p,xn)^{91m}\text{Nb}$ process

In addition to the ground state ( $T_{1/2} = 680$  y), one metastable state ( $T_{1/2} = 60.86$  d) is also populated during the formation of this radionuclide. The four reactions responsible for  $^{91m}\text{Nb}$  production are:  $^{91}\text{Zr}(p,n)^{91m}\text{Nb}$ ,  $^{92}\text{Zr}(p,2n)^{91m}\text{Nb}$ ,  $^{94}\text{Zr}(p,4n)^{91m}\text{Nb}$  and  $^{96}\text{Zr}(p,6n)^{91m}\text{Nb}$ . The metastable state decays both to the ground state of  $^{91}\text{Nb}$  (95%) and to  $^{91}\text{Zr}$  (5%). The very

long-lived  $^{91g}\text{Nb}$  decays to stable  $^{91}\text{Zr}$ . There are no precursors, thus the reported cross sections are for the direct production of  $^{91m}\text{Nb}$ .

Four previous works presented independent cross sections for the  $^{\text{nat}}\text{Zr}(p,xn)^{91m}\text{Nb}$  process [16,22,23,27], shown in Fig. 8. Blaser *et al.* [16] and Vysotskij *et al.* [27] presented data only for the  $^{91}\text{Zr}(p,n)^{91m}\text{Nb}$  reaction below 8 MeV. These data, obtained using enriched targets, have been converted to the natural isotopic composition of  $^{91}\text{Zr}$  (11.22%). In general, the available data show relative big scatter. The results of Blaser *et al.* and Vysotskij *et al.* show good agreement with each other. The results of Murakami *et al.* [23] seem to support their data. In contrast, the results of Michel *et al.* [22] are significantly shifted towards lower energies. Indeed, similar shifts were observed for the  $^{\text{nat}}\text{Zr}(p,xn)^{92m}\text{Nb}$  and  $^{\text{nat}}\text{Zr}(p,X)^{95g}\text{Nb}$  processes.

Three peaks can be distinguished in the excitation function, corresponding to the three participating reactions mentioned above. The maxima are located around 10, 14 and 38 MeV. The data of Murakami *et al.* is compatible with a maximum of about 30 mb for the first peak. In the case of the second peak, the maxima vary between 58 mb (Michel *et al.*) and 65 mb (Murakami *et al.*). Only Michel *et al.* presented cross sections for the third peak near 38 MeV, reporting a maximum of about 12 mb.

The present measurements (24 new values, see Table 2 and Fig. 8) are in good agreement with the results of Murakami *et al.* and support their data concerning the positions and the maxima of the two lower-energy peaks, as shown in Fig. 8. The agreement between the present data and those of Michel *et al.* is generally poor.

The TENDL-2013 data [5] exhibit the three expected peaks and show good agreement with the present results up to about 28 MeV. There is, however, a systematic overestimation of all the experimental results in the region of the third peak.

### 3.2.6. The $^{\text{nat}}\text{Zr}(p,xn)^{90(m+g)}\text{Nb}$ process

Proton bombardment of natural Zr opens five reaction channels below 70 MeV that form  $^{90}\text{Nb}$ . Details of these reactions can be found in Table 1. Besides the ground state ( $T_{1/2} = 14.6$  h) a relatively short-lived metastable state,  $^{90m}\text{Nb}$  ( $T_{1/2} = 18.8$  s), is also populated during the irradiations but it decays completely to the ground state. The  $^{90g}\text{Nb}$  state has no other precursors. Taking into account the usual measuring set-ups, it is possible to evaluate the excitation function only after the complete decay of the directly-formed metastable state. The measured cross sections are therefore cumulative.

The previously published cross sections are also cumulative, denoted by  $^{90(m+g)}\text{Nb}$  for clarity, and reproduced in Fig. 9. This process was investigated by the majority of the authors: nine of the fourteen groups who studied  $^{\text{nat}}\text{Zr}+p$  presented cross sections for this process in different energy regions [15,18–23,25,26].

Just as in subsection 3.2.5, three peaks can also be observed in the excitation function of the  $^{\text{nat}}\text{Zr}(p,xn)^{90(m+g)}\text{Nb}$  process. Except in the case of one work [20], all results locate the position of the first peak between 14 and 15 MeV [15,18,19,21–23,25,26]. The entire excitation function based on the work of Kondrat'ev *et al.* [20] seems to be shifted by 3–5 MeV towards higher energies. In addition, their data are systematically lower than those of the other authors. The data of Khandaker *et al.* [19] also seem shifted towards higher energies

but by a lesser amount, only about 1–2 MeV. The various maxima for the first peak vary between 350 and 520 mb. The curious disagreement between the data sets of Khandaker *et al.* [19] and Uddin *et al.* [26], which were performed in the same laboratory and reported within one year from another, continues to surprise us. While for the  $^{nat}\text{Zr}(p,xn)^{92m}\text{Nb}$  process Khandaker *et al.* presented systematically higher values than Uddin *et al.* (see subsection 3.2.4), in the present case the trend is largely in the opposite direction. Uddin *et al.* now have 10–20% higher cross sections than Khandaker *et al.* In contrast to the previous two nuclear processes (subsections 3.2.4 and 3.2.5), the data of Michel *et al.* [22] show good agreement with the general trend of the excitation function. Interestingly, the data of Busse *et al.* [18], measured on enriched targets above 15.5 MeV, show a sharper decrease beyond the first peak maximum than any of the other data sets. However, their lower energy data points measured on both natural and enriched Zr samples are consistent with the majority of the previous results.

Five authors reported cross sections in the region of the second peak [19–22, 26]. Based on their results, the second peak is located around 32 MeV with maxima ranging between 120 and 150 mb, except Kondrat'ev *et al.* who presented the lowest maximum for this peak, around 60 mb at 34 MeV. Likewise, the results of Kondrat'ev *et al.* are also systematically lower than those of Michel *et al.* in the region of the third peak (maxima of 40 and 60 mb, respectively).

The present work produced 30 measured cross sections for the  $^{nat}\text{Zr}(p,xn)^{90(m+g)}\text{Nb}$  process, also shown in Fig. 9 with numerical values in Table 2. The new data are consistent with the majority of the previous results, especially with the most recent values [15,23]. The respective peak maxima are around 420 mb (at 17 MeV), 130 mb (at 31 MeV), and 60 mb (at 56 MeV).

The TENDL-2013 data [5] show acceptable agreement with the majority of the experimental results. Beyond the first peak, however, there is a slight systematic underestimation compared to the general trend, if the data of Kondrat'ev *et al.* are disregarded. Also, the peak positions are slightly shifted towards lower energies (16, 30 and 50 MeV, respectively).

### 3.2.7. The $^{nat}\text{Zr}(p,xn)^{89m}\text{Nb}$ process

Similar to the case of the previous process (subsection 3.2.6), five reactions are also responsible for the formation of  $^{89m}\text{Nb}$  ( $T_{1/2} = 1.10$  h) and  $^{89g}\text{Nb}$  ( $T_{1/2} = 2.03$  h) in the energy range studied (see Table 1). Both the metastable and the ground states decay separately via EC to  $^{89}\text{Zr}$ , which further decays to stable  $^{89}\text{Y}$ . The proton activation of  $^{nat}\text{Zr}$  targets does not produce any precursors of  $^{89m,g}\text{Nb}$ .

The available experimental cross sections were measured on highly enriched targets (Levkovskij [21]:  $^{90}\text{Zr}(p,2n)^{89m}\text{Nb}$  and  $^{91}\text{Zr}(p,3n)^{89m}\text{Nb}$ ; Busse *et al.* [18]:  $^{90}\text{Zr}(p,2n)^{89m}\text{Nb}$ ). Their converted results are reproduced in Fig. 10. The data of the two groups show very good agreement with each other in the comparable energy region. Unfortunately, Busse *et al.* reported only 4 cross sections in the threshold region of the excitation function. Thus, the energy position of the maximum cross section and its magnitude can be estimated only from the work of Levkovskij (about 85 mb near 24 MeV).

Our present work not only resulted in 23 cross sections, but extended the available data set of this process with 16 new values beyond 30 MeV (see Table 2 and Fig. 10). The present measurements agree well with the existing literature results except for a slightly lower maximum of 73 mb.

For this process, the TENDL-2013 data [5] significantly underestimate the experimental values in the entire investigated energy region except near the threshold. Note that due to the high natural abundance of  $^{90}\text{Zr}$  in the targets (51.45%), the shape of the excitation function is dominated by the  $^{90}\text{Zr}(p,2n)^{89\text{m}}\text{Nb}$  reaction.

### 3.2.8. The $^{\text{nat}}\text{Zr}(p,xn)^{89\text{g}}\text{Nb}$ process

For the production and decay of  $^{89\text{g}}\text{Nb}$  ( $T_{1/2} = 2.03$  h) please refer to the previous section and also to Table 1. Only three cross-section values near the threshold were reported by Busse *et al.* [18], the only previous investigators of the  $^{90}\text{Zr}(p,2n)^{89\text{g}}\text{Nb}$  nuclear reaction, to our knowledge. Their converted data are shown in Fig. 11. These data are too sparse to conclude anything concerning the shape of the excitation function.

According to the present results (24 data points, see Table 2 and Fig. 11), the excitation function exhibits a broad peak with a maximum of about 380 mb near 26 MeV.

Similar to the case of the  $^{\text{nat}}\text{Zr}(p,2n)^{89\text{m}}\text{Nb}$  processes, the TENDL-2013 data [5] also under-predict the measured values significantly. The shape of the theoretical curve seems to be in reasonable agreement with the measured data but the maximum is somewhat shifted towards a lower energy (about 220 mb near 24 MeV).

### 3.3. Formation of Zr radionuclides

Among the seven radionuclides of zirconium that has half-lives between 0.8 h and 200 d, six can also be produced via proton-induced reactions on  $^{\text{nat}}\text{Zr}$  targets ( $^{95}\text{Zr}$ ,  $^{93}\text{Zr}$ ,  $^{89}\text{Zr}$ ,  $^{88}\text{Zr}$ ,  $^{87}\text{Zr}$ , and  $^{86}\text{Zr}$ ). Below 70 MeV, seven authors reported cross sections for metastable and/or ground states of  $^{95}\text{Zr}$ ,  $^{89}\text{Zr}$ ,  $^{88}\text{Zr}$  and  $^{86}\text{Zr}$  radionuclides in different energy regions [17,19,21–24,26]. Besides the above 4 radionuclides, the formation of  $^{87}\text{Zr}$  was also studied in this work. The results of the present work for  $^{95}\text{Zr}$ ,  $^{89(0.94\text{m+g})}\text{Zr}$ ,  $^{88}\text{Zr}$ ,  $^{87(\text{m+g})}\text{Zr}$  and  $^{86}\text{Zr}$  are shown in Figs. 12–17, respectively, while the numerical values are compiled in Table 3. The available literature values, corrected where necessary, are also shown in the appropriate figures.

The measurements of Michel *et al.* [22] exhibit a rather strange phenomenon. Between 30 and 60 MeV, three or four outlying data points (associated with very big energy and cross-section uncertainties) differ significantly from the excitation-function trends depicted by the rest of the data. No details are available in the original paper as to whether those values are from different irradiation(s) or not. We shall discuss this problem in some detail below. It should also be noted that this phenomenon is evident not only for Zr but for Y and Sr radionuclides as well.

Due to the relatively large number of experimental works, the energy and cross-section uncertainties are not added to the data points in the figures, except in the cases of the present work and the  $^{\text{nat}}\text{Zr}(p,X)^{88}\text{Zr}$  and  $^{\text{nat}}\text{Zr}(p,X)^{86}\text{Zr}$  processes.

### 3.3.1. The $^{nat}\text{Zr}(p,X)^{95}\text{Zr}$ process

As already mentioned in subsection 3.2.2, only the ground state of  $^{95}\text{Zr}$  ( $T_{1/2} = 64.032$  d) is populated directly by two reactions (see also Table 1.). There is, however, another reaction on  $^{96}\text{Zr}$  that produce the precursor  $^{95g}\text{Y}$  ( $T_{1/2} = 10.3$  m) which feed  $^{95}\text{Zr}$ . Therefore, the contribution of  $^{95}\text{Y}$  decay to the cross sections of the  $^{nat}\text{Zr}(p,X)^{95}\text{Zr}$  nuclear process should be taken into account. Since the threshold of the  $^{96}\text{Zr}(p,2p)^{95}\text{Y}$  reaction (11.64 MeV) is located at a higher energy than those of the direct reactions populating  $^{95}\text{Zr}$  (7.94 and 5.69 MeV, respectively), the influence of  $^{95}\text{Y}$  would be observed only at higher energies. Without a proper and quick chemical separation, however, one cannot remove  $^{95}\text{Y}$  from the activated samples, consequently only cumulative cross sections can be evaluated for the  $^{nat}\text{Zr}(p,X)^{95}\text{Zr}$  process. Unfortunately, there is a potential interfering process that can also form  $^{95}\text{Zr}$ , namely activation by secondary neutrons via the  $^{96}\text{Zr}(n,2n)^{95}\text{Zr}$  reaction. Such experiment-dependent contributions are difficult to quantify but should be kept in mind – hopefully they are small enough to neglect.

Searching the literature, we found only three authors who previously reported cumulative cross section for the  $^{nat}\text{Zr}(p,X)^{95}\text{Zr}$  nuclear process [21–23]. None of the literature sources discussed the possible problem of the neutron-induced reaction on  $^{96}\text{Zr}$ . Their results are reproduced in Fig. 12. The cross sections of Levkovskij [21] and Murakami *et al.* [23] support each other in the overlapping energy region below 14 MeV. As is evident in the figure, the cross sections of Levkovskij are rather scanty at higher energies (above 20 MeV). Although the data of Michel *et al.* are also largely in agreement with the previous results, their excitation function seems to be shifted towards lower energies by about 1–2 MeV. Above 30 MeV, only the latter author published cross sections. Based on the available data, the excitation function reaches a single maximum of about 4.8 mb near 30 MeV (neglecting the outlier points of Ref. [22]) and slowly decreases afterwards up to 70 MeV.

The present study provides 25 new cumulative values to the database of the  $^{nat}\text{Zr}(p,X)^{95}\text{Zr}$  nuclear process (see Table 3 and Fig. 12). Our measurements support the literature results and is in excellent agreement, especially, with the two lower-energy studies [21,23].

In general, the TENDL-2013 data [5] reproduce the shape of the experimental trend rather well but seem to be shifted towards higher energies (2–4 MeV). Due to this, the energy position of the maximum (5.3 mb) is also moved to a somewhat higher value of 36 MeV.

### 3.3.2. The $^{nat}\text{Zr}(p,X)^{89(0.94m+g)}\text{Zr}$ process

There are two relatively long-lived states in  $^{89}\text{Zr}$ . The metastable state ( $T_{1/2} = 4.18$  m) has a much shorter half-life than the ground state ( $T_{1/2} = 78.41$  h). The metastable state feeds both  $^{89g}\text{Zr}$  (IT: 93.77%) and  $^{89}\text{Y}$  (stable). The ground state decays 100% to  $^{89}\text{Y}$ . Besides nucleons, the emission of clusters (deuterons and tritons) may significantly contribute, thus as many as 14 reactions participate (see Table 1). In addition,  $^{89}\text{Zr}$  is also formed through the decay of  $^{89}\text{Nb}$  (see subsections 3.2.7 and 3.2.8). Taking into account this rather complex production route for  $^{89}\text{Zr}$  and the experimental conditions reported in the available works [19,21,22,26], it was possible for those authors to extract cross section only after the complete decay of the directly-formed metastable state as well as the precursors  $^{89m}\text{Nb}$  and  $^{89g}\text{Nb}$ . Thus, cumulative cross sections for  $^{89(0.94m+g)}\text{Zr}$  were measured in those experiments. Similar to the previous

case (see subsection 3.3.1) secondary neutrons can also form the residual nucleus  $^{89}\text{Zr}$  (via the  $^{90}\text{Zr}(n,2n)$ ,  $^{91}\text{Zr}(n,3n)$ ,  $^{92}\text{Zr}(n,4n)$ ,  $^{94}\text{Zr}(n,6n)$  and  $^{96}\text{Zr}(n,8n)$  reactions).

As can be concluded from Fig. 13, the two earlier studies [21,22] show good agreement with each other and exhibit a broad peak around 26 MeV. Their respective maxima are also similar, about 520 mb. The results of Uddin *et al.* [26] also support this maximum, however, their curve seems to be shifted a little towards higher energies (by about 2 MeV). In the threshold region of the excitation function, Khandaker *et al.* [19] agrees well with the data of Uddin *et al.* but above 20 MeV they reported systematically lower values. Their maximum is almost 45% lower. As before, it has to be remarked as surprising that experimental values reported from the same laboratory within one year show such a large difference. In addition, both authors [19,26] reported cross-section values much below the threshold of the  $^{90}\text{Zr}(p,d)^{89}\text{Zr}$  reaction (9.85 MeV, marked with a black arrow in Fig. 13). This may be due to neutron activation of the target foils.

The present study produced 19 cross-section values up to 66 MeV (see Table 3 and Fig. 13). The new results agree well with the data of Uddin *et al.* and predict almost the same maximum (490 mb at 28 MeV) as in Refs. 21,22 and 26. Beyond the peak region, our values largely support the results of Michel *et al.*

Surprisingly, the TENDL-2013 data [5] not only underestimate the experimental results but, as can be seen in Fig. 13, two rather prominent additional peaks (at 18 and 40 MeV) are predicted for this process (maxima of 280, 310 and 240 mb at 18, 26 and 40 MeV, respectively).

### 3.3.3. The $^{nat}\text{Zr}(p,X)^{88}\text{Zr}$ process

Numerous nuclear reactions (12 in total, see Table 1) contribute to the formation of the ground state of  $^{88}\text{Zr}$  ( $T_{1/2} = 83.40$  d). Among them, four emit protons and neutrons only while eight involve complex-particle emission as well. There are no long-lived isomeric states and the  $^{88}\text{Zr}$  ground state decays to  $^{88}\text{Y}$  ( $T_{1/2} = 106.61$  d) which again feeds stable  $^{88}\text{Sr}$ . As is usual in the case of  $\text{Zr}+p$  reactions that form radioactive zirconium isotopes, there are also co-produced niobium radionuclides ( $^{88m}\text{Nb}$  and  $^{88g}\text{Nb}$ , with half-lives 7.8 m and 14.3 m, respectively) which decay to  $^{88}\text{Zr}$  (see Table 1.). Due to their short half-lives, only cumulative cross sections for the formation of  $^{88}\text{Zr}$  can be extracted after the complete decay of these precursors. Similar to a few previous cases (see subsections 3.3.1 and 3.3.2), reactions by secondary neutrons can also contribute to the formation of  $^{88}\text{Zr}$ .

The data available in the literature also contain contributions from the decay of  $^{88}\text{Nb}$ . Prior to the present work, five authors reported data for this process [17, 19, 22, 24, 26] (see Fig. 14). However, two studies published only two data points (Bringas *et al.* [17]) and one data point (Rignier *et al.* [24]) below 70 MeV. Systematic work was performed by Michel *et al.* [22] and recently by Uddin *et al.* [26] and Khandaker *et al.* [19]. The excitation functions of the latter two authors show good agreement with each other except near the threshold. Unfortunately, both authors reported values only for the rising part of the curve. The work of Michel *et al.* shows that the excitation function has one prominent maximum of about 350 mb near 41 MeV. Also, the values of Michel *et al.* are systematically higher than those of Uddin *et al.* and Khandaker *et al.* The two data points of Bringas *et al.* seem to support the values of Michel *et al.* and Uddin *et al.*, while the only cross section of Rignier *et al.* at 59 MeV seems

to be and outlier with an extremely high value. None of the literature sources discussed the possible problem of neutron-induced reactions on  $^{nat}\text{Zr}$  leading to  $^{88}\text{Zr}$  formation.

We measured the excitation function of the  $^{nat}\text{Zr}(p,X)^{88}\text{Zr}$  process from threshold up to 66 MeV (see Table 3 and Fig. 14). The 15 new cross-section values confirm the results of Michel *et al.*, except for a relatively small shift towards lower energies (2–3 MeV).

The shape of the excitation function is reproduced satisfactorily by the TENDL-2013 data [5], however, the predicted curve is shifted towards lower energies by about 3–4 MeV. The peak maximum is also slightly lower, about 310 mb near 36 MeV.

#### 3.3.4. The $^{nat}\text{Zr}(p,X)^{87(m+g)}\text{Zr}$ process

Twelve reactions are responsible for the production of  $^{87}\text{Zr}$ , similar to the case of  $^{88}\text{Zr}$  (see subsection 3.3.3 and Table 1). Both the  $^{87m}\text{Zr}$  metastable state ( $T_{1/2} = 14$  s) and the  $^{87g}\text{Zr}$  ground state ( $T_{1/2} = 1.68$  h) are populated by those reactions. The metastable state feeds the ground state via IT (100%), with  $^{87g}\text{Zr}$  further decaying to  $^{87}\text{Y}$  which again feeds  $^{87}\text{Sr}$  (stable). In addition to the direct reactions, both  $^{87m}\text{Nb}$  ( $T_{1/2} = 3.75$  m) and  $^{87g}\text{Nb}$  ( $T_{1/2} = 2.6$  m) are short-lived precursors (see Table 1.). Consequently, only cumulative cross sections for the formation of  $^{87(m+g)}\text{Zr}$  can be measured via the usual non-destructive  $\gamma$ -ray spectroscopy. Neutron-induced reactions can also contribute, as mentioned before.

Probably due to the relatively short half-life of  $^{87}\text{Zr}$ , no experimental data could be found in the literature. The present measurements constitute a set of 12 new cross sections between 40 and 66 MeV. Although our dataset exhibits some scatter in the peak region (see Fig. 15 and Table 3), it is clear that the excitation function has a single broad maximum – about 180 mb at 56 MeV.

The TENDL-2013 data [5] reproduces the shape of the excitation function satisfactorily, however the entire curve seems to be shifted towards lower energies (2–3 MeV). This is similar to the previous case (see subsection 3.3.3). Also, the theoretical curve underestimates the experimental values, predicting a maximum of about 140 mb near 54 MeV.

#### 3.3.5. The $^{nat}\text{Zr}(p,X)^{86}\text{Zr}$ process

The number of reactions participating in the formation of the  $^{86}\text{Zr}$  ground state ( $T_{1/2} = 16.5$  h) is the least among the investigated  $^{nat}\text{Zr}+p\rightarrow\text{Zr}$  nuclear processes (9 reactions, see Table 1). As a result of the decay of  $^{86}\text{Zr}$ , both the metastable and ground states of  $^{86}\text{Y}$  are populated. Finally, the latter radionuclide decays to stable  $^{86}\text{Sr}$ . Unfortunately, the decay of the co-produced  $^{86}\text{Nb}$  ( $T_{1/2} = 1.45$  m) also contributes to the  $^{86}\text{Zr}$  yield in the activated samples, making it difficult to extract direct-formation cross sections for the  $^{nat}\text{Zr}(p,X)^{86}\text{Zr}$  process (see Table 1.). The cumulative cross sections, on the other hand, can be measured after the complete decay of  $^{86}\text{Nb}$ . One should also consider the possibility that neutron-induced reactions may play a role.

Only Michel *et al.* [22] published cumulative cross sections for this process above 50 MeV. As shown in Fig. 16, the data covers the steep rise in the threshold region without quite reaching the expected peak maximum. The new results (7 cross sections, see Table 3 and Fig 16) are in good agreement with the values of Michel *et al.*

Although the shape of the TENDL-2013 curve [5] is in good agreement with the measurements, it is clearly shifted towards lower energies by about 2–3 MeV. The TENDL-2013 data set exhibits a maximum near 67 MeV with a value of about 41 mb.

### 3.4 Formation of *Y* radionuclides

There are eight radionuclides of yttrium that have half-lives between 0.8 h and 200 d and can be produced via proton induced nuclear reactions on natural Zr targets. Eight research groups reported cross sections for  $^{nat}\text{Zr}+p$  processes resulting in metastable and/or ground states of  $^{88}\text{Y}$ ,  $^{87}\text{Y}$  and  $^{86}\text{Y}$  radionuclides in different energy regions [15,19,20–23,26,27]. Concerning the formation of yttrium radionuclides, strontium and zirconium isobars can be significant precursors. The neutron background may also contribute production paths via neutron-induced reactions however such contributions will probably be negligible except near the effective excitation-function thresholds.

Besides the above three radionuclides, new cross-section data for the formation of  $^{91}\text{Y}$ ,  $^{90}\text{Y}$ ,  $^{86}\text{Y}$  and  $^{85}\text{Y}$  are presented for the first time, to the best of our knowledge. The results for  $^{91m}\text{Y}$ ,  $^{90m}\text{Y}$ ,  $^{88}\text{Y}$ ,  $^{87m}\text{Y}$ ,  $^{87(m+g)}\text{Y}$ ,  $^{86m}\text{Y}$ ,  $^{86g}\text{Y}$ ,  $^{85m}\text{Y}$  and  $^{85g}\text{Y}$  are presented in Figs. 17–25, respectively, while the numerical values are compiled in Table 4. The available literature values (corrected where necessary) are also reproduced in the appropriate figures. The energy and cross-section uncertainties of the literature values are not shown in the figures except in the cases of the  $^{nat}\text{Zr}(p,X)^{87m}\text{Y}$  and  $^{nat}\text{Zr}(p,X)^{88}\text{Y}$  processes.

#### 3.4.1. The $^{nat}\text{Zr}(p,X)^{91m}\text{Y}$ process

Proton-induced reactions on  $^{nat}\text{Zr}$  populate both the metastable and ground states of  $^{91}\text{Y}$ . The 15 contributing reactions are listed in Table 1. The  $^{91m}\text{Y}$  ( $T_{1/2} = 49.71$  m) decays completely (IT) to  $^{91g}\text{Y}$  ( $T_{1/2} = 58.51$  d) which further decays to stable  $^{91}\text{Zr}$ . The precursor  $^{91}\text{Sr}$  ( $T_{1/2} = 9.63$  h) is formed via 10 contributing reactions on  $^{94,96}\text{Zr}$  above 20 MeV and decays completely to  $^{91}\text{Y}$  (see Table 1.). Note that the  $^{91g}\text{Y}$  decay is accompanied by only very weak  $\gamma$ -ray emissions, thus, data were measured only for the metastable state.

No previous results were found in the literature for either the  $^{nat}\text{Zr}(p,X)^{91}\text{Sr}$  or the  $^{nat}\text{Zr}(p,X)^{91m}\text{Y}$  processes. Due to our experimental conditions, we could not identify the presence of  $^{91}\text{Sr}$  in the activated samples, therefore independent cross sections could not be extracted for the  $^{nat}\text{Zr}(p,X)^{91m}\text{Y}$  process. However, taking into account the large difference in the respective half-lives and the decay branching ratio of  $^{91}\text{Sr}$  to  $^{91m}\text{Y}$  (55.57%), the influence of the  $^{nat}\text{Zr}(p,X)^{91}\text{Sr}$  process is expected to be negligible. This means that, for all practical purposes, independent cross sections for the  $^{nat}\text{Zr}(p,X)^{91m}\text{Y}$  process were measured shortly after EOB.

Our results of 23 new cross sections up to 66 MeV are presented in Table 4 and Fig. 17. The excitation function is monotonically increasing over the studied energy region (20–66 MeV) with no discernable peaks. In contrast, the TENDL-2013 data [5] predict a clear peak near 17 MeV with a maximum of about 1.1 mb. Between 24 and 40 MeV, the predicted curve is consistent with the experimental results, but beyond this energy it overestimates the measured values.

#### 3.4.2. The $^{nat}\text{Zr}(p,X)^{90m}\text{Y}$ process

Altogether 16 reactions contribute to  $^{90}\text{Y}$  formation in  $^{\text{nat}}\text{Zr}+\text{p}$  (see Table 1). The metastable state  $^{90\text{m}}\text{Y}$  ( $T_{1/2} = 3.19$  h) largely decays to the ground state  $^{90\text{g}}\text{Y}$  ( $T_{1/2} = 2.671$  d, IT: 99.99%) which further decays to stable  $^{90}\text{Zr}$ . Only  $^{90\text{g}}\text{Y}$  is fed by decay of the precursor  $^{90}\text{Sr}$ , thus, independent cross sections can be measured for the  $^{\text{nat}}\text{Zr}(\text{p},\text{X})^{90\text{m}}\text{Y}$  process.

Prior to the present investigation, no other group reported cross sections for this process. The new data (24 cross sections) are shown in Fig. 18 and compiled in Table 4. The excitation function shows a discernable peak with a maximum of about 1.6 mb near 25 MeV. Beyond the peak it increases monotonically in the investigated energy region.

Up to the energy position of the peak, the theoretical TENDL-2013 data [5] show good agreement with the experimental results. However, the theoretical data systematically overestimate the measured values (see Fig. 18) beyond 25 MeV. This overestimation is about a factor of 2 at the highest measured energy.

### 3.4.3. The $^{\text{nat}}\text{Zr}(\text{p},\text{X})^{88}\text{Y}$ process

The ground state of  $^{88}\text{Y}$  ( $T_{1/2} = 106.63$  d) is formed via numerous (23) proton-induced nuclear processes on  $^{\text{nat}}\text{Zr}$  (see Table 1). Note that no higher-lying states of this radionuclide have half-lives long enough to be observed in the present investigation. The decay of  $^{88}\text{Y}$  feeds  $^{88}\text{Sr}$ , which is stable. The formation of  $^{88}\text{Y}$  is also possible through a decay chain ( $^{88}\text{Nb} \rightarrow ^{88}\text{Zr} \rightarrow ^{88}\text{Y}$ ) above 19 MeV. The excitation function of  $^{88}\text{Zr}$  has already been discussed above (see subsection 3.3.3). The excitation function of  $^{88}\text{Y}$  exhibits a significant contribution from precursor decay (see Fig. 19). Since the half-lives of  $^{88}\text{Y}$  and  $^{88}\text{Zr}$  are very similar, the  $^{88}\text{Y}$  activity in the activated  $^{\text{nat}}\text{Zr}$  samples cannot be measured post complete precursor decay. Consequently, the measured activities must be corrected according to Ref. [22] for purposes of extracting cross sections. The cross sections obtained are consistent with the independent formation of  $^{88}\text{Y}$ .

The available literature data [15,21–23,26,27] are presented in Fig. 19. Since the measured cross sections are in the range of 0.001 to 100 mb, a logarithmic presentation is employed in this figure. Three authors reported cross sections below 20 MeV [15,23,27] where  $^{88}\text{Y}$  are not formed via precursor decay. Only Al-Abyad *et al.* [15] and Murakami *et al.* [23] have an overlapping energy region between 11 and 14 MeV. These results seem to support each other, however, the values of Al-Abyad *et al.* are rather scattered below 14 MeV. As shown in Fig. 19, the results of Murakami *et al.* and Vysotskij *et al.* [27] exhibit a large discrepancy. According to the Vysotskij data, the excitation function starts at a much lower energy. The formation of  $^{88}\text{Y}$  via the decay of  $^{88}\text{Zr}$  formed by neutron-induced reactions in a relative high secondary neutron flux may be a possible explanation (also see subsection 3.3.3). Levkovskij [21] and Michel *et al.* [22] show acceptable agreement in their overlap energy region. According to the paper of Michel *et al.* they published corrected cross sections. They measured cumulative cross sections for the mother nuclide ( $^{88}\text{Zr}$ ) and independent cross section for the product was determined using their correction method. Due to the lack of experimental details, it is only an assumption that the cross sections of Levkovskij are corrected for precursor decay. The Michel *et al.* data show rather large scatter between 34 and 50 MeV with some noticeable outliers, as mentioned also in several previous cases.

The cross sections of Uddin *et al.* [26] have been corrected for precursor decay. Note that the Uddin data constitute the lowest values among the various authors. It is noteworthy that

only Michel *et al.* and Uddin *et al.* reported cross sections for the formation of both  $^{88}\text{Y}$  and  $^{88}\text{Zr}$ .

It can be concluded that the excitation function peaks near 20 and 45 MeV with maxima of about 3.3 and 30 mb, respectively. We investigated the  $^{\text{nat}}\text{Zr}(p,X)^{88}\text{Y}$  process only from 14 MeV up to higher energies. Naturally, we have also corrected our data for precursor decay, using the method described in Ref. [22], beyond 19 MeV. The 18 new cross sections are also presented in Fig. 19 and Table 4. Up to 30 MeV, the new data show good agreement with the values of Al-Abyad *et al.*, Murakami *et al.*, Levkovskij and Michel *et al.* Above 30 MeV, however, our values are slightly higher than those of other authors.

The TENDL-2013 theoretical data [5] exhibit a rather good overall agreement with the measured data (see Fig. 19). Some overestimation, however, is evident above 30 MeV.

#### 3.4.4. The $^{\text{nat}}\text{Zr}(p,X)^{87\text{m}}\text{Y}$ process

Proton-induced reactions on  $^{\text{nat}}\text{Zr}$  populate one metastable state of  $^{87}\text{Y}$  ( $T_{1/2} = 13.37$  h) besides the ground state ( $T_{1/2} = 79.8$  h) in the investigated energy region. The 23 contributing reactions are compiled in Table 1. The decay of  $^{87\text{m}}\text{Y}$  feeds  $^{87\text{g}}\text{Y}$  (IT: 98.43%) as well as stable  $^{87}\text{Sr}$  (1.57%). The  $^{87\text{g}}\text{Y}$  ground state decays completely to stable  $^{87}\text{Sr}$ . The production conditions of the shorter-lived precursor  $^{87}\text{Zr}$  (also present in the decay chain  $^{87}\text{Nb} \rightarrow ^{87}\text{Zr} \rightarrow ^{87}\text{Y}$ ) have already been discussed in subsection 3.3.4. Its influence to the formation of  $^{87}\text{Y}$  is clearly observable above about 30 MeV. Note that  $^{87\text{g}}\text{Zr}$  completely decays to the metastable state  $^{87\text{m}}\text{Y}$ .

Until now, four authors [19,21,22,26] reported independent cross sections for this process but only one author measured data above 40 MeV [22]. Their results are reproduced in Fig. 20. Due to the large range of values, a logarithmic presentation of the results was selected. All data sets predict a similar shape for the excitation function with a prominent peak around 23 MeV. In contrast to the agreement for the peak position, the various data sets show large differences in the measured values. Uddin *et al.* [26] published the lowest values and their maximum is only about 3 mb at the peak maximum. Although the data of Khandaker *et al.* [19] and Uddin are relative close to each other at low energies, above 17 MeV the Khandaker data are systematically higher, by about a factor of 2. As observed above for other cases, it is curious that data from the same laboratory published within one year can differ so much. Both authors [19,26] mentioned the presence of the precursor but they neglected its influence to their data. The cross sections of Levkovskij [21] are systematically (about 10–20%) higher than the values of Khandaker *et al.* Michel *et al.* [22] reported the highest values. Their peak maximum near 23 MeV is above 10 mb. There are, however, two cross-section values of Michel *et al.* (this time between 18 and 34 MeV) which are much closer to the results of Levkovskij and Khandaker *et al.* than to their own mainstream (see also the similar problem of Michel data in the case of the  $^{\text{nat}}\text{Zr}(p,X)^{88}\text{Y}$  process). The data of Michel *et al.* also exhibits a second peak close to 56 MeV with a maximum of about 250 mb.

Our new cumulative cross sections (18 values, see Fig. 20 and Table 4) are consistent with the data of Levkovskij and above 45 MeV agree quite well with the results of Michel *et al.* The disagreements at lower energies are rather curious.

The TENDL-2013 [5] curve seems to agree in absolute value only with the values of Khandaker *et al.* and underpredicts the results of Levkovskij, Michel *et al.* and the present

work. This rather low-lying curve relative to the majority of the experimental data is nevertheless consistently higher than the results of Uddin *et al.*

### 3.4.5. The $^{nat}\text{Zr}(p,X)^{87(0.984m+g)}\text{Y}$ process

Concerning the production and decay of  $^{87g}\text{Y}$  ( $T_{1/2} = 79.80$  h), please refer to Table 1 and subsection 3.4.4. Prior to the present work, six groups investigated the  $^{nat}\text{Zr}(p,x)^{87(0.984m+g)}\text{Y}$  process. Their results are presented in Fig. 21. Murakami *et al.* [23], Khandaker *et al.* [19], Kondrat'ev *et al.* [20] and Uddin *et al.* [26] reported cumulative cross sections after the complete decay of  $^{87m}\text{Y}$ . We summed the independent cross sections of Levkovskij [21] measured on  $^{90}\text{Zr}$  and  $^{91}\text{Zr}$  to get cumulative values. According to Ref. [31], Michel *et al.* [22] reported independent cross sections by subtracting the contribution of the isomeric transition. Consequently, their values are also independent cross sections. It is therefore expected that the Michel *et al.* data should be lower than the results of the other authors.

Below 13 MeV, the available data [19,20,22,23,26] are rather scattered (see Fig. 21). As in several previous instances, the data of Uddin *et al.* [26] are the lowest among the various data sets. They reported a peak maximum of about 5 mb near 25 MeV. Interestingly, Levkovskij [21] seems to support the values of Uddin *et al.* while Khandaker *et al.* [19] reported systematically higher values (10–20%), especially above 15 MeV (maximum of 8 mb near 25 MeV). Similar to the above process (see subsection 3.4.4), Michel *et al.* published the highest values among the authors over the whole investigated energy region, with a maximum of about 15 mb near 25 MeV. This is contrary to expectations (see the previous paragraph).

Above 30 MeV, the excitation function rises again, reaching a second maximum at about 58 MeV. The data of Michel *et al.* and Kondrat'ev *et al.* exhibit very different second maxima, about 250 and 60 mb, respectively. The behavior of the Kondrat'ev data is very interesting. At low energies it is consistent with the data of Michel *et al.* but above 16 MeV it seems to support the results of Khandaker *et al.* However, between 35 and 40 MeV there is good agreement with the data of Uddin *et al.* Above 40 MeV, Kondrat'ev *et al.* reported significantly smaller values than Michel *et al.*, by a factor of between 4 and 6. If we assume that the cross-section values of Michel *et al.* are independent ones, this deviation is even more difficult to understand.

The new results (20 cumulative cross sections, see Table 4 and Fig. 21) are consistent with the values of Michel *et al.*

The TENDL-2013 data seem to support the values of Khandaker *et al.* and Murakami *et al.* in the overlapping energy regions. The entire curve is low-lying compared to the present data and those of Michel *et al.*

### 3.4.6. The $^{nat}\text{Zr}(p,X)^{86m}\text{Y}$ process

Numerous nuclear reactions on  $^{90,91,92,94}\text{Zr}$  contribute to the formation of  $^{86}\text{Y}$  in the activation of  $^{nat}\text{Zr}$  with protons up to 66 MeV. The 15 participating reactions are compiled in Table 1. In addition to the ground state, the metastable state  $^{86m}\text{Y}$  ( $T_{1/2} = 48$  m) is also populated during the activation. The metastable state decays almost completely to the ground state (IT: 99.3%) while  $^{86g}\text{Y}$  ( $T_{1/2} = 14.74$  h) in turn completely decays to stable  $^{86}\text{Sr}$ . Since

the precursor ( $^{86}\text{Zr}$ ) decays only to the  $^{86}\text{Y}$  ground state, independent cross sections can be measured for the  $^{nat}\text{Zr}(p,X)^{86m}\text{Y}$  process.

As far as we know, the present work reports measured cross sections for the first time. The numerical data (21 values) are shown in Fig. 22 and compiled in Table 4. The excitation function has a distinct peak with a maximum of about 10 mb near 35 MeV. Above 52 MeV, it increases monotonically to the highest investigated energy.

The TENDL-2013 [5] theoretical data predict the shape of the excitation function reasonably well and show a peak at the same energy as the experimental results. The maximum of the peak, however, is under-predicted and at energies above 55 MeV the theoretical values are systematically higher.

### 3.4.7. The $^{nat}\text{Zr}(p,X)^{86(0.99m+g)}\text{Y}$ process

For the production and decay of  $^{86g}\text{Y}$  ( $T_{1/2} = 14.74$  h), please refer to the previous section and also to Table 1. As mentioned in subsection 3.4.7,  $^{86g}\text{Y}$  is populated by the decay of  $^{86m}\text{Y}$  as well as the precursor  $^{86}\text{Zr}$ . Formation of these radionuclides has already been discussed above (see subsections 3.4.6. and 3.3.5). The contribution from  $^{86}\text{Zr}$  decay is observable only above 40 MeV.

The available literature results [19–22,26] are reproduced in Fig. 23. Levkovskij [21] measured cross sections for the  $^{90}\text{Zr}(p,X)^{86(m+g)}\text{Y}$  process up to 30 MeV. For comparison his cumulative data were converted to a natural target composition. According to the EXFOR database [31] both Michel *et al.* [22] and Kondrat'ev *et al.* [20] reported cumulative cross sections. Likewise, Uddin *et al.* [26] and Khandaker *et al.* [19] measured the activities after the complete decay of the metastable state.

The published data for this excitation function are rather contradictory. The data of Kondrat'ev *et al.* exhibit an effective threshold almost 10 MeV lower than the others. Due to this 'energy shift', the position of their peak maximum is also located at a lower energy (30 MeV). The data of Michel *et al.* exhibit a peak maximum at 35 MeV. The maxima of the above two authors are close to each other (30 and 28 mb, respectively). The renormalized data of Levkovskij show excellent agreement with the values of Michel *et al.* The recently published cross sections of Uddin *et al.* and Khandaker *et al.* up to 40 MeV seem to be reasonably consistent with each other, especially in the threshold region, however, their respective maxima are somewhat different. Uddin *et al.* reported 18 mb at 35 MeV while Khandaker *et al.* measured a little higher value of about 21 mb at 37 MeV. In addition, the cross sections of Uddin *et al.* are systematically lower than those of Khandaker *et al.* at higher energies beyond the peak. Above 40 MeV, only Kondrat'ev *et al.* and Michel *et al.* reported experimental cross sections. Although their results seem to be in relatively good agreement, the energy shift in the Kondrat'ev data is still observable. The results of Kondrat'ev *et al.* show a second peak with a maximum of about 30 mb near 64 MeV. This second peak is notably absent in the data of Michel *et al.*

The data set measured in the present work comprises 15 cross sections between 25 and 66 MeV (see Table 4 and Fig. 23). It seems to support the recent results of Khandaker *et al.* [19] and Uddin *et al.* [26] in the overlapping energy region. Between 40 and 60 MeV, our values are systematically lower than those of Kondrat'ev *et al.* [20] and Michel *et al.* [22]. Above 60

MeV, however, the new values are significantly higher, exhibiting a much steeper slope compared to the other data sets.

The TENDL-2013 data [5] satisfactorily reproduce the shape of the excitation function and predict only one prominent peak below 70 MeV. While the position of the peak around 34 MeV is close to that observed experimentally, the maximum of only about 12 mb is significantly lower.

#### 3.4.8. The $^{nat}\text{Zr}(p,X)^{85m}\text{Y}$ process

A metastable state ( $^{85m}\text{Y}$ ,  $T_{1/2} = 4.86$  h) and the ground state of  $^{85}\text{Y}$  have both been observed experimentally in the investigated energy region. Details of the relevant reactions are given in Table 1. Both states decay separately to  $^{85}\text{Sr}$ . The decay chain ends at stable  $^{85}\text{Rb}$ . The co-produced precursor ( $^{85}\text{Zr}$ ) also has two longer-lived states ( $^{85g}\text{Zr}$ ,  $T_{1/2} = 7.86$  m and  $^{85m}\text{Zr}$ ,  $T_{1/2} = 10.9$  s). The decay of these states feed both states of  $^{85}\text{Y}$  (95% to  $^{85g}\text{Y}$  and 5% to  $^{85m}\text{Y}$ ). Since the threshold energy for the formation of  $^{85}\text{Zr}$  via the  $^{90}\text{Zr}(p,t3n)^{85}\text{Y}$  reaction is much higher than that of the  $^{90}\text{Zr}(p,\alpha 2n)^{85}\text{Y}$  reaction, the influence of the  $^{nat}\text{Zr}(p,X)^{85}\text{Zr}$  process is negligible below 48 MeV. Above 48 MeV, therefore, only cumulative cross sections can be measured for the  $^{nat}\text{Zr}(p,X)^{85m,g}\text{Y}$  processes. Both these processes have not been investigated before, as far as we know.

The present results include 8 cumulative cross sections for the  $^{nat}\text{Zr}(p,X)^{86m}\text{Y}$  nuclear process above 45 MeV (see Table 4 and Fig. 24). Unfortunately, due to the rather large uncertainties and the sparseness of the experimental data, not much can be concluded concerning the shape of the excitation function from the measurements alone. A better idea can be formed by also including theoretical predictions.

The theoretical data according to the TENDL-2013 compilation [5] show a prominent peak near 45 MeV with a maximum of about 14 mb. The excitation function has a local minimum near 59 MeV and increases again towards higher energies. Figure 24 shows that the agreement between the TENDL-2013 data and the experimental results is satisfactory within the rather large uncertainties of the latter.

#### 3.4.9. The $^{nat}\text{Zr}(p,X)^{85g}\text{Y}$ process

For the production and decay of  $^{85g}\text{Y}$  ( $T_{1/2} = 2.68$  h), please refer to the previous section and also Table. 1. The new measurements comprise 9 cumulative cross sections but only above 42 MeV (see Table 4 and Fig. 25). No previous data was found in the literature for this process. The experimental results show a probable peak near 46 MeV with a maximum of about 9.5 mb.

The TENDL-2013 data [5] also predict a peak for this process but at a somewhat lower energy (about 42 MeV). The peak maximum is significantly lower, at a value of only 2 mb. In addition, above 58 MeV the theoretical curve starts to increase sharply but the experimental data do not show this trend. This is possibly due to an overall energy shift between the theoretical prediction and the measurements.

### 3.5. Formation of Sr radionuclides

Several Sr radionuclides can be produced below 66 MeV via  $^{nat}\text{Zn}+p$  processes. Among them, seven have half-lives between 0.8 h and 200 d. However, excitation functions for only  $^{83}\text{Sr}$  and  $^{85}\text{Sr}$  were found in the literature. The experimental conditions of the present investigation allowed the observation of only  $^{85}\text{Sr}$  in the activated samples.

### 3.5.1 The $^{nat}\text{Zr}(p,X)^{85(0.87m+g)}\text{Sr}$ process

In addition to the ground state, one metastable state is also populated during the formation of  $^{85}\text{Sr}$ . When this shorter-lived metastable state ( $T_{1/2} = 1.126$  h) decays, both the ground states of  $^{85}\text{Sr}$  (via IT: 87%) and  $^{85}\text{Rb}$  (via EC: 13%) are populated. The  $^{85g}\text{Sr}$  ( $T_{1/2} = 64.84$  d) feeds only the ground state of  $^{85}\text{Rb}$ , which is stable. Table 1 contains the list of contributing reactions (on  $^{90,91,92}\text{Zr}$ ) up to 66 MeV. Besides the direct reactions, the decay of both  $^{85m}\text{Y}$  and  $^{85g}\text{Y}$  (precursors) feed the isomeric and ground states of  $^{85}\text{Sr}$ . As already discussed above (see subsections 3.4.8. and 3.4.9), those states of  $^{85}\text{Y}$  are also populated by the decay of the metastable and ground states of  $^{85}\text{Zr}$ .

Only one group previously reported cross sections for the above process in the investigated energy region, namely Michel *et al.* [22] (see Fig. 26). It has to be mentioned that due to the complex nature of the formation of  $^{85}\text{Sr}$ , it is practically impossible to measure the cross sections for the direct formation of  $^{85}\text{Sr}$  without chemical separation and complete knowledge of the excitation functions of the  $^{nat}\text{Zr}(p,X)^{85}\text{Zr}$  and the  $^{nat}\text{Zr}(p,X)^{85}\text{Y}$  nuclear processes. According to Ref. [22], the published cross sections for the  $^{nat}\text{Zr}(p,X)^{85}\text{Sr}$  process were obtained without chemistry and after the complete decay of  $^{85}\text{Zr}$ ,  $^{85}\text{Y}$  and  $^{85m}\text{Sr}$  – thus cumulative cross sections were reported. As shown in Fig. 26, their excitation function reaches a peak maximum of about 40 mb at 48 MeV. Above 60 MeV, the data exhibit an increasing trend.

The present measurements provided 11 new cross sections for this process (see Table 3 and Fig. 26). Within the uncertainties, these results show excellent agreement with the data of Michel *et al.* Note that below 40 MeV, however, the data of Michel *et al.* seem to be shifted towards lower energies, as seen in several previous cases as well.

Although the TENDL-2013 data [5] describe the shape of the excitation function quite well, a significant underprediction of the cross sections for this process is evident. The peak maximum of about 6 mb near 48 MeV is almost a factor of 7 lower than obtained experimentally.

## 4. Conclusions

This work constitutes a systematic investigation, up to 66 MeV, of those  $^{nat}\text{Zr}+p$  nuclear processes which lead to the formation of different Nb, Zr, Y and Sr radionuclides with half-lives between 0.8 h and 200 d. For several processes, measured cross sections are presented for the first time. We also compared the present results with the available literature data and the predictions of the TALYS code as compiled in the TENDL-2013 library. These comparisons revealed several discrepancies between the available experimental data sets and also with the theoretical calculations. We have attempted to explain the most obvious cases where, for example, targetry problems, neglected nuclear processes, disturbing nuclear

reactions, etc., could have contributed to the observed discrepancies. Further experimental work is still required in some cases, especially close to the effective thresholds of the excitation functions and at higher energies (above 40 MeV) to get reliable databases for all the investigated processes.

## Acknowledgements

The authors wish to thank the cyclotron operators in Hungary, Japan and South Africa for their technical assistance. This work was financially supported by the Hungarian Research Foundation (Budapest, OTKA K108669) and the National Research Foundation (NRF) of South Africa (Grant specific unique reference number UID 85507). It is acknowledged that opinions, findings and conclusions or recommendations expressed in any publication generated with the NRF supported research are those of the authors, and that the NRF accepts no liability whatsoever in this regard. The authors thank Dr. J. Timár (ATOMKI) for valuable discussions and comments.

## References

- [1] NEA/OECD, Accelerator-driven Systems (ADS) and Fast Reactors (FR) in Advanced Nuclear Fuel Cycles – A comparative study, Report NEA3109, 2002, pp 1–350, and references therein. Available from URL: [www.oecd-nea.org/](http://www.oecd-nea.org/).
- [2] W. Ren, Z. Zhang, Y. Han, Calculation and analysis of cross-sections for  $p+^{90,91,92,94,96,\text{nat}}\text{Zr}$  reactions up to 200 MeV, Nucl. Instr. Meth. Phys. Res. B 269 (2011) 472–483.
- [3] V. Radchenko, H. Hauser, M. Eisenhut, D.J. Vugts, G.A.M.S. van Dongen, F. Roesch,  $^{90}\text{Nb}$  – a potential PET nuclide: production and labeling of monoclonal antibodies, Radiochim. Acta 100 (2012) 857–864.
- [4] F. Tárkányi, A. Hermanne, S. Takács, F. Ditrói, A.I Dityuk, Yu.N Shubin, Excitation functions for production of radionuclides of niobium, zirconium and yttrium by irradiation of zirconium with deuterons, Nucl. Instr. Meth. Phys. Res. B 217 (2004) 373–386.
- [5] A.J. Koning, D. Rochman, S.C. van der Marck, J. Kopecky, J. Ch. Sublet, S. Pomp, H. Sjostrand, R. Forrest, E. Bauge, H. Henriksson, O. Cabellos, S. Goriely, J. Leppanen, H. Leeb, A. Plompen, R. Mills, TENDL-2013: TALYS-based evaluated nuclear data library, Available from URL: <http://www.talys.eu/tendl-2013/> (last updated December 2013).
- [6] F. Szelecsényi, G.F. Steyn, Z. Kovács, C. Vermeulen, N.P. van der Meulen, S.G. Dolley, T.N. van der Walt, K. Suzuki, K. Mukai, Investigation of the  $^{66}\text{Zn}(p,2p)^{64}\text{Cu}$  and  $^{68}\text{Zn}(p,x)^{64}\text{Cu}$  nuclear processes up to 100 MeV: Production of  $^{64}\text{Cu}$ , Nucl. Instr. Meth. Phys. Res. B 240 (2005) 625–637.
- [7] Z. Kormány, A new method and apparatus for measuring the mean energy of cyclotron beams, Nucl. Instr. Meth. Phys. Res. A 337 (1994) 258–264.

- [8] G. Székely, FGM – A flexible gamma-spectrum analysis program for a small computer, *Comput. Phys. Commun.* 34 (1985) 313–319.
- [9] NuDat 2.6, National Nuclear Data Center, Brookhaven National Laboratory, 2012, Available from URL: [www.nndc.bnl.gov/nudat2/](http://www.nndc.bnl.gov/nudat2/).
- [10] WWW Chart of the Nuclides 2010, Nuclear Data Centre, Japan Atomic Energy Agency. Available from URL: <http://wwwndc.jaea.go.jp/CN10/>.
- [11] I. Cata-Danil, M. Ivascu, T. Glodariu, N.V. Zamfir, D. Bucurescu, D. Filipescu, G. Cata-Danil, L. Stroe, C. Mihai, D. Ghita, G. Suliman, T. Sava, Measurement of cross sections and thick target yields for ( $\alpha,\gamma$ ) process on  $^{63}\text{Cu}$ , *Rom. Rep. Phys.* 60 (2008) 555–561.
- [12] K. Gul, A. Hermanne, M.G. Mustafa, F. M. Nortier, P. Obložinský, S.M. Qaim, B. Scholten, Yu. Shubin, S. Takács, F. T. Tárkányi, Z. Zhuang, Charged particle cross-section database for medical radionuclide production: diagnostic radionuclides and monitor reactions, IAEA-TECDOC-1211, IAEA, Vienna, May 2001. Available from URL: [www-nds.iaea.org/medical/](http://www-nds.iaea.org/medical/) (last updated May 2013).
- [13] H.H. Andersen, J.F. Ziegler, Hydrogen stopping powers and ranges in all elements, In: *The Stopping and Ranges of Ions in Matter* (Ed. J.F. Ziegler), vol. 3, Pergamon, New York, 1977, p. 1.
- [14] J.F. Ziegler, *The Stopping and Range of Ions in Matter (SRIM-2013)*, Available from URL: <http://www.srim.org/>.
- [15] M. Al-Abyad, A.S. Abdel-Hamid, F. Tárkányi, F. Ditrói, S. Takács, U. Seddik, I.I. Bashter, Cross-section measurements and nuclear model calculation for proton induced nuclear reaction on zirconium, *Appl. Radiat. Isot.* 70 (2012) 257–262.
- [16] J.P. Blaser, F. Boehm, P. Marmier, P. Scherrer, Anregungsfunktionen und Wirkungsquerschnitte der (p,n)-Reaktion (II), *Helvetica Physica Acta* 24 (1951) 441–464.
- [17] F. Bringas, M.T. Yamashita, I.D. Goldman, P.R. Pascholati, V. Sciani, Measurement of proton-induced reaction cross sections in Ti, Ni and Zr near the threshold, In: *Proc. Int. Conf. on Nuclear Data for Science and Technology (ND2004)*, Eds. R.C. Haight, M.B. Chadwick, T. Kawano, P. Talou), Santa Fe, 2004, *AIP Conf. Proc.* 769 (2005) 1374–1377.
- [18] S. Busse, F. Rösch, S. M. Qaim, Cross section data for the production of the positron emitting niobium isotope  $^{90}\text{Nb}$  via the  $^{90}\text{Zr}(p,n)$ -reaction, *Radiochim. Acta* 90 (2002) 1–5.
- [19] M.U. Khandaker, K. Kim, M.W. Lee, K.S. Kim, G.N. Kim, Y.S. Cho, Y.O. Lee, Experimental determination of proton-induced cross-sections on natural zirconium, *Appl. Radiat. Isot.* 67 (2009) 1341–1347.

- [20] S.N. Kondrat'ev, V.A. Kuzmenko, Yu.N. Lobach, V.S. Prokopenko, V.D. Sklyarenko, V.V. Tokarevskii, Cross sections for forming radionuclides from the interaction of protons with energies up to 70 MeV with zirconium (in Russian), *Atomnaya Energiya* 71 (1991) 325–331. (English translation is available: *Soviet Atomic Energy* 71(1991) 832–838).
- [21] V.N. Levkovskij, Activation cross section of nuclides of average masses ( $A = 40\text{--}100$ ) by protons and alpha-particles with average energies ( $E = 10\text{--}50$  MeV), *Inter Vesi*, Moscow, 1991.
- [22] R. Michel, R. Bodemann, H. Busemann, R. Daunke, M. Gloris, H.-J. Lange, B. Klug, A. Krins, I. Leya, M. Lüpke, S. Neumann, H. Reinhardt, M. Schnatz-Büttgen, U. Herpers, Th. Schiekkel, F. Sudbrock, B. Holmqvist, H. Condé, P. Malmborg, M. Suter, B. Dittrich-Hannen, P.-W. Kubik, H.-A. Synal, D. Filges, Cross sections for the production of residual nuclides by low- and medium-energy protons from the target elements C, N, O, Mg, Al, Si, Ca, Ti, V, Mn, Fe, Co, Ni, Cu, Sr, Y, Zr, Nb, Ba and Au, *Nucl. Instr. Meth. Phys. Res. B* 129 (1997) 153–193.
- [23] M. Murakami, H. Haba, S. Goto, J. Kanaya, H. Kudo, Production cross sections of niobium and tantalum isotopes in proton-induced reactions on  $^{nat}\text{Zr}$  and  $^{nat}\text{Hf}$  up to 14 MeV, *Appl. Radiat. Isot.* 90 (2014) 149–157.
- [24] S. Regnier, B. Lavielle, M. Simonoff, G.N. Simonoff, Nuclear reactions in Rb, Sr, Y, and Zr targets, *Phys. Rev. C* 26 (1982) 931–943.
- [25] E.A. Skakun, V.G. Batij, Yu.N. Rakivnenko, O.A. Rastrepin, Excitation functions and isomer ratios for up-to-9-MeV proton interactions with Zr and Mo isotope nuclei (in Russian), *Yadernaya Fizika* 46 (1987) 28–39.
- [26] M.S. Uddin, M.U. Khandaker, K.S. Kim, Y.S. Lee, M.W. Lee, G.N. Kim, Excitation functions of the proton induced nuclear reactions on natural zirconium, *Nucl. Instr. Meth. Phys. Res. B* 266 (2008) 13–20.
- [27] O.N. Vysotskij, A.V. Gonchar, O.K. Gorpinich, S.N. Kondrat'ev, V.S. Prokopenko, S.B. Rakitin, V.D. Sklyarenko, V.V. Tokarevskij, Excitation functions of the  $\text{Zr}+p,d \rightarrow {}^{91m}\text{Nb}$ ,  ${}^{92m}\text{Nb}$ ,  ${}^{95}\text{Nb}$ ,  ${}^{95}\text{Zr}$ ,  ${}^{88}\text{Y}$  reactions (in Russian). In: *Proc. 41<sup>th</sup> Conf. on Nuclear Spectroscopy and Nuclear Structure*, Minsk, Belarus, 16–19 April 1991, pp 486–492.
- [28] F.R. Chloupek, A.St.J. Murphy, R.N. Boyd, A.L. Cole, J. Görres, R.T. Guray, G. Raimann, J.J. Zach, T. Rauscher, J.V. Schwarzenberg, P. Tischhauser, M.C. Wiescher, Measurements of proton radiative capture cross sections relevant to the astrophysical rp- and  $\gamma$ -processes. *J. Nucl. Phys. A* 652 (1999) 391–405.
- [29] S. Takács, F. Tárkányi, M. Sonck, A. Hermanne, Investigation of the  $^{nat}\text{Mo}(p,x)^{96m}\text{Tc}$  nuclear reaction to monitor proton beams: New measurements and consequences on the earlier reported data, *Nucl. Instr. Meth. Phys. Res. B* 198 (2002) 183–196.
- [30] S.K. Basu, G. Mukherjee, A.A. Sonzogni, Nuclear Data sheets for  $A = 95$ , *Nucl. Data Sheets* 111 (2010) 2555–2737.

[31] Experimental Nuclear Reaction Data (EXFOR) Database, Nuclear Data Section, International Atomic Energy Agency (Version of July 11, 2014) Available from URL: [www-nds.iaea.org/exfor/](http://www-nds.iaea.org/exfor/)

**Figure caption:**

**Fig.1.** Reference excitation function of the  $^{nat}\text{Ti}(p,xn)^{48}\text{V}$  monitor reaction [12] and cross sections of the same reaction measured in this study for beam monitoring purposes.

**Fig.2.** Reference excitation function of the  $^{nat}\text{Cu}(p,xn)^{62}\text{Zn}$  monitor reaction [12] and cross sections of the same reaction measured in this study for beam monitoring purposes.

**Fig.3.** Reference excitation function of the  $^{nat}\text{Cu}(p,n)^{65}\text{Zn}$  monitor reaction [12] and cross sections of the same reaction measured in this study for beam monitoring purposes.

**Fig.4.** Independent cross sections for the formation of  $^{96}\text{Nb}$  via the  $^{nat}\text{Zr}(p,n)^{96}\text{Nb}$  nuclear reaction.

**Fig.5.** Independent cross sections for the formation of  $^{95m}\text{Nb}$  via the  $^{nat}\text{Zr}(p,2n)^{95m}\text{Nb}$  nuclear process.

**Fig.6.** Independent cross sections for the formation of  $^{95g}\text{Nb}$  via the  $^{nat}\text{Zr}(p,X)^{95g}\text{Nb}$  nuclear process.

**Fig.7.** Independent cross sections for the formation of  $^{92m}\text{Nb}$  via the  $^{nat}\text{Zr}(p,xn)^{92m}\text{Nb}$  nuclear process.

**Fig.8.** Independent cross sections for the formation of  $^{91m}\text{Nb}$  via the  $^{nat}\text{Zr}(p,xn)^{91m}\text{Nb}$  nuclear process.

**Fig.9.** Cumulative cross sections for the formation of  $^{90(m+g)}\text{Nb}$  via the  $^{nat}\text{Zr}(p,xn)^{90(m+g)}\text{Nb}$  nuclear process.

**Fig.10.** Independent cross sections for the formation of  $^{89m}\text{Nb}$  via the  $^{nat}\text{Zr}(p,xn)^{89m}\text{Nb}$  nuclear process.

**Fig.11.** Independent cross sections for the formation of  $^{89g}\text{Nb}$  via the  $^{nat}\text{Zr}(p,xn)^{89g}\text{Nb}$  nuclear process.

**Fig.12.** Cumulative cross sections for the formation of  $^{95}\text{Zr}$  via the  $^{nat}\text{Zr}(p,X)^{95}\text{Zr}$  nuclear process.

**Fig.13.** Cumulative cross sections for the formation of  $^{89(0.94m+g)}\text{Zr}$  via the  $^{nat}\text{Zr}(p,X)^{89(0.94m+g)}\text{Zr}$  nuclear process.

**Fig.14.** Cumulative cross sections for the formation of  $^{88}\text{Zr}$  via the  $^{nat}\text{Zr}(p,X)^{88}\text{Zr}$  nuclear process.

**Fig.15.** Cumulative cross sections for the formation  $^{87(m+g)}\text{Zr}$  via the  $^{\text{nat}}\text{Zr}(p,X)^{87(m+g)}\text{Zr}$  nuclear process.

**Fig.16.** Cumulative cross sections for the formation  $^{86}\text{Zr}$  via the  $^{\text{nat}}\text{Zr}(p,X)^{86}\text{Zr}$  nuclear process.

**Fig.17.** Independent cross sections for the formation of  $^{91m}\text{Y}$  via the  $^{\text{nat}}\text{Zr}(p,X)^{91m}\text{Y}$  nuclear process.

**Fig.18.** Independent cross sections for the formation of  $^{90m}\text{Y}$  via the  $^{\text{nat}}\text{Zr}(p,X)^{90m}\text{Y}$  nuclear process

**Fig.19.** Independent cross sections for the formation of  $^{88}\text{Y}$  via the  $^{\text{nat}}\text{Zr}(p,X)^{88}\text{Y}$  nuclear process.

**Fig.20.** Cumulative cross sections for the formation of  $^{87m}\text{Y}$  via the  $^{\text{nat}}\text{Zr}(p,X)^{87m}\text{Y}$  nuclear process.

**Fig.21.** Cumulative cross sections for the formation of  $^{87(0.984m+g)}\text{Y}$  via the  $^{\text{nat}}\text{Zr}(p,X)^{87m}\text{Y}$  nuclear process.

**Fig.22.** Independent cross sections for the formation of  $^{86m}\text{Y}$  via the  $^{\text{nat}}\text{Zr}(p,X)^{86m}\text{Y}$  nuclear process.

**Fig.23.** Cumulative cross sections for the formation of  $^{86(0.99m+g)}\text{Y}$  via the  $^{\text{nat}}\text{Zr}(p,X)^{86(0.99m+g)}\text{Y}$  nuclear process.

**Fig.24.** Cumulative cross sections for the formation of  $^{85m}\text{Y}$  via the  $^{\text{nat}}\text{Zr}(p,X)^{85m}\text{Y}$  nuclear process.

**Fig.25.** Cumulative cross sections for the formation of  $^{85g}\text{Y}$  via the  $^{\text{nat}}\text{Zr}(p,X)^{85g}\text{Y}$  nuclear process.

**Fig.26.** Cumulative cross sections for the formation of  $^{86(0.87m+g)}\text{Sr}$  via the  $^{\text{nat}}\text{Zr}(p,X)^{86(0.87m+g)}\text{Sr}$  nuclear process.

Fig.1.

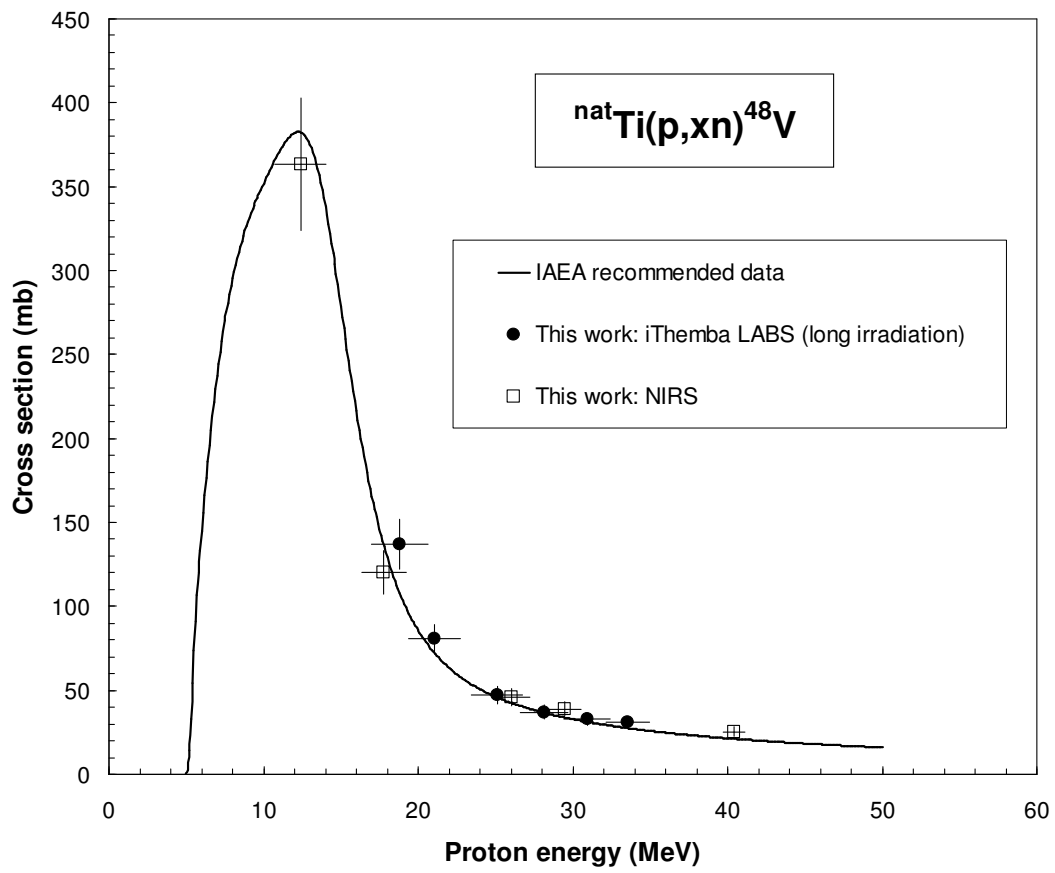


Fig.2.

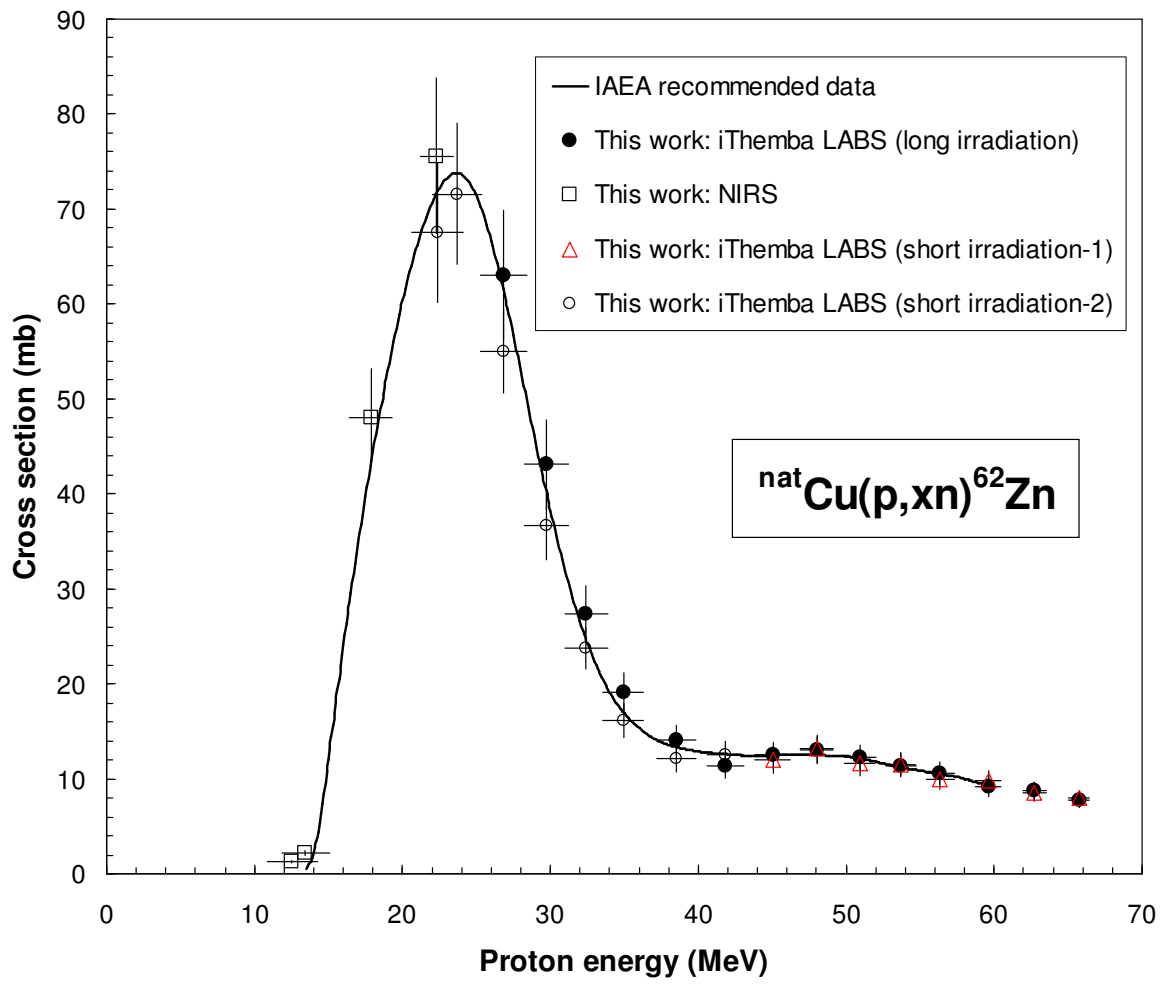


Fig.3.

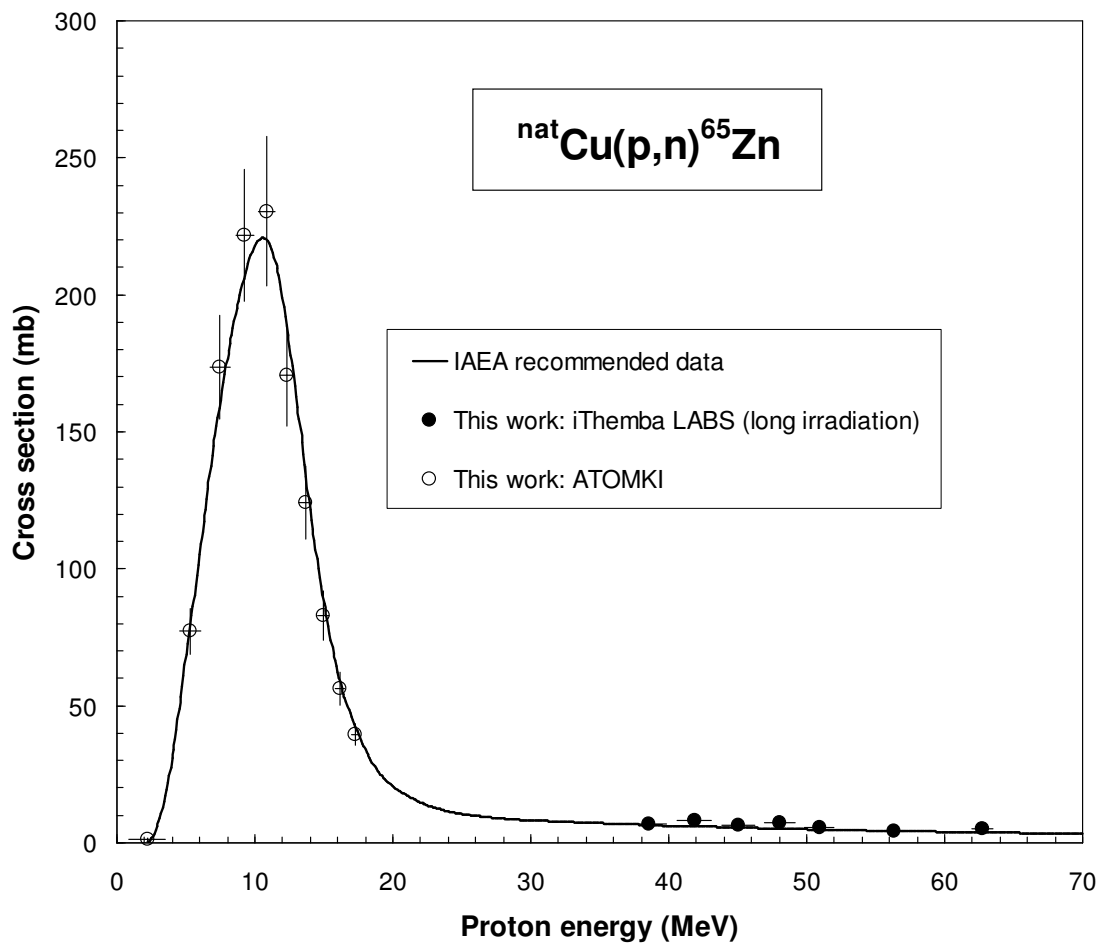


Fig.4.

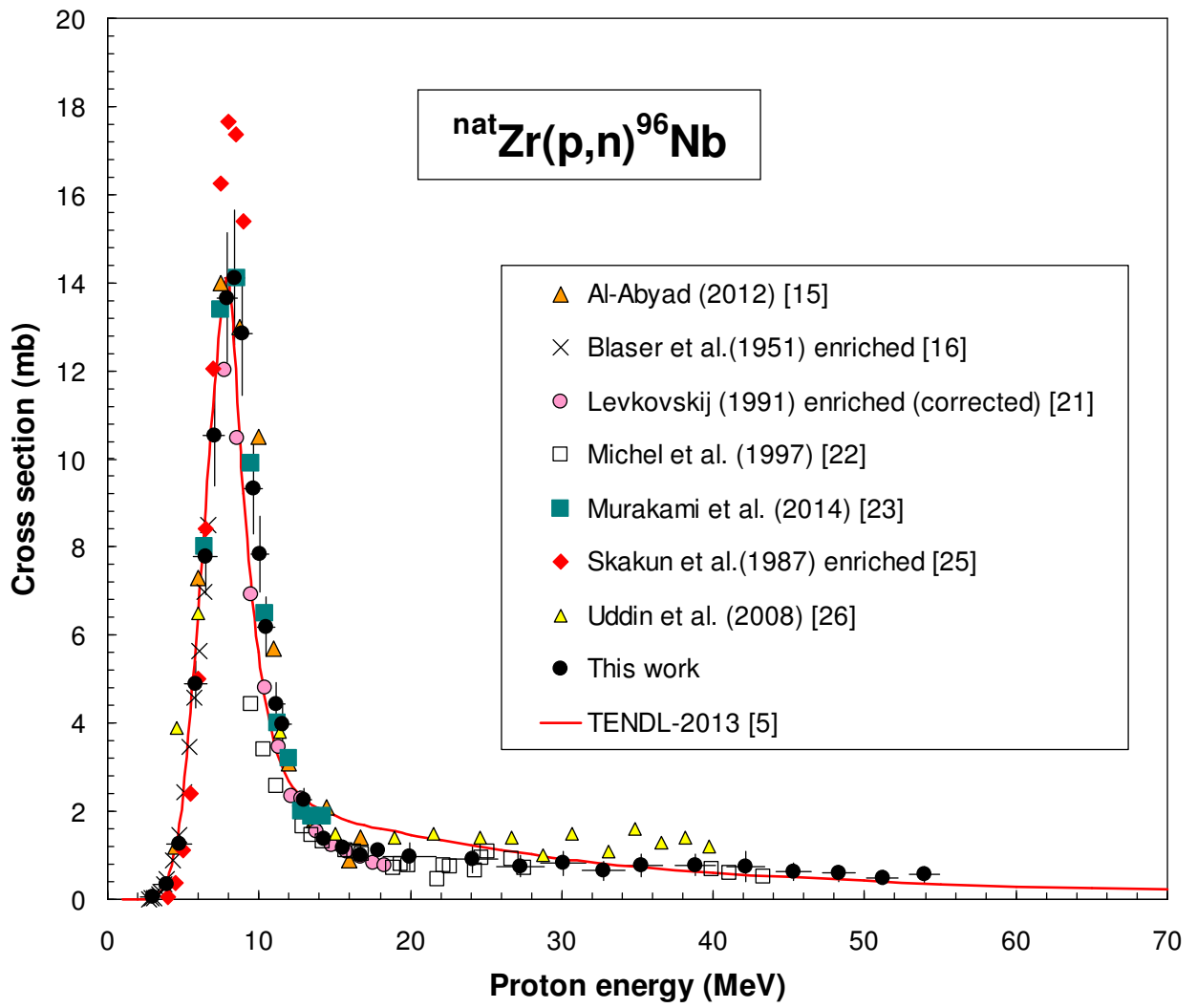


Fig.5.

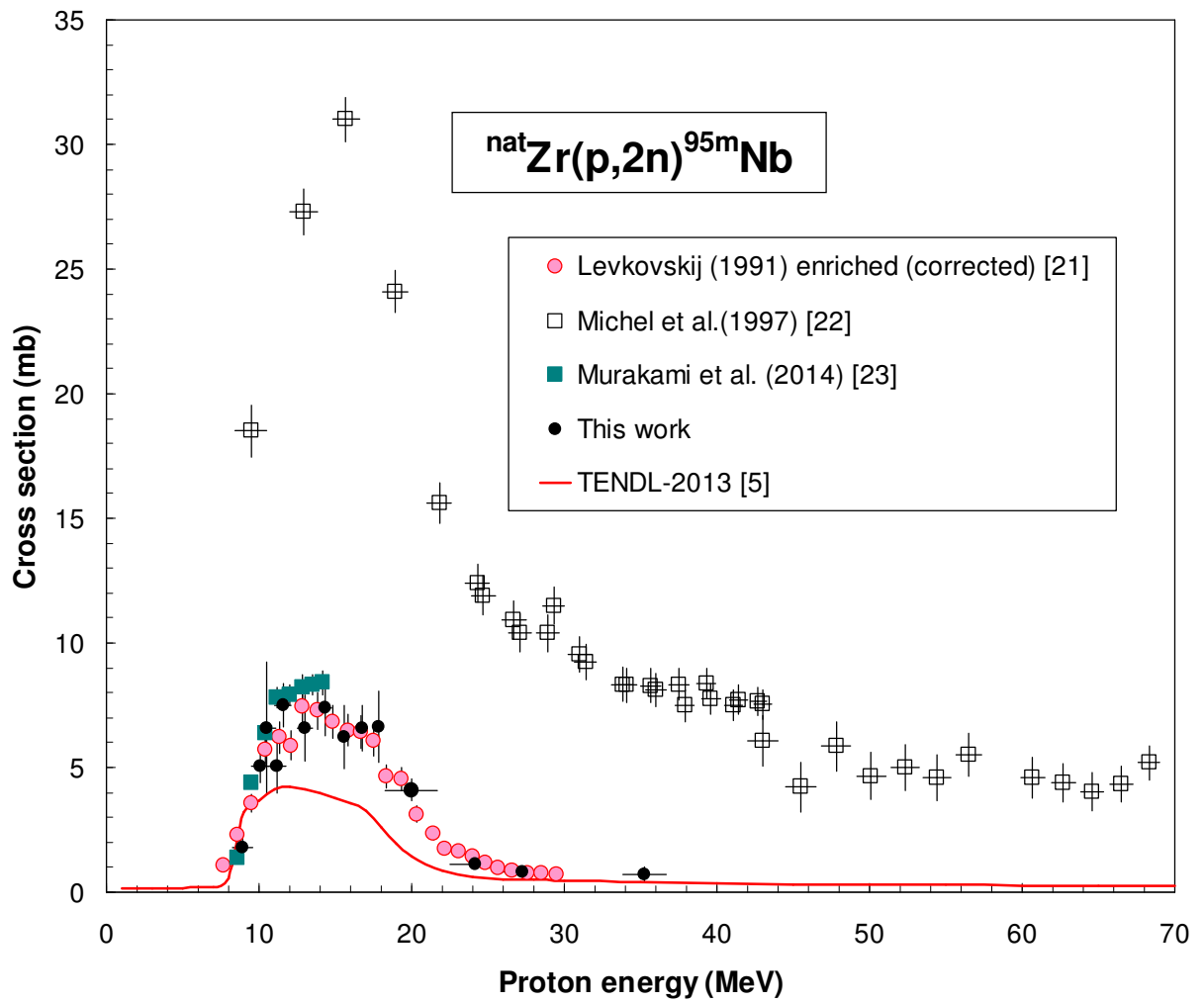


Fig.6

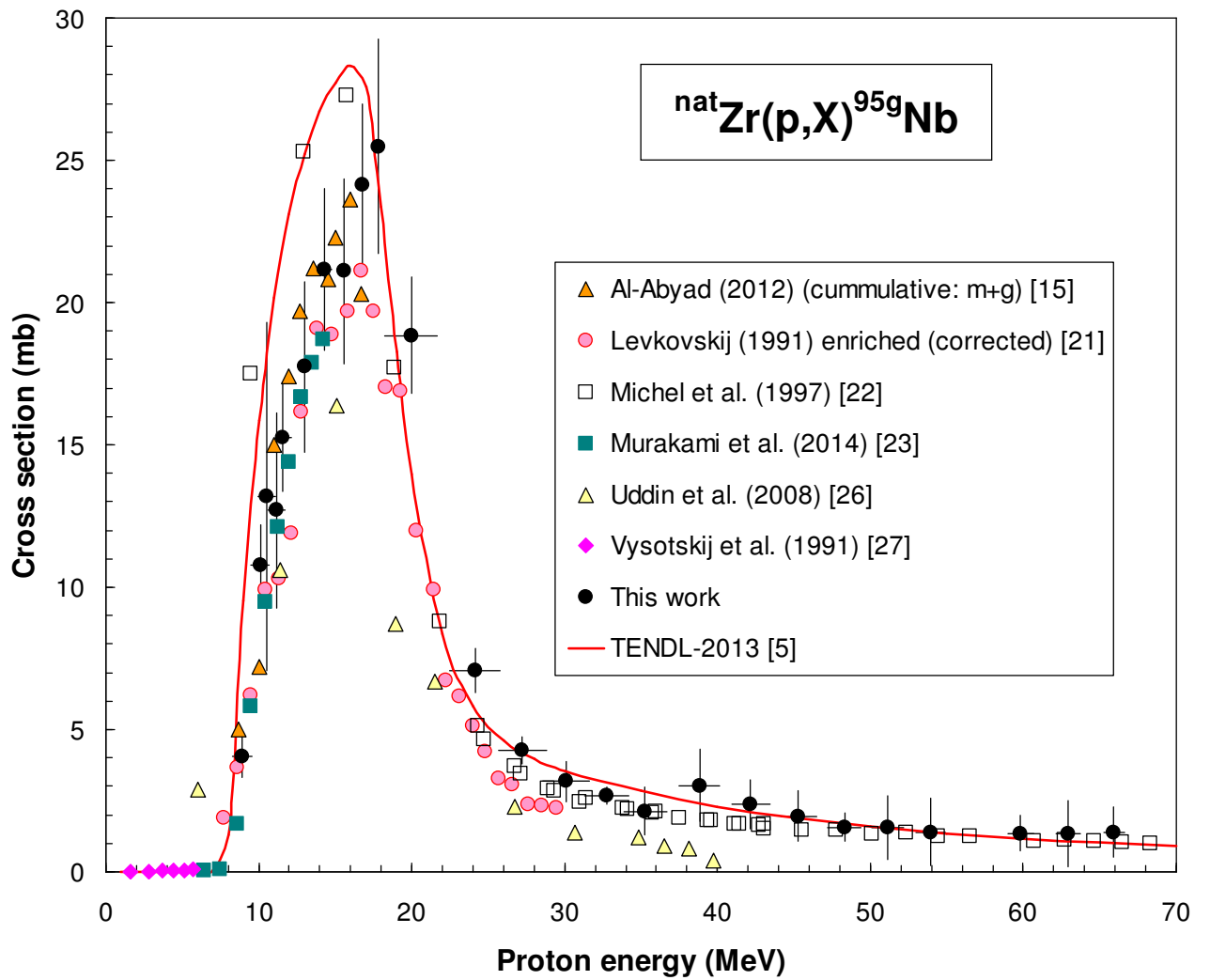


Fig.7

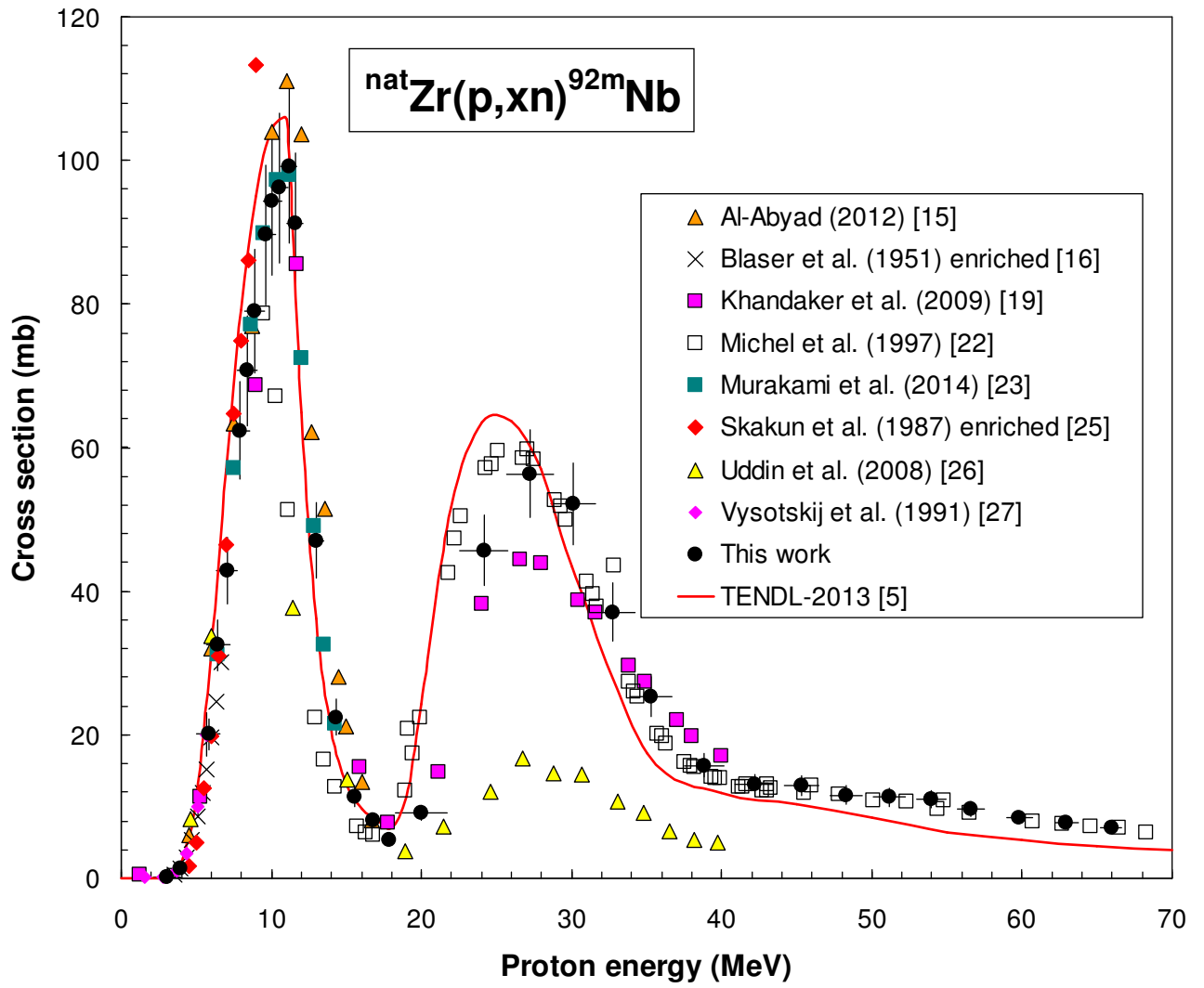


Fig.8

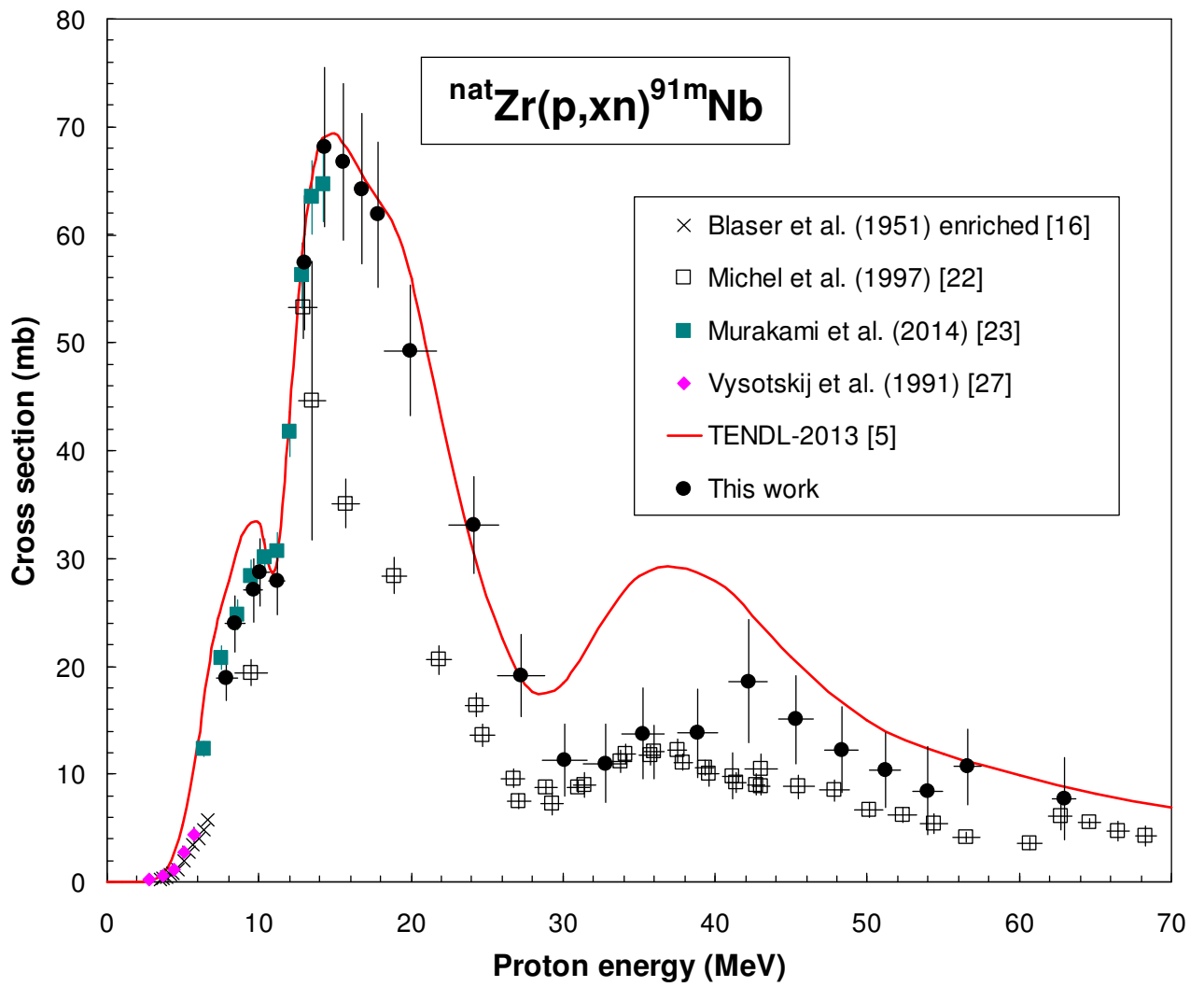


Fig.9

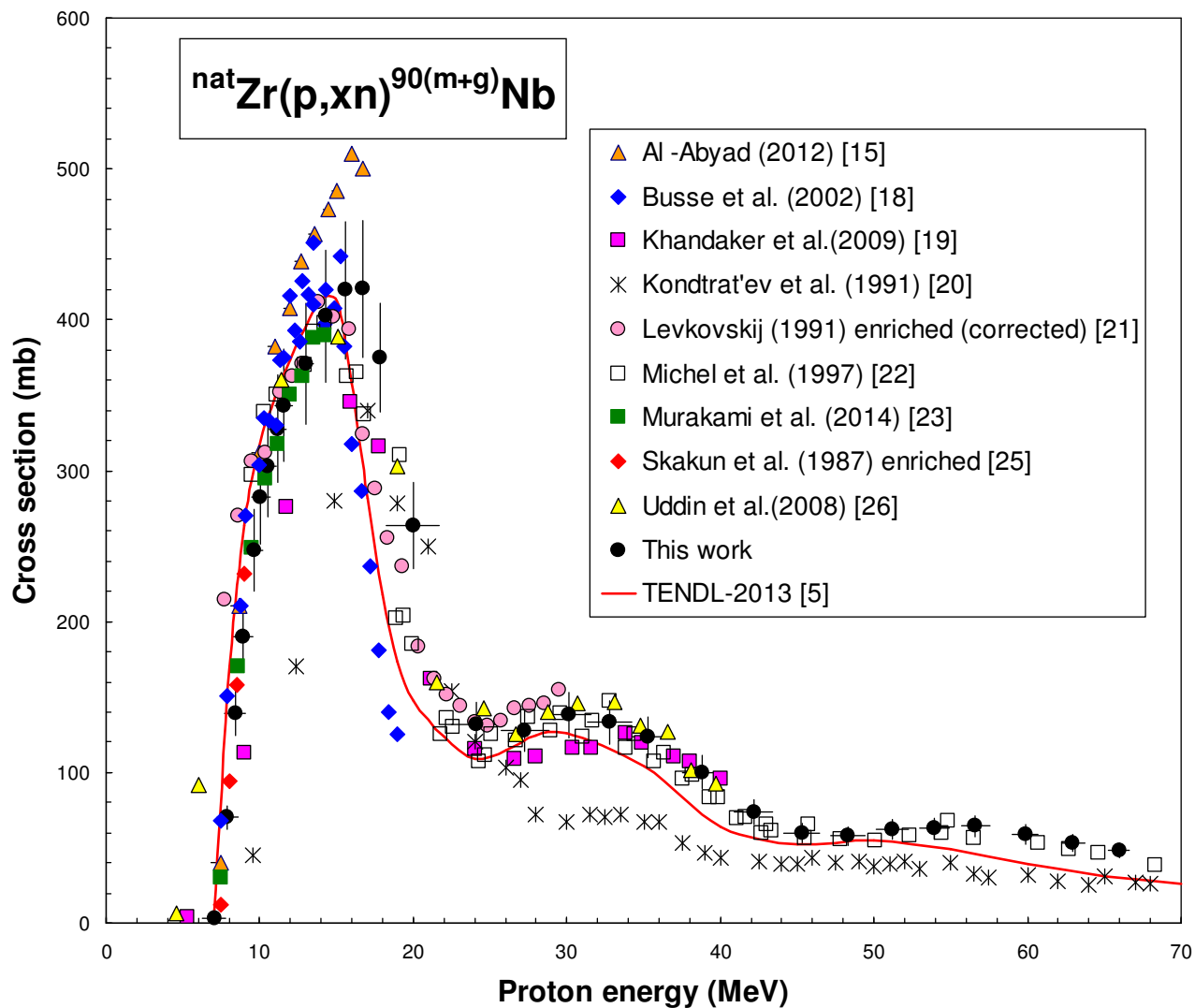


Fig.10

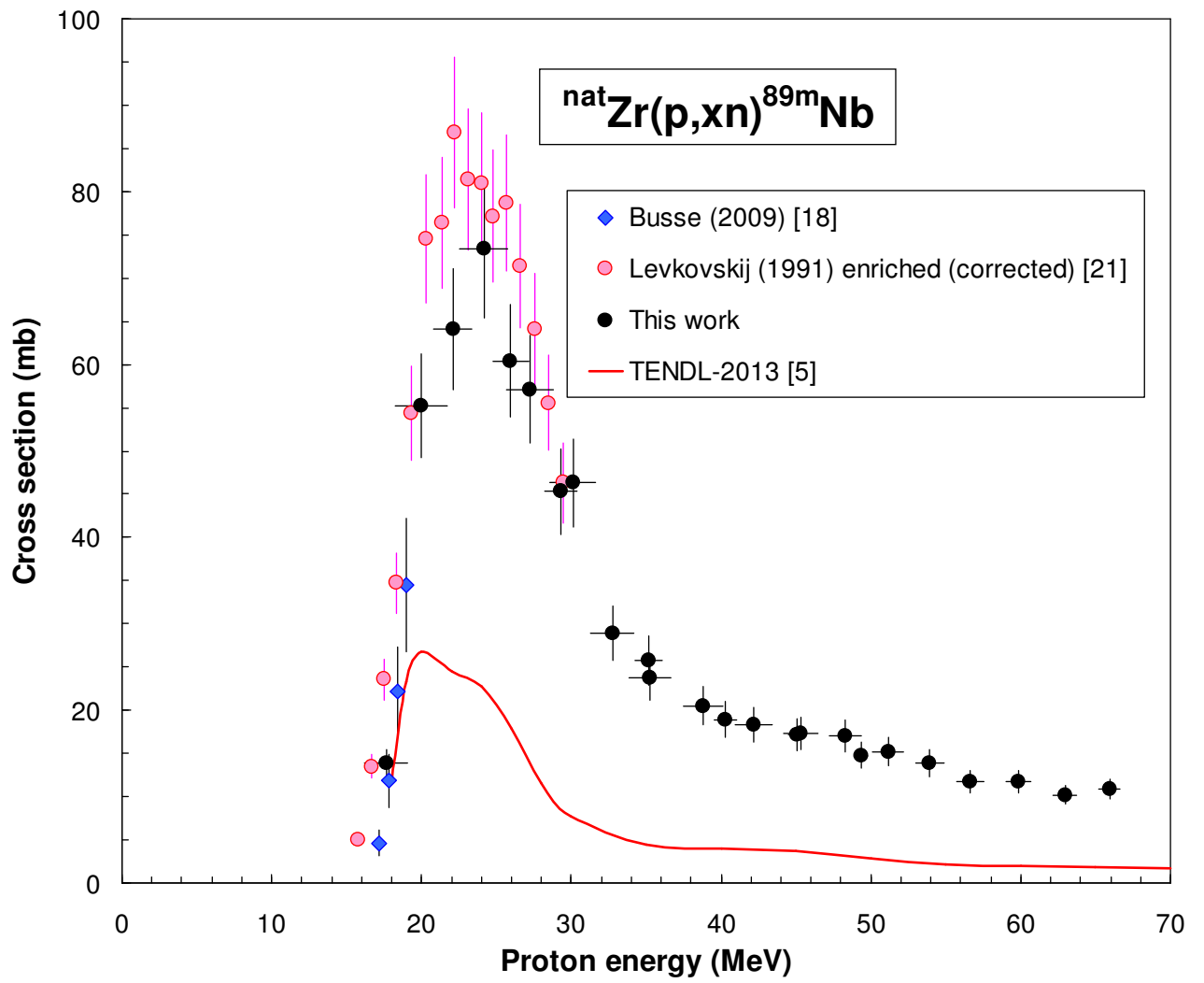


Fig.11

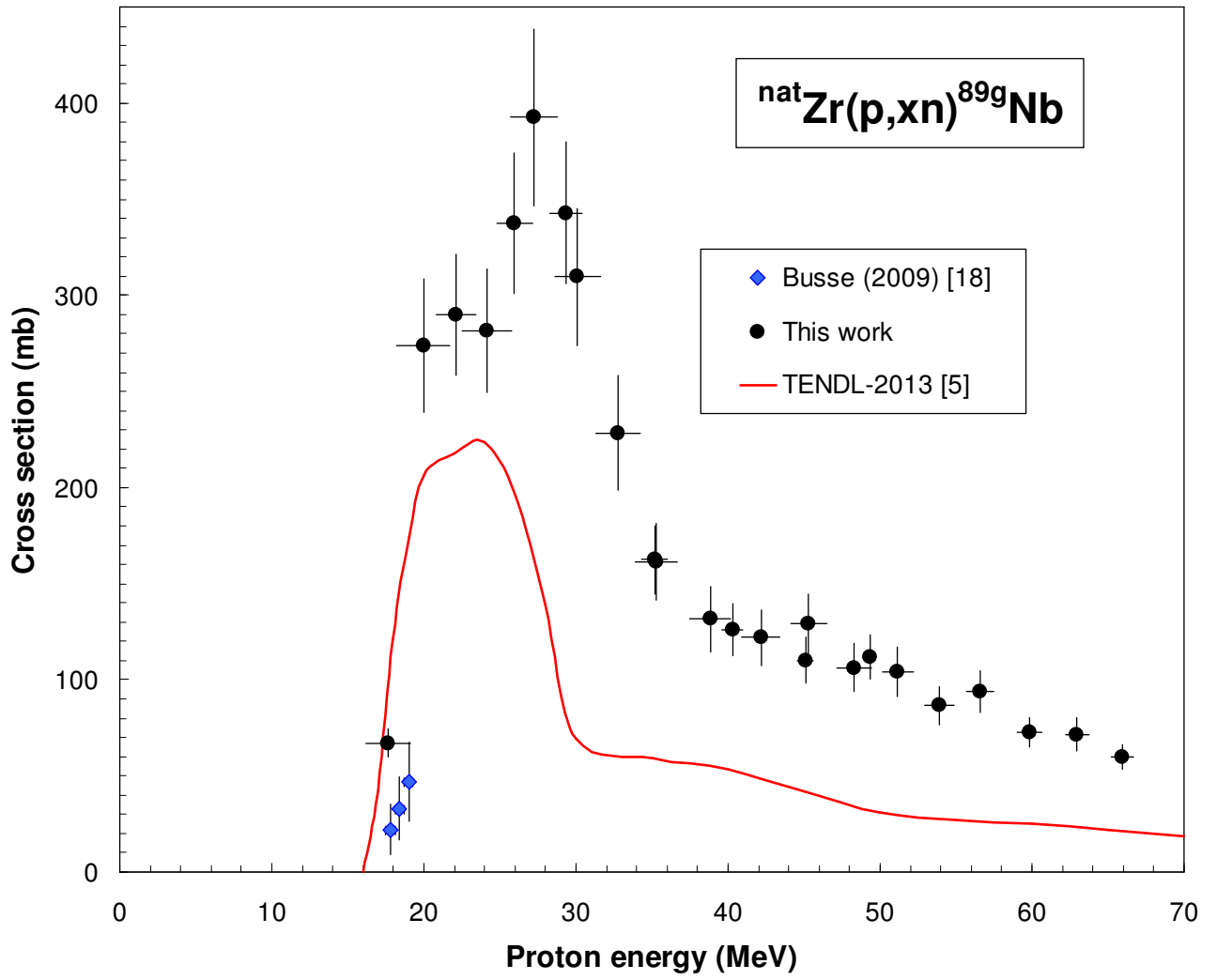


Fig.12

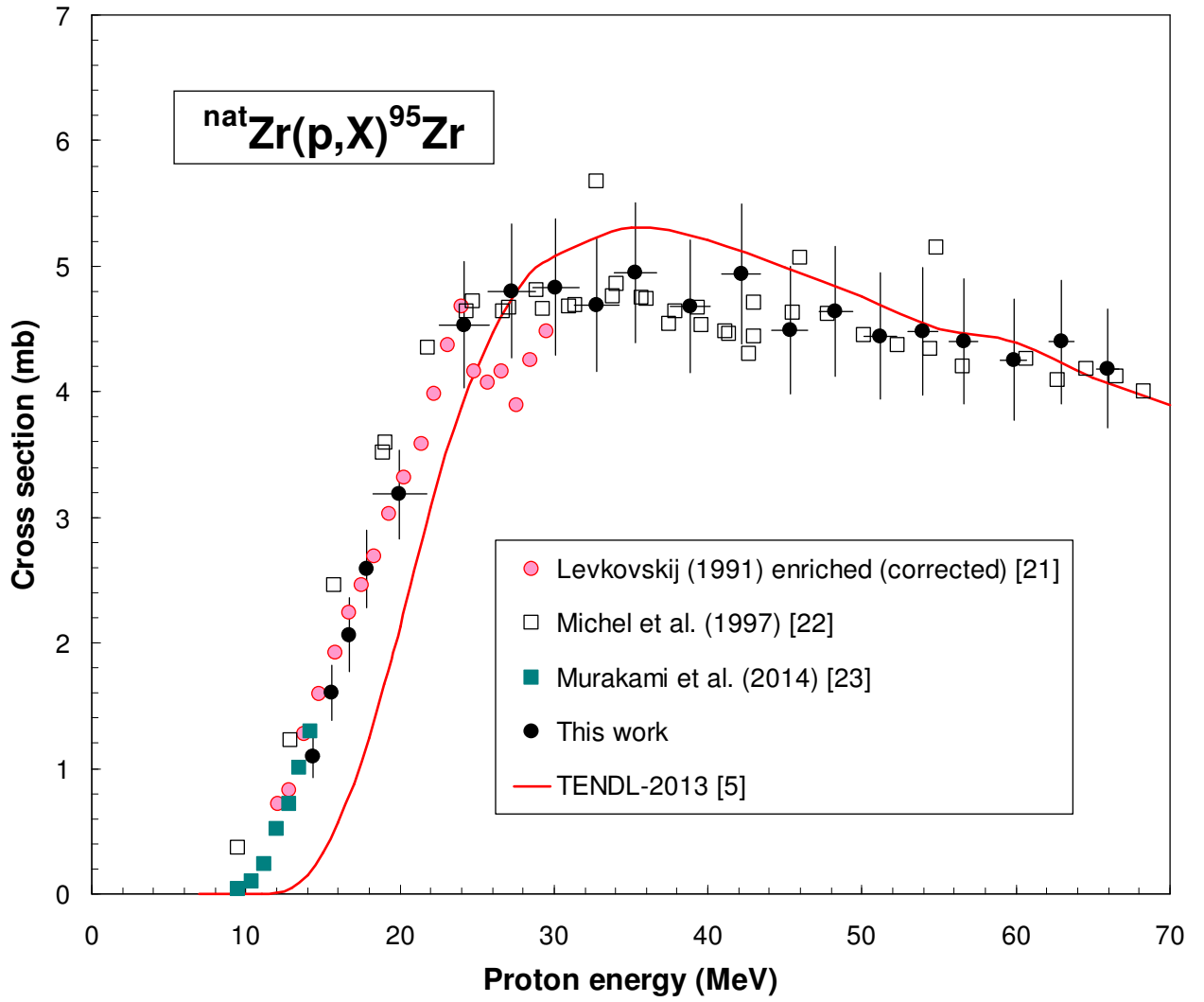


Fig.13

Fig.13

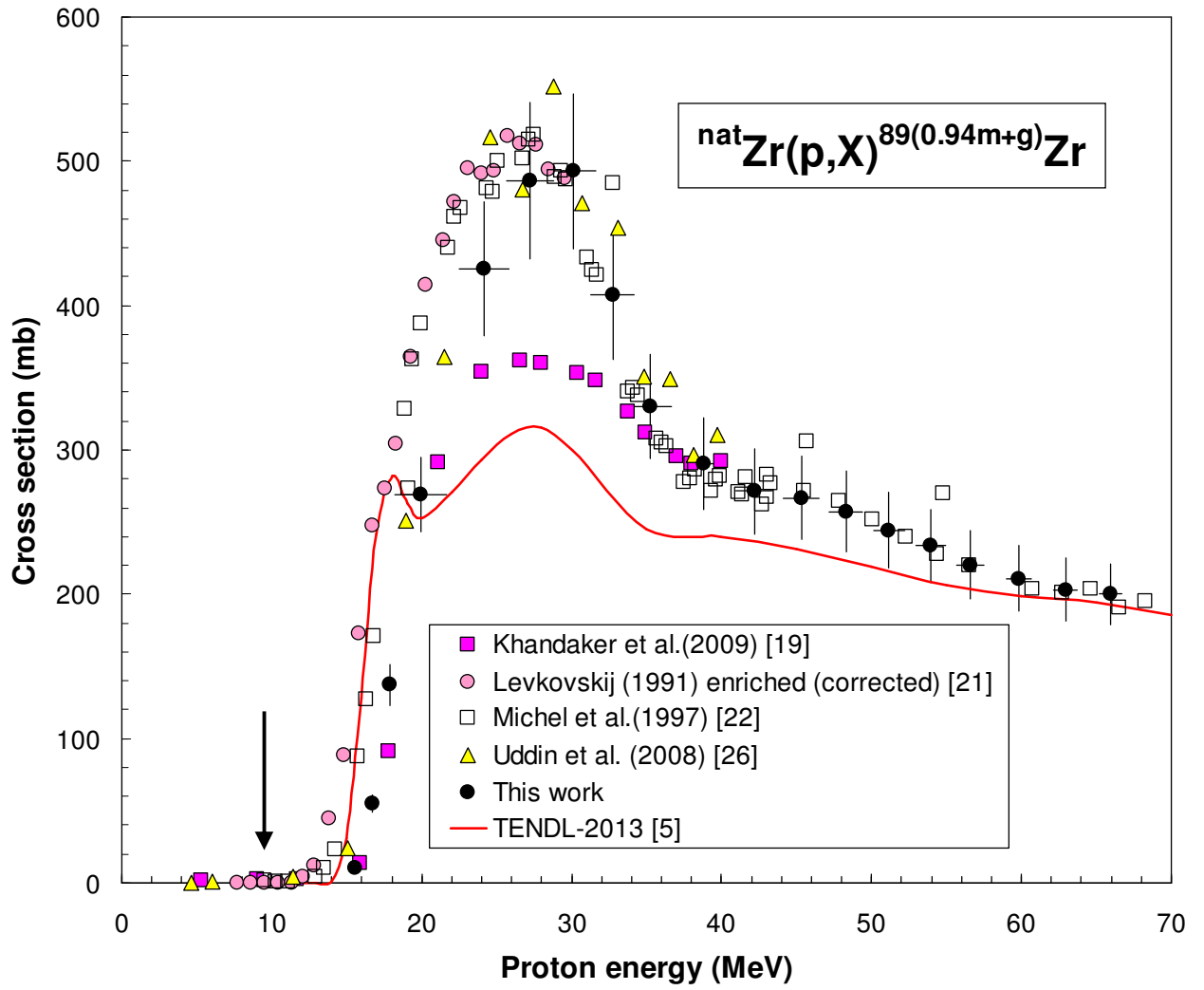


Fig.14

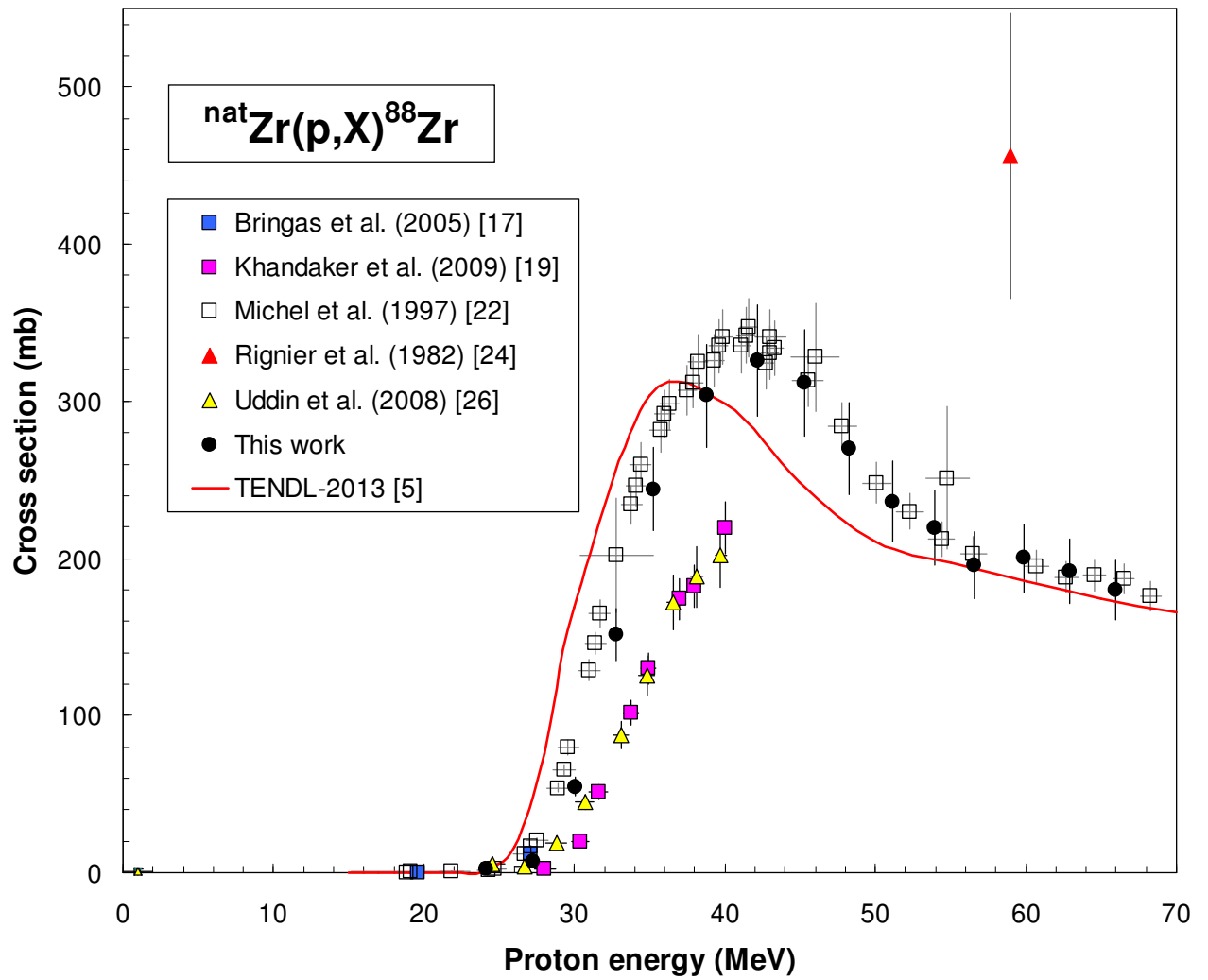


Fig.15

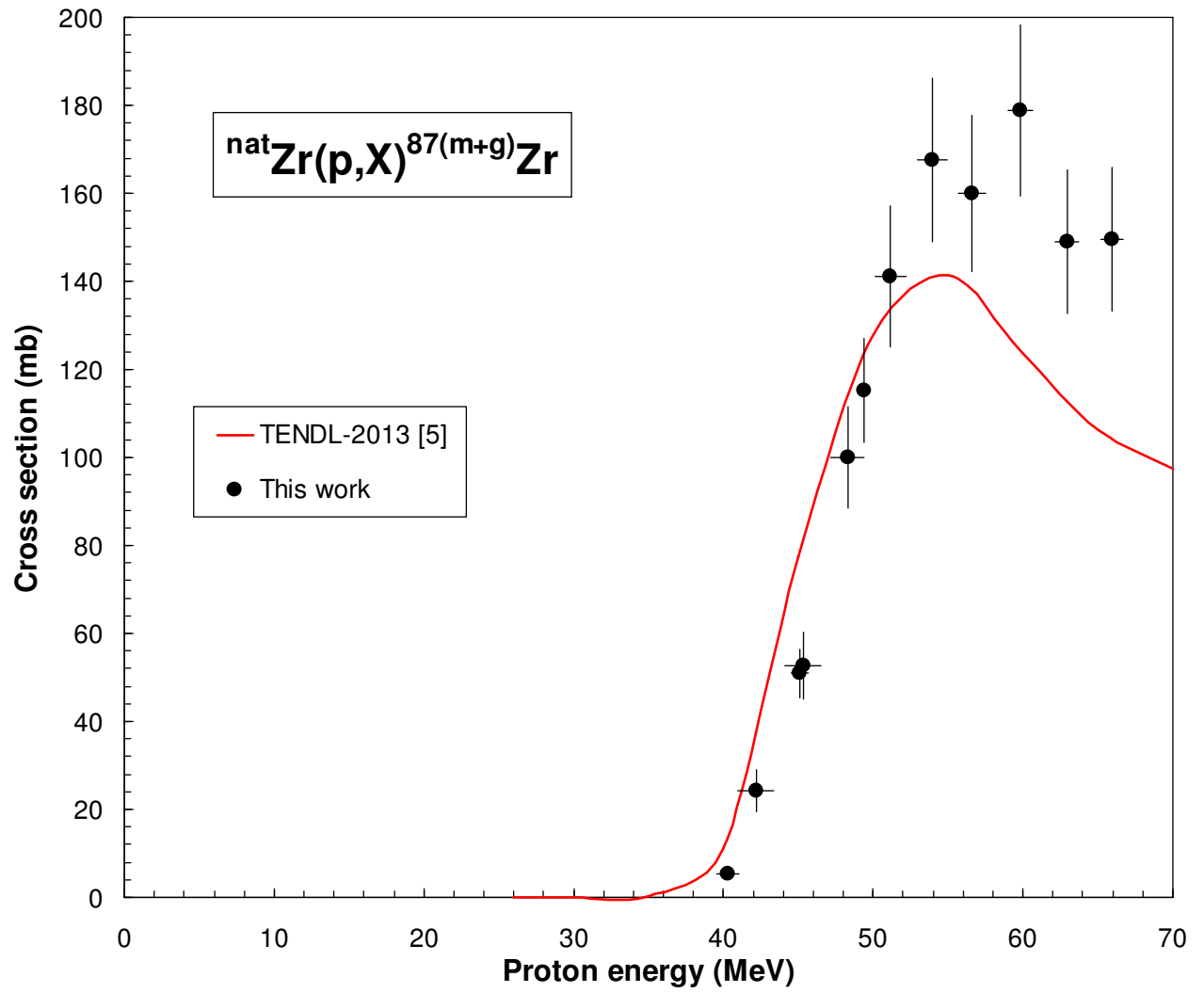


Fig.16

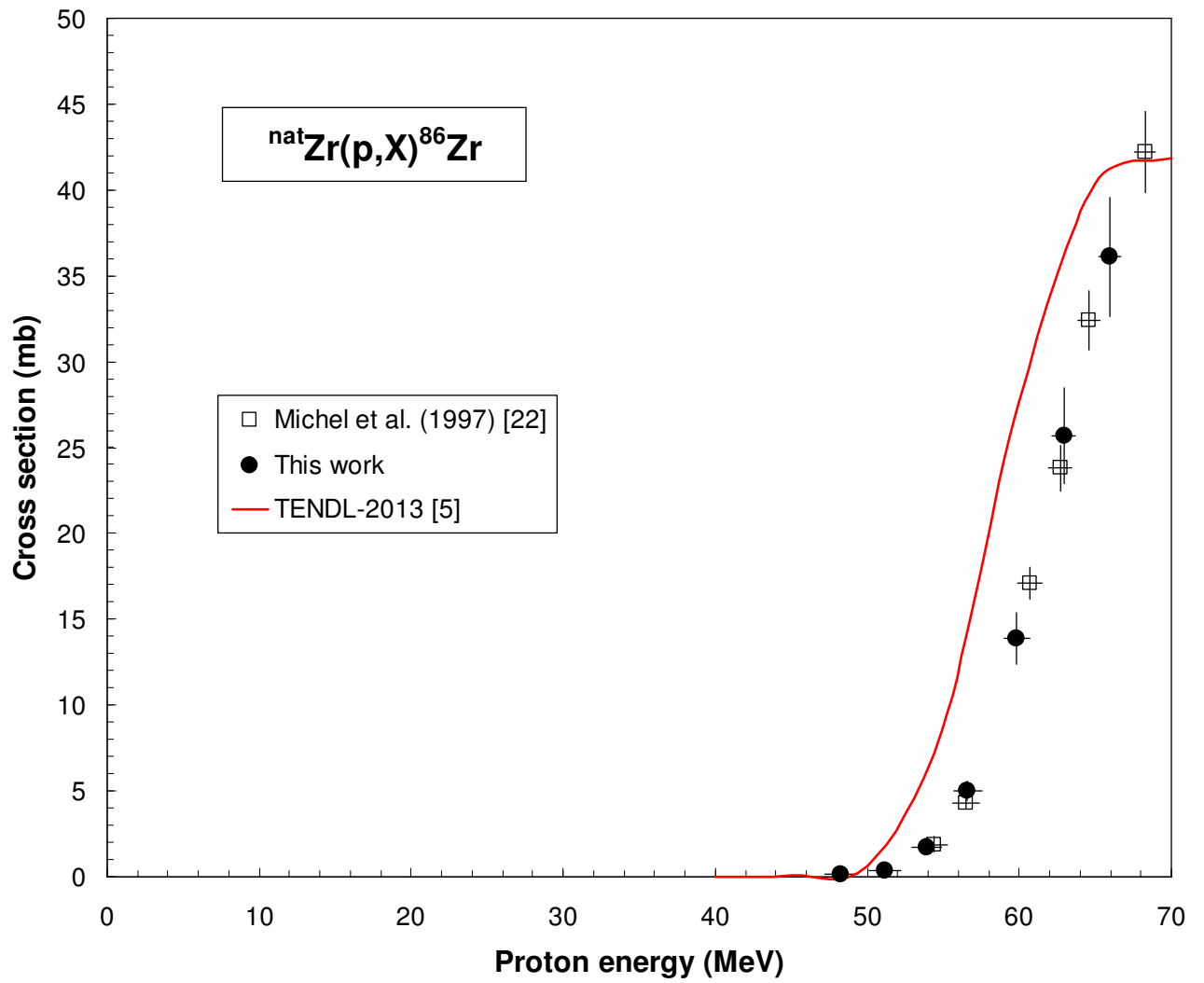


Fig.17

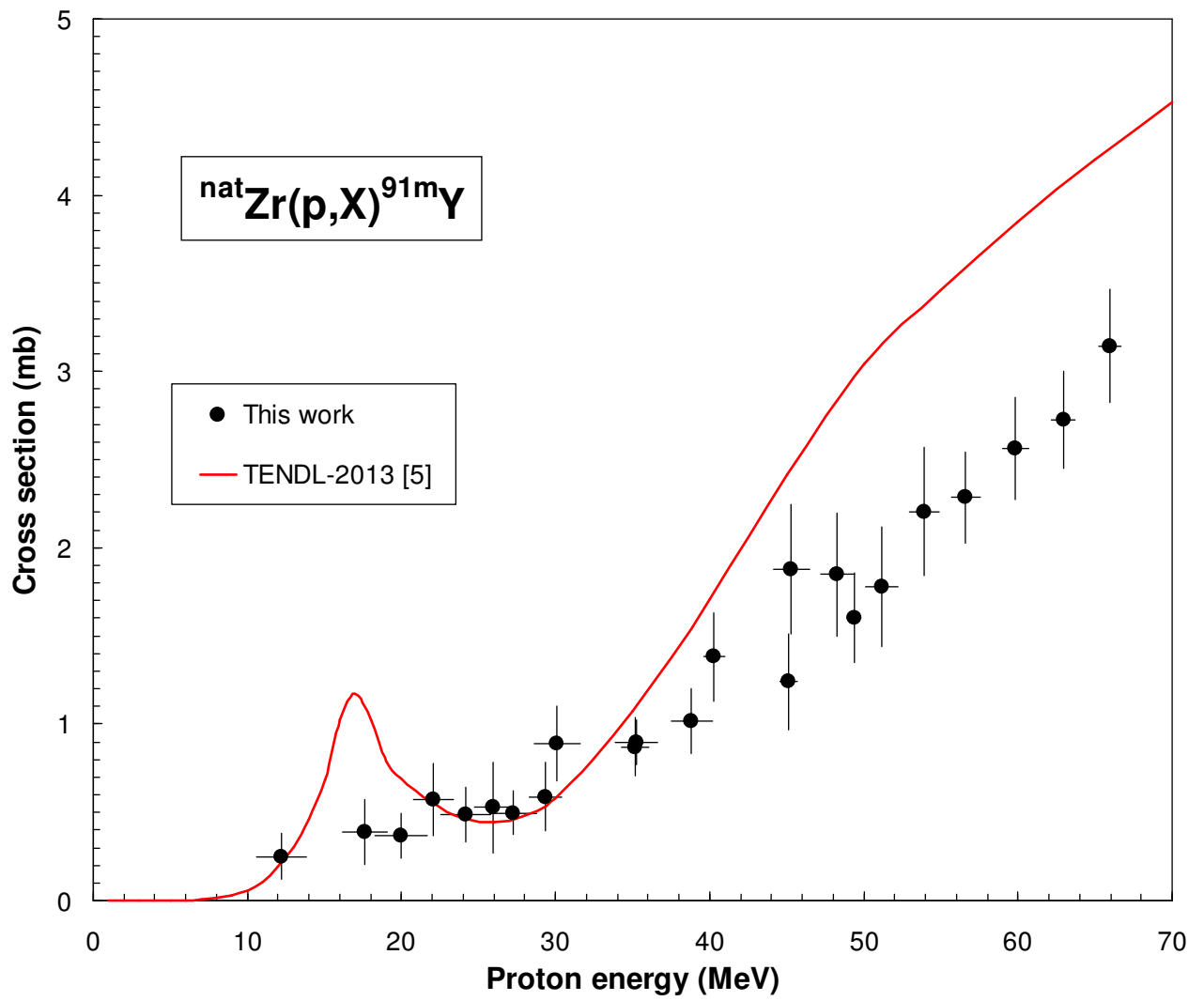


Fig.18

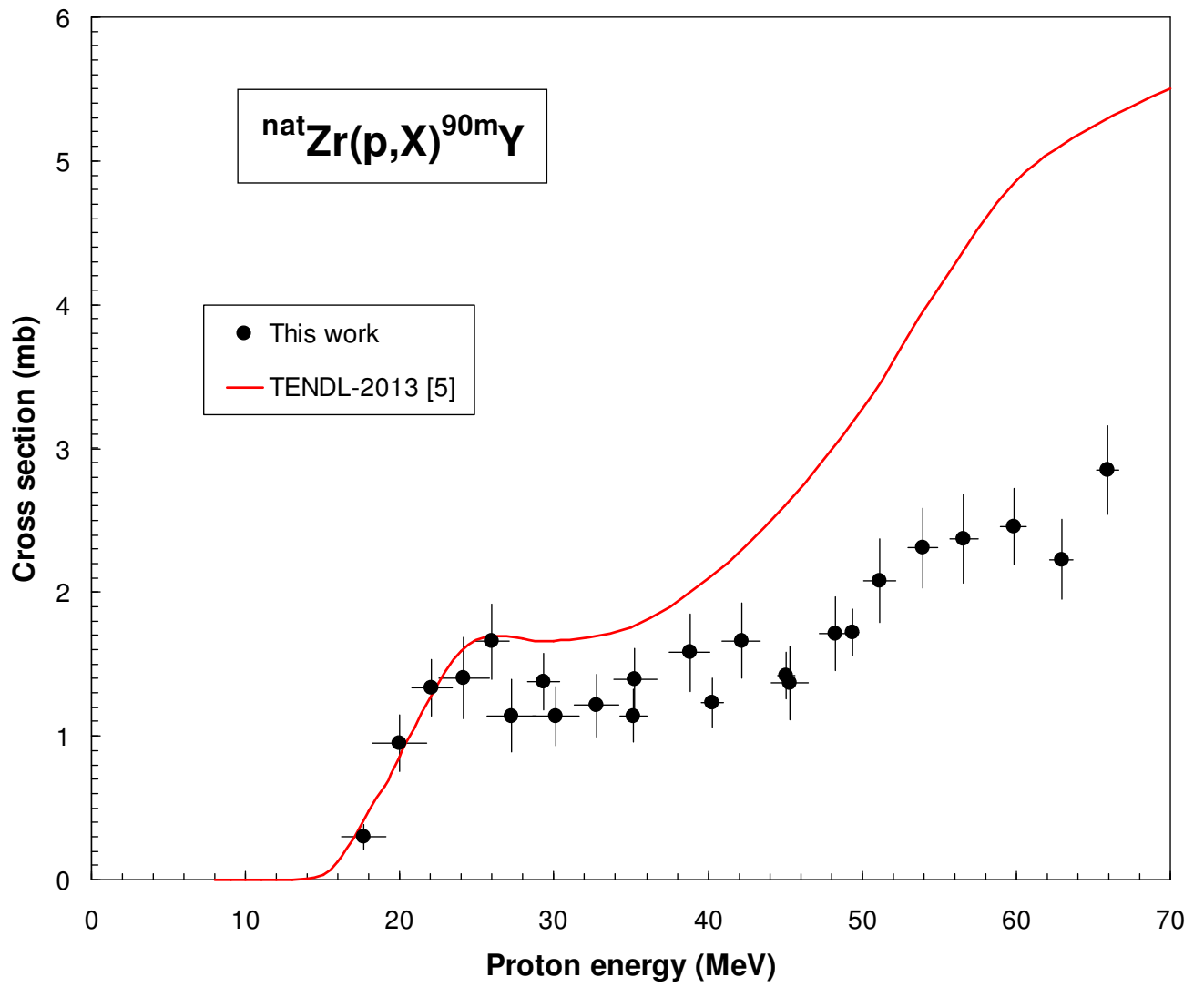


Fig.19

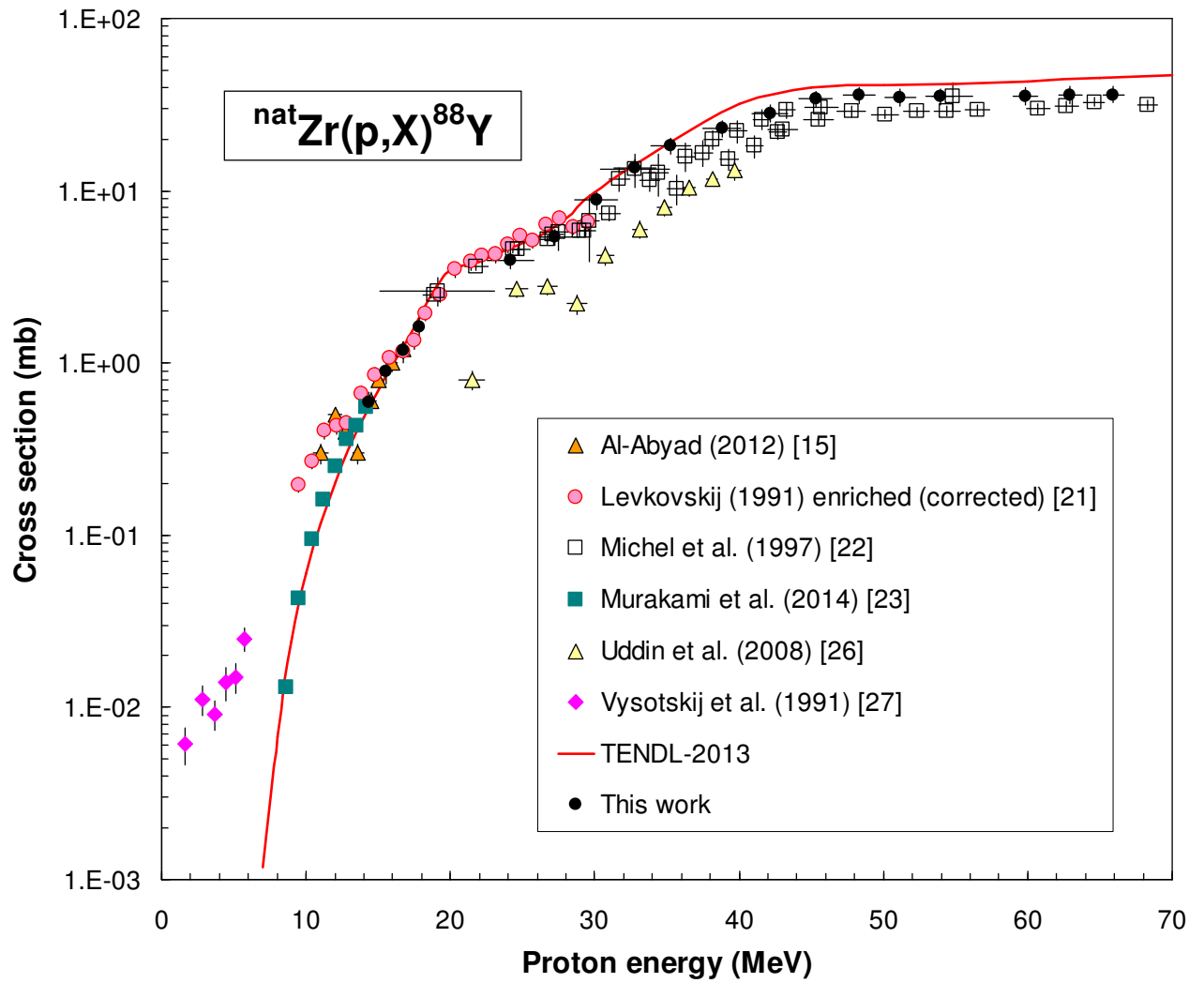


Fig.20

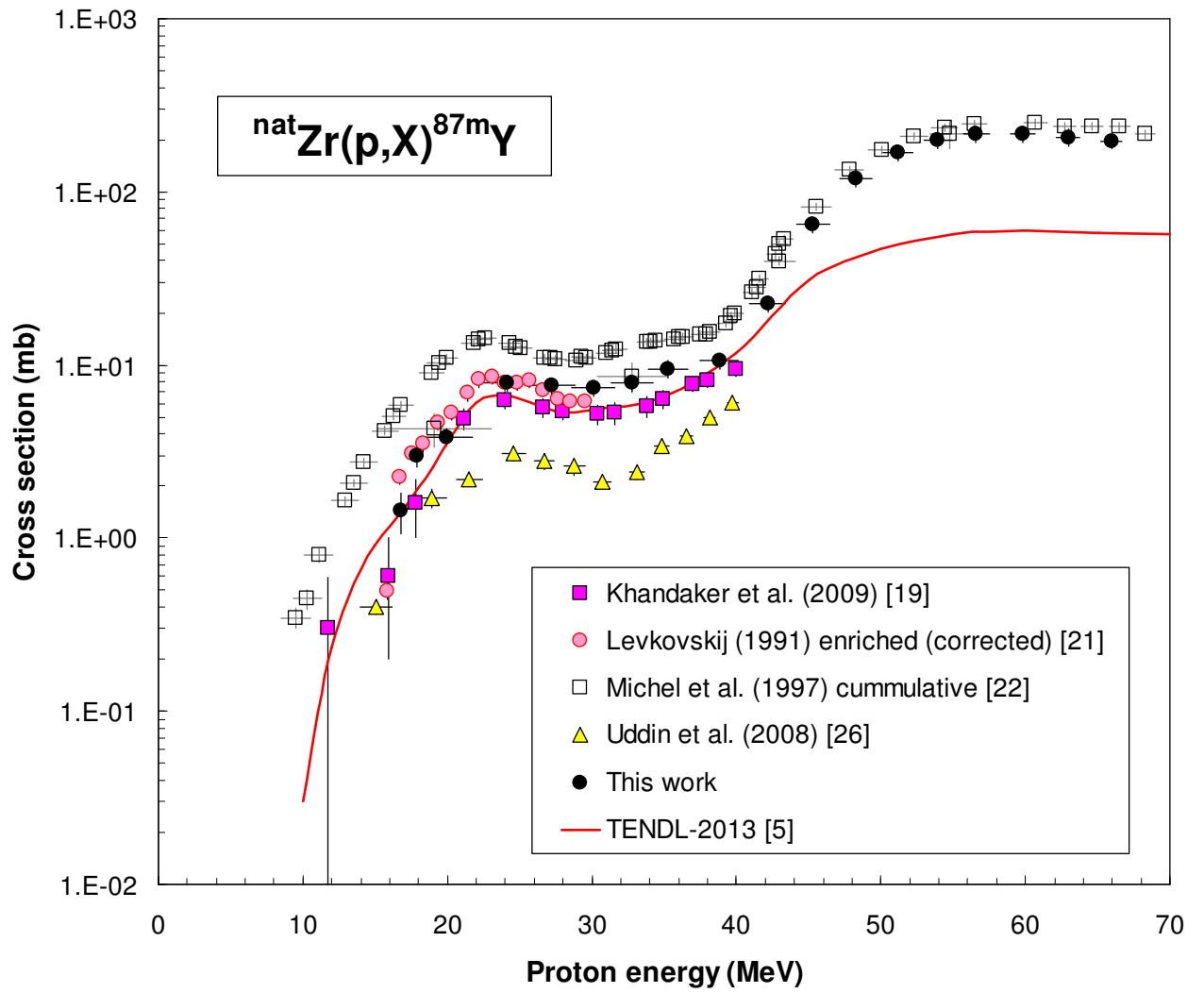


Fig.21

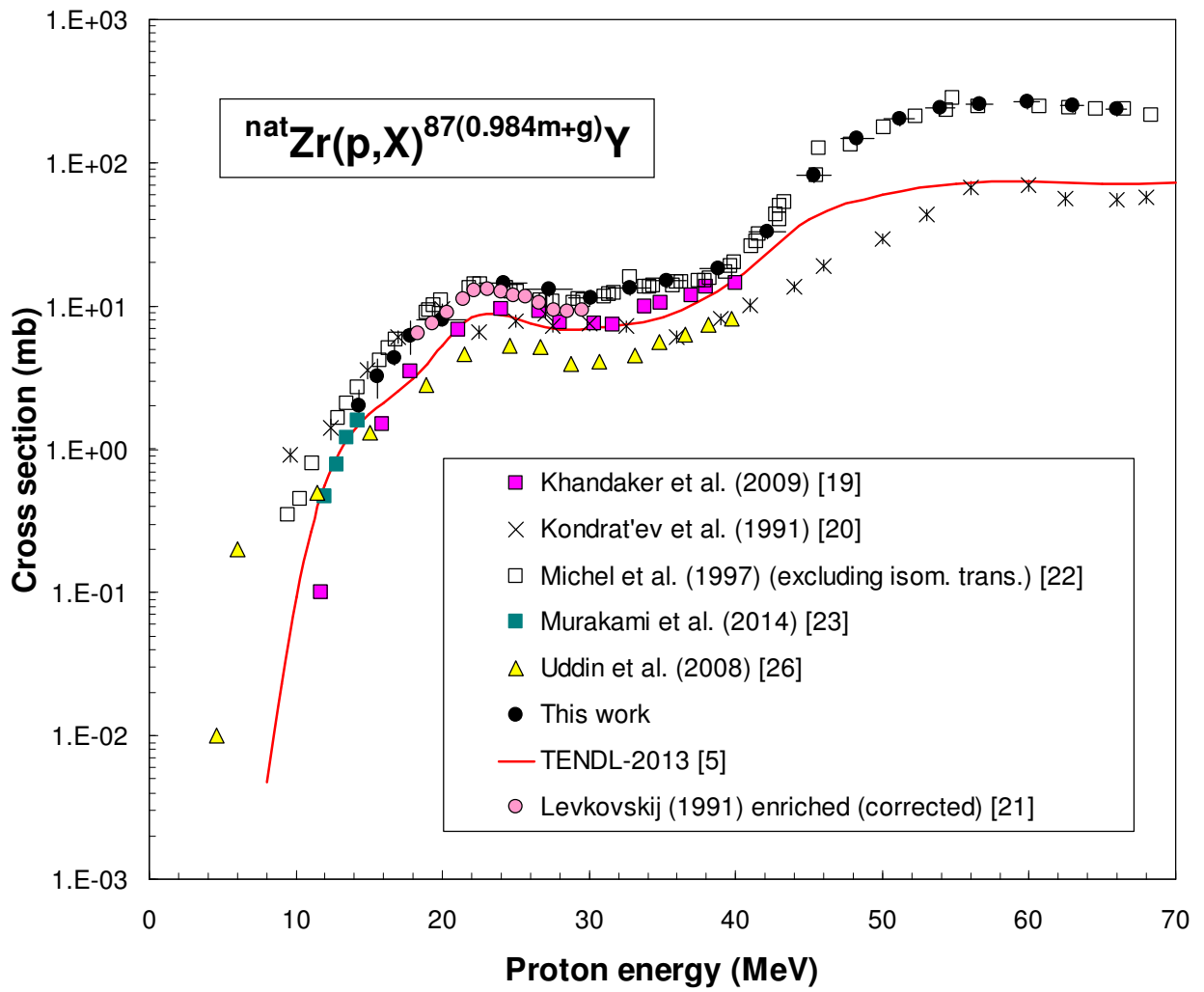


Fig.22

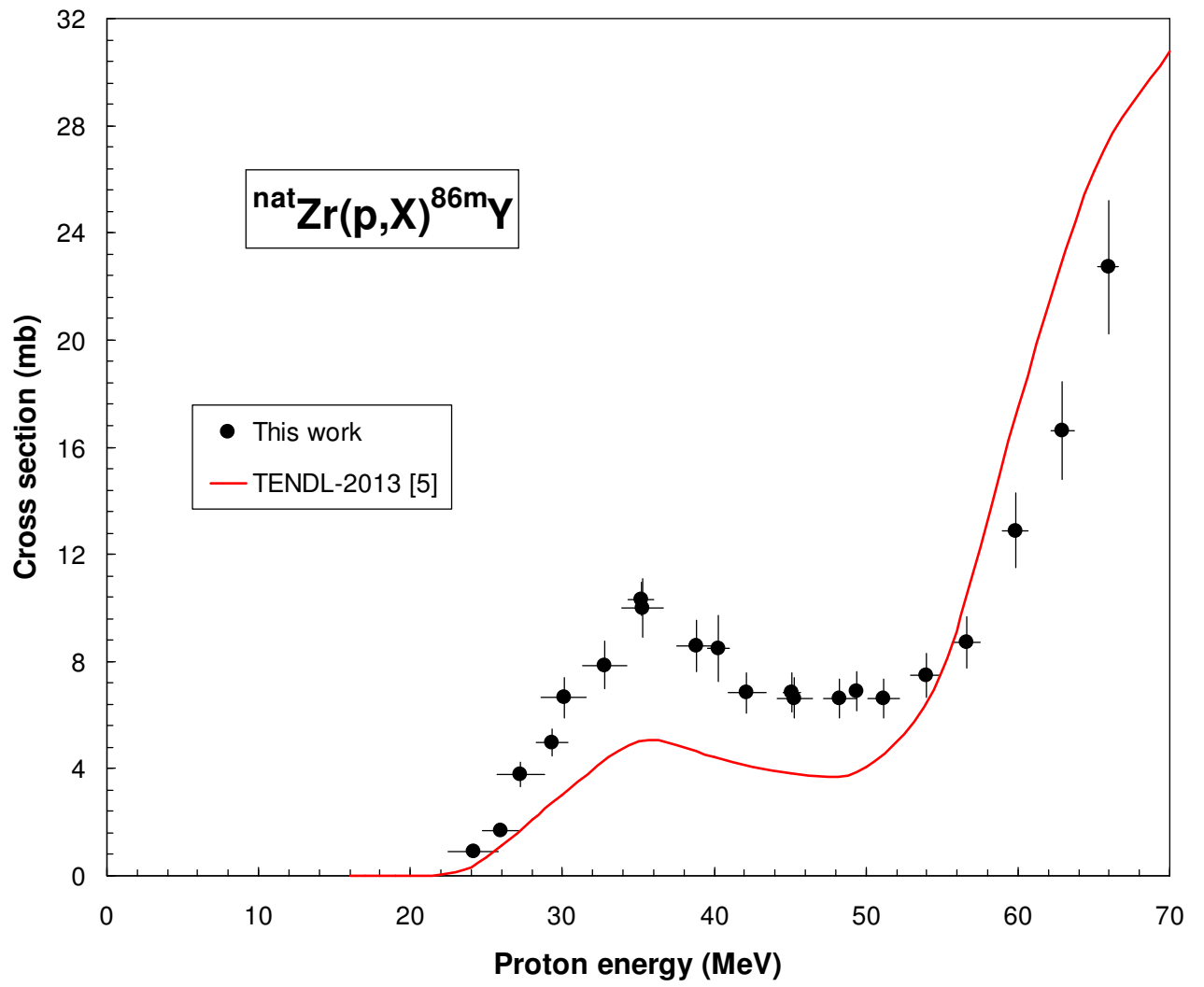


Fig.23

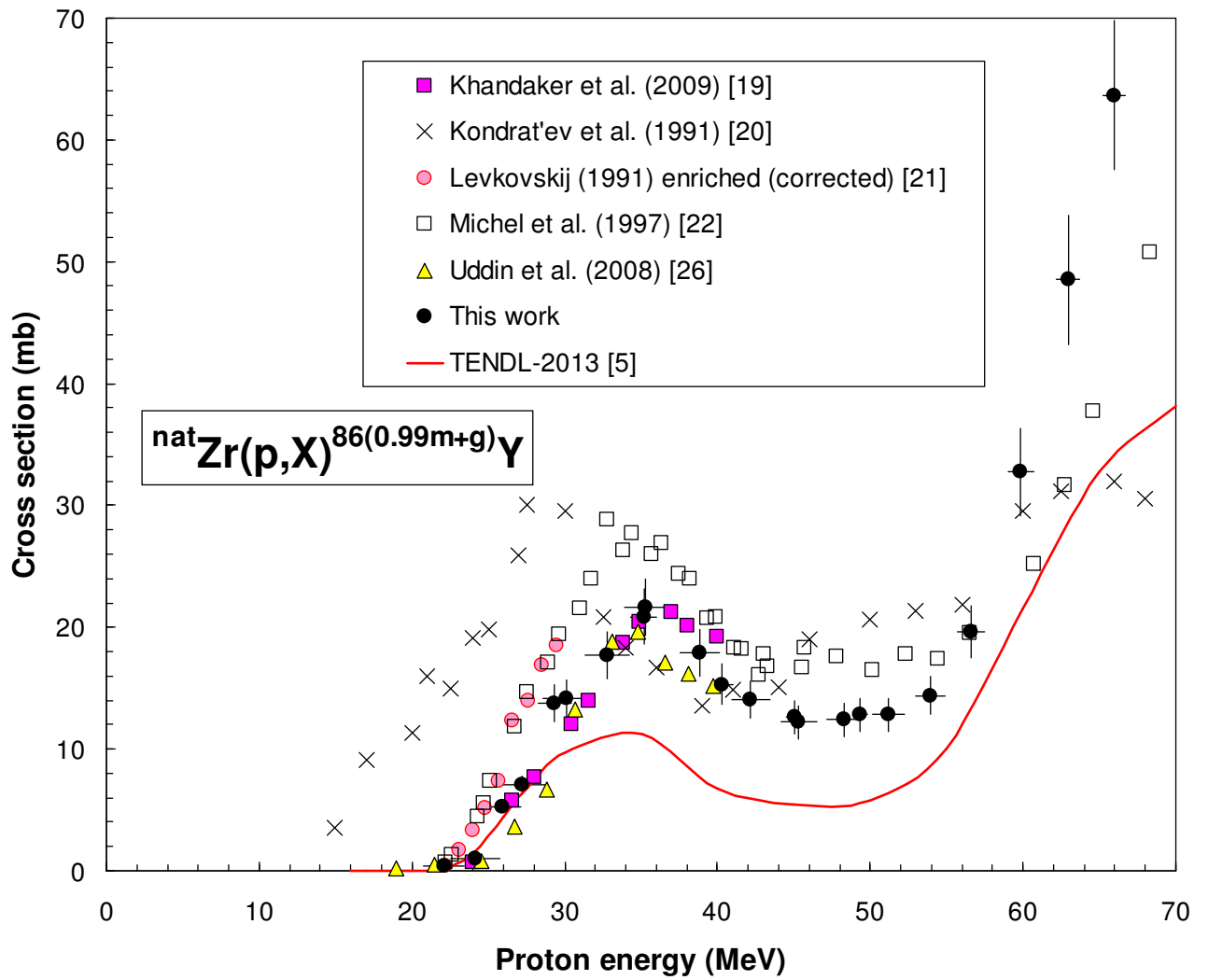


Fig.24

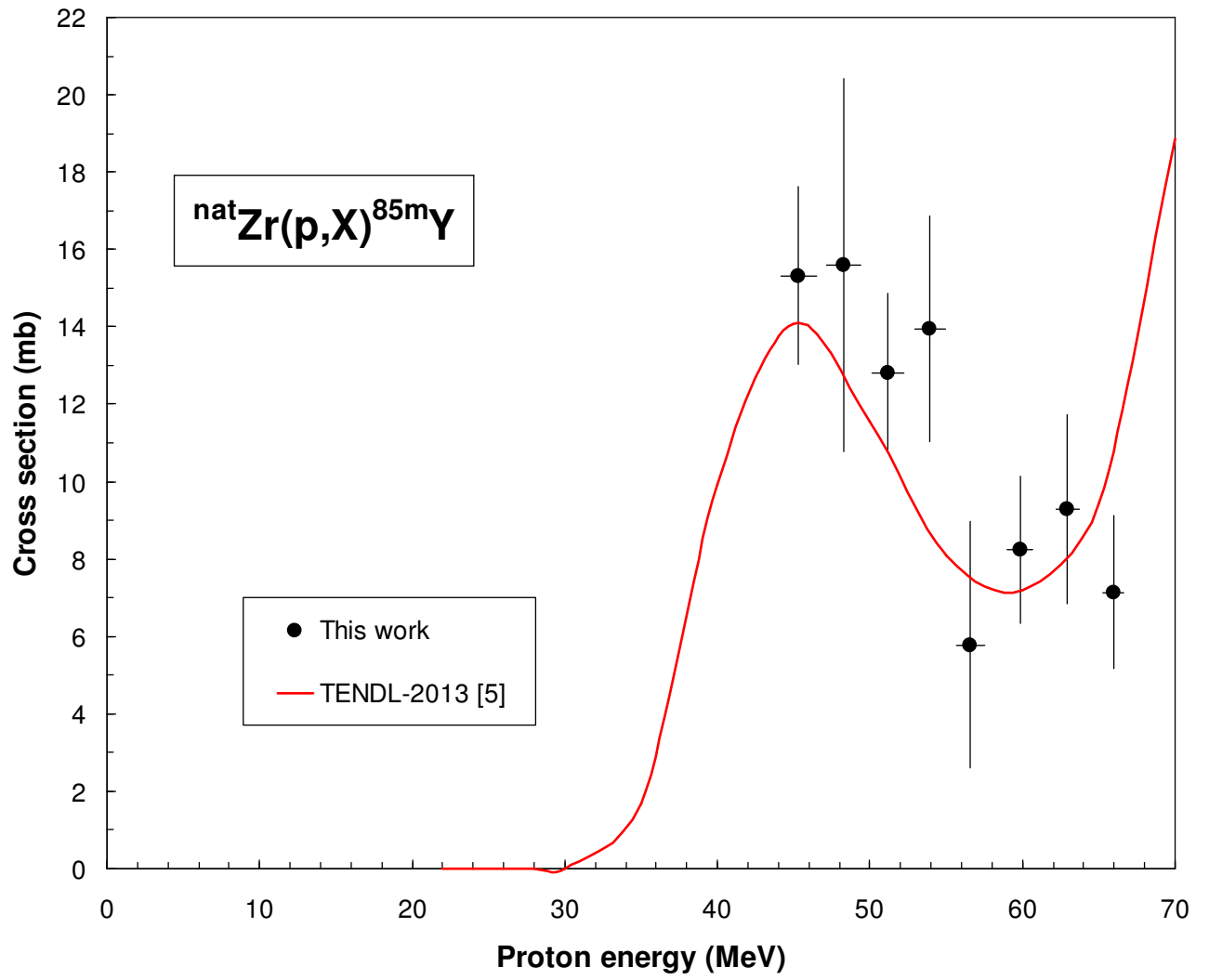


Fig.25

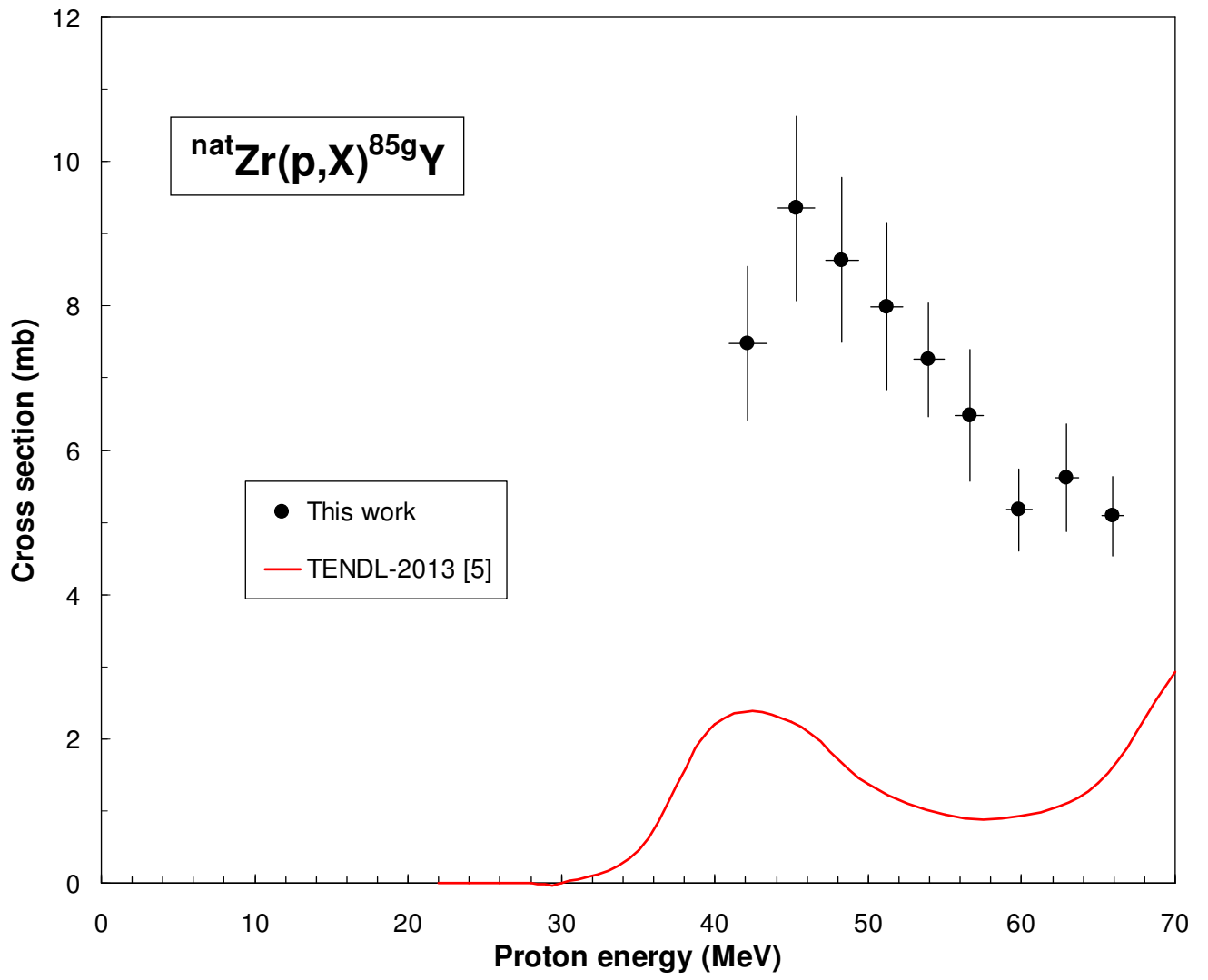
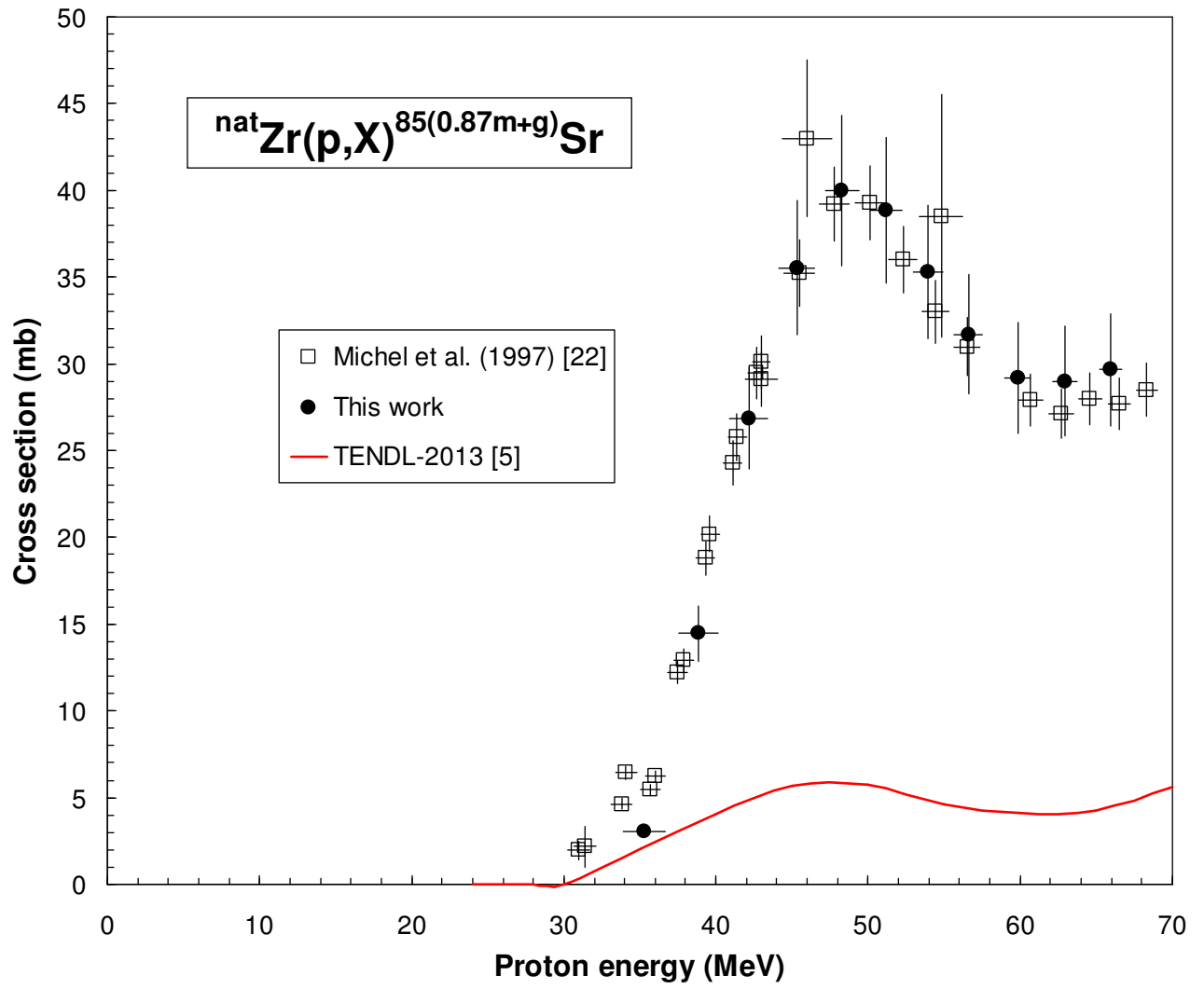


Fig.26



**Table 1.** Decay data of the investigated Nb, Zr, Y and Sr radionuclides produced via  $^{nat}\text{Zr}+\text{p}$  nuclear processes.

Isotope	Half-life	Energy <sup>a</sup> (MeV)	Branching ratio (%)	Contributing reactions <sup>b</sup>	Q-value <sup>c</sup> (MeV)
$^{96\text{g}}\text{Nb}$	23.35 h	460.04 568.87 778.22	26.62 58.00 96.45	$^{96}\text{Zr}(\text{p},\text{n})^{96}\text{Nb}$	-0.62
$^{95\text{m}}\text{Nb}$	3.61 d	235.69	24.8	$^{96}\text{Zr}(\text{p},2\text{n})^{95}\text{Nb}$ <i>Decay of <math>^{95}\text{Zr}</math> (<math>T_{1/2} = 64.0</math> d)</i> <i>(see below)</i>	-7.51
$^{95\text{g}}\text{Nb}$	34.99 d	765.80	99.81	<i>The same as for <math>^{95\text{m}}\text{Nb}</math></i> <i>(see above)</i>	
$^{92\text{m}}\text{Nb}$	10.15 d	934.44	99.15	$^{92}\text{Zr}(\text{p},\text{n})^{92}\text{Nb}$ $^{94}\text{Zr}(\text{p},3\text{n})^{92}\text{Nb}$ $^{96}\text{Zr}(\text{p},5\text{n})^{92}\text{Nb}$	-2.79 -17.74 -32.06
$^{91\text{m}}\text{Nb}$	60.86 d	1204.67	2.02 <sup>#</sup>	$^{91}\text{Zr}(\text{p},\text{n})^{91}\text{Nb}$ $^{92}\text{Zr}(\text{p},2\text{n})^{91}\text{Nb}$ $^{94}\text{Zr}(\text{p},4\text{n})^{91}\text{Nb}$ $^{96}\text{Zr}(\text{p},6\text{n})^{91}\text{Nb}$	2.06 -10.67 -25.63 -39.94
$^{90\text{g}}\text{Nb}$	14.60 h	141.18 1129.22	66.80 92.70	$^{90}\text{Zr}(\text{p},\text{n})^{90}\text{Nb}$ $^{91}\text{Zr}(\text{p},2\text{n})^{90}\text{Nb}$ $^{92}\text{Zr}(\text{p},3\text{n})^{90}\text{Nb}$ $^{94}\text{Zr}(\text{p},5\text{n})^{90}\text{Nb}$ $^{96}\text{Zr}(\text{p},7\text{n})^{90}\text{Nb}$	-6.89 -14.09 -22.72 -37.68 -51.99
$^{89\text{m}}\text{Nb}$	1.10 h	580.00	95.57	$^{90}\text{Zr}(\text{p},2\text{n})^{89}\text{Nb}$ $^{91}\text{Zr}(\text{p},3\text{n})^{89}\text{Nb}$ $^{92}\text{Zr}(\text{p},4\text{n})^{89}\text{Nb}$ $^{94}\text{Zr}(\text{p},6\text{n})^{89}\text{Nb}$ $^{96}\text{Zr}(\text{p},8\text{n})^{89}\text{Nb}$	-17.00 -24.20 -32.83 -47.78 -62.10
$^{89\text{g}}\text{Nb}$	2.03 h	920.50 1627.00	1.40 3.50 <sup>#</sup>	<i>The same as for <math>^{89\text{m}}\text{Nb}</math></i> <i>(see above)</i>	
$^{95}\text{Zr}$	64.032 d	724.19 756.73	44.27 54.38	$^{96}\text{Zr}(\text{p},\text{pn})^{95}\text{Zr}$ <i>Decay of <math>^{95}\text{Y}</math> (<math>T_{1/2} = 10.3</math> m):</i> $^{96}\text{Zr}(\text{p},2\text{p})^{95}\text{Y} \rightarrow ^{95}\text{Zr}$	-7.85 -11.52
$^{89\text{g}}\text{Zr}$	78.41 h	909.15	99.04	$^{90}\text{Zr}(\text{p},\text{pn})^{89}\text{Zr}$ $^{91}\text{Zr}(\text{p},\text{p}2\text{n})^{89}\text{Zr}$ $^{92}\text{Zr}(\text{p},\text{p}3\text{n})^{89}\text{Zr}$ $^{94}\text{Zr}(\text{p},\text{p}5\text{n})^{89}\text{Zr}$ $^{96}\text{Zr}(\text{p},\text{p}7\text{n})^{89}\text{Zr}$ <i>Decay of <math>^{89}\text{Nb}</math> (see above)</i>	-11.97 -19.16 -27.80 -42.75 -57.07
$^{88}\text{Zr}$	83.40 d	392.87	97.29	$^{90}\text{Zr}(\text{p},\text{p}2\text{n})^{88}\text{Zr}$ $^{91}\text{Zr}(\text{p},\text{p}3\text{n})^{88}\text{Zr}$ $^{92}\text{Zr}(\text{p},\text{p}4\text{n})^{88}\text{Zr}$ $^{94}\text{Zr}(\text{p},\text{p}6\text{n})^{88}\text{Zr}$ <i>Decay of <math>^{88\text{m},\text{g}}\text{Nb}</math> (<math>T_{1/2} = 7.8</math> m</i> <i>and 10.3 m):</i> $^{90}\text{Zr}(\text{p},3\text{n})^{88}\text{Nb} \rightarrow ^{88}\text{Zr}$	-21.29 -28.48 -37.12 -52.07 -29.52

				$^{91}\text{Zr}(p,4n)^{88}\text{Nb} \rightarrow ^{88}\text{Zr}$ $^{92}\text{Zr}(p,5n)^{88}\text{Nb} \rightarrow ^{88}\text{Zr}$ $^{94}\text{Zr}(p,7n)^{88}\text{Nb} \rightarrow ^{88}\text{Zr}$	-36.72 -45.35 -60.31
$^{87g}\text{Zr}$	1.68 h	1227.00	2.8 <sup>#</sup>	$^{90}\text{Zr}(p,p3n)^{87}\text{Zr}$ $^{91}\text{Zr}(p,p4n)^{87}\text{Zr}$ $^{92}\text{Zr}(p,p5n)^{87}\text{Zr}$ $^{94}\text{Zr}(p,p7n)^{87}\text{Zr}$ <i>Decay of <math>^{87m,g}\text{Nb}</math> (<math>T_{1/2} = 3.8</math> m and 2.6 m):</i> $^{90}\text{Zr}(p,4n)^{87}\text{Nb} \rightarrow ^{87}\text{Zr}$ $^{91}\text{Zr}(p,5n)^{87}\text{Nb} \rightarrow ^{87}\text{Zr}$ $^{92}\text{Zr}(p,6n)^{87}\text{Nb} \rightarrow ^{87}\text{Zr}$	-33.64 -40.83 -49.47 -64.42  -39.90 -47.09 -55.73
$^{86}\text{Zr}$	16.5 h	242.80	95.84	$^{90}\text{Zr}(p,p4n)^{86}\text{Zr}$ $^{91}\text{Zr}(p,p5n)^{86}\text{Zr}$ $^{92}\text{Zr}(p,p6n)^{86}\text{Zr}$ <i>Decay of <math>^{86}\text{Nb}</math> (<math>T_{1/2} = 1.45</math> m):</i> $^{90}\text{Zr}(p,5n)^{86}\text{Nb} \rightarrow ^{86}\text{Zr}$ $^{91}\text{Zr}(p,6n)^{86}\text{Nb} \rightarrow ^{86}\text{Zr}$	-43.09 -50.28 -58.92  -52.71 -59.90
$^{91m}\text{Y}$	49.71 m	555.57	95.00	$^{92}\text{Zr}(p,2p)^{91}\text{Y}$ $^{94}\text{Zr}(p,2p2n)^{91}\text{Y}$ $^{96}\text{Zr}(p,2p4n)^{91}\text{Y}$ <i>Decay of <math>^{91}\text{Sr}</math> (<math>T_{1/2} = 9.63</math> h):</i> $^{94}\text{Zr}(p,3pn)^{91}\text{Sr} \rightarrow ^{91}\text{Y}$ $^{96}\text{Zr}(p,3p3n)^{91}\text{Sr} \rightarrow ^{91}\text{Y}$	-9.40 -24.35 -38.67  -26.27 -40.58
$^{90m}\text{Y}$	3.19 h	202.53 479.51	97.30 90.74	$^{91}\text{Zr}(p,2p)^{90}\text{Y}$ $^{92}\text{Zr}(p,2pn)^{90}\text{Y}$ $^{94}\text{Zr}(p,2p3n)^{90}\text{Y}$ $^{96}\text{Zr}(p,2p5n)^{90}\text{Y}$	-8.69 -17.33 -32.28 -46.60
$^{88}\text{Y}$	106.63 d	898.04	93.70	$^{90}\text{Zr}(p,2pn)^{88}\text{Y}$ $^{91}\text{Zr}(p,2p2n)^{88}\text{Y}$ $^{92}\text{Zr}(p,2p3n)^{88}\text{Y}$ $^{94}\text{Zr}(p,2p5n)^{88}\text{Y}$ $^{96}\text{Zr}(p,2p7n)^{88}\text{Y}$ <i>Decay of <math>^{88}\text{Nb}</math> and <math>^{88}\text{Zr}</math> (see above)</i>	-19.84 -27.03 -35.66 -50.62 -64.93
$^{87m}\text{Y}$	13.37 h	380.79	78.06	$^{90}\text{Zr}(p,2p2n)^{87}\text{Y}$ $^{91}\text{Zr}(p,2p3n)^{87}\text{Y}$ $^{92}\text{Zr}(p,2p4n)^{87}\text{Y}$ $^{94}\text{Zr}(p,2p6n)^{87}\text{Y}$ <i>Decay of <math>^{87}\text{Nb}</math> and <math>^{87}\text{Zr}</math> (see above)</i>	-29.19 -36.38 -45.02 -59.97
$^{87g}\text{Y}$	79.80 h	388.53 484.81	82.20 89.80	<i>See above</i>	
$^{86m}\text{Y}$	0.8 h	208.10	93.70	$^{90}\text{Zr}(p,2p3n)^{86}\text{Y}$ $^{91}\text{Zr}(p,2p4n)^{86}\text{Y}$ $^{92}\text{Zr}(p,2p5n)^{86}\text{Y}$ <i>Decay of <math>^{86}\text{Nb}</math> and <math>^{86}\text{Zr}</math> (see above)</i>	-40.99 -48.19 -56.82
$^{86g}\text{Y}$	14.74 h	1076.63	82.5	<i>See above</i>	

$^{85m}\text{Y}$	4.86 h	535.60	3.50	$^{90}\text{Zr}(p,2p4n)^{85}\text{Y}$ $^{91}\text{Zr}(p,2p5n)^{85}\text{Y}$ <i>Decay of <math>^{85m,g}\text{Zr}</math> (<math>T_{1/2} = 10.9\text{ s}</math>  and <math>7.86\text{ m}</math>):</i> $^{90}\text{Zr}(p,p5n)^{85}\text{Zr} \rightarrow ^{85}\text{Y}$ $^{91}\text{Zr}(p,p6n)^{85}\text{Zr} \rightarrow ^{85}\text{Y}$	-50.51 -57.70 -55.96 -63.15
$^{85g}\text{Y}$	2.68 h	913.89 <sup>+</sup>	9.0 <sup>#</sup>	<i>See above</i>	
$^{85g}\text{Sr}$	64.84 d	514.01	96.00	$^{90}\text{Zr}(p,3p3n)^{85}\text{Sr}$ $^{91}\text{Zr}(p,3p4n)^{85}\text{Sr}$ $^{92}\text{Zr}(p,3p5n)^{85}\text{Sr}$ <i>Decay of <math>^{85}\text{Nb}</math> (<math>T_{1/2} = 20.9\text{ s}</math>):</i> $^{90}\text{Zr}(p,6n)^{85}\text{Nb} \rightarrow ^{85}\text{Zr} \rightarrow ^{85}\text{Y}$ <i>Decay of <math>^{85}\text{Zr}</math> and <math>^{85}\text{Y}</math> (see  above)</i>	-46.46 -53.65 -62.29 -63.63

<sup>a</sup> Characteristic  $\gamma$ -ray energies used for identification and quantification of the radionuclides investigated in this work.

<sup>b</sup> Nuclear reactions forming the radionuclide below 66 MeV.

<sup>c</sup> In the case of emission of complex particles, the Q-values must be modified by the respective binding energies of the compound particles:  $np \rightarrow d$  (+2.2 MeV),  $2np \rightarrow t$  (+8.48 MeV),  $2pn \rightarrow ^3\text{He}$  (+7.72 MeV),  $2p2n \rightarrow \alpha$  (+28.30 MeV). Note that Q-values for isomeric states must also be decreased with the respective level energies of those states.

<sup>#</sup> Data taken from **Ref.[10]**.



**Table 2.** Cross sections of  $^{nat}\text{Zr}+p$  nuclear processes leading to the formation of Nb radionuclides.

Energy (MeV)	Cross section (mb)							
	$^{96}\text{Nb}$	$^{95m}\text{Nb}$	$^{95g}\text{Nb}$	$^{92m}\text{Nb}$	$^{91m}\text{Nb}$	$^{90(m+g)}\text{Nb}$	$^{89m}\text{Nb}$	$^{89g}\text{Nb}$
3.0±0.9 <sup>a</sup>	0.048±0.005	-	-	0.27±0.03	-	-	-	-
4.0±0.9 <sup>a</sup>	0.33±0.04	-	-	1.44±0.16	-	-	-	-
4.7±0.8 <sup>a</sup>	1.27±0.14	-	-	-	-	-	-	-
5.8±0.8 <sup>a</sup>	4.88±0.53	-	-	20.07±2.18	-	-	-	-
6.5±0.8 <sup>a</sup>	7.78±0.85	-	-	32.50±3.53	-	-	-	-
7.0±0.7 <sup>a</sup>	10.52±1.14	-	-	42.82±4.65	-	3.35±0.36	-	-
7.9±0.7 <sup>a</sup>	13.66±1.48	-	-	62.40±6.78	18.89±2.05	70.15±7.62	-	-
8.4±0.7 <sup>a</sup>	14.11±1.53	-	-	70.67±7.68	23.93±2.56	139.21±15.12	-	-
8.9±0.7 <sup>a</sup>	12.83±1.39	1.79±0.40	4.04±0.70	78.98±8.58	-	190.17±20.66	-	-
9.6±0.6 <sup>a</sup>	9.32±1.01	-	10.15±1.10	89.62±9.74	27.04±2.94	247.27±26.86	-	-
10.1±0.6 <sup>a</sup>	7.83±0.85	5.08±0.66	10.79±1.43	94.31±10.25	28.65±3.11	282.21±30.66	-	-
10.5±0.6 <sup>a</sup>	6.19±0.67	6.60±2.62	13.20±6.12	96.16±10.45	-	302.48±32.86	-	-
11.2±0.6 <sup>a</sup>	4.44±0.48	5.07±1.08	12.71±3.43	99.18±10.78	27.85±3.02	327.80±35.61	-	-
11.6±0.5 <sup>a</sup>	3.96±0.43	7.50±0.89	15.26±1.89	91.21±9.91	-	343.06±37.27	-	-
13.0±0.5 <sup>a</sup>	2.27±0.25	6.58±1.35	17.75±2.99	47.05±5.22	57.42±6.24	370.94±40.29	-	-
14.3±0.4 <sup>a</sup>	1.38±0.15	7.40±1.13	21.16±2.84	22.39±2.50	68.11±7.40	402.58±43.73	-	-
15.6±0.4 <sup>a</sup>	1.18±0.13	6.22±1.26	21.10±3.27	11.43±1.51	66.78±7.25	419.72±45.61	-	-
16.7±0.3 <sup>a</sup>	1.02±0.11	6.59±0.92	24.12±2.89	8.03±0.94	64.22±6.98	420.39±45.67	-	-
17.7±1.5 <sup>c</sup>	-	-	-	-	-	-	13.89±1.51	67.09±7.29
17.9±0.3 <sup>a</sup>	1.11±0.11	6.64±1.44	24.50±3.78	5.33±0.83	61.87±6.72	374.77±36.15	-	-
20.0±1.7 <sup>b,d</sup>	0.97±0.32	4.10±0.45	18.85±2.05	9.11±0.99	49.26±6.08	263.69±28.64	55.23±6.02	273.92±34.70
22.1±1.3 <sup>c</sup>	-	-	-	-	-	-	64.11±6.96	289.98±31.50
24.2±1.6 <sup>b,d</sup>	0.91±0.30	1.12±0.17	7.06±0.77	45.71±4.97	33.08±5.53	132.04±14.34	73.43±7.99	281.68±32.22
25.9±1.2 <sup>c</sup>	-	-	-	-	-	-	60.44±6.57	337.45±36.66
27.3±1.6 <sup>b,d</sup>	0.76±0.25	0.81±0.19	4.27±0.46	56.37±6.13	19.18±3.79	128.06±13.91	57.12±6.22	392.63±45.88
29.3±1.1 <sup>c</sup>	-	-	-	-	-	-	45.33±4.92	342.96±37.26
30.1±1.5 <sup>b,d</sup>	0.83±0.27	-	3.18±0.71	52.16±5.67	11.32±3.33	137.97±14.99	46.31±5.04	309.65±35.86
32.8±1.5 <sup>b,d</sup>	0.65±0.21	-	2.67±0.30	37.08±4.03	10.98±3.60	133.15±14.46	28.84±3.16	228.39±29.76
35.2±0.9 <sup>c</sup>	-	-	-	-	-	-	25.75±2.80	162.62±17.67
35.3±1.4 <sup>b,d</sup>	0.78±0.25	0.74±0.30	2.13±0.84	25.37±2.76	13.76±4.25	123.47±13.41	23.80±2.60	161.43±20.13

38.8±1.3 <sup>b,d</sup>	0.79±0.26	-	3.04±1.28	15.75±1.71	13.81±4.12	100.05±10.87	20.50±2.24	131.47±17.12
40.3±0.7 <sup>c</sup>	-	-	-	-	-	-	18.92±2.06	125.93±13.68
42.2±1.2 <sup>b,d</sup>	0.75±0.36	-	2.38±0.87	13.04±1.42	18.61±5.67	73.50±7.98	18.31±2.00	121.87±14.48
45.1±0.6 <sup>c</sup>	-	-	-	-	-	-	17.23±1.87	110.11±11.96
45.3±1.2 <sup>b,e</sup>	0.62±0.20	-	1.95±0.89	12.88±1.40	15.08±4.11	59.82±6.50	17.30±1.90	129.11±15.59
48.3±1.1 <sup>b,e</sup>	0.59±0.19	-	1.56±0.49	11.60±1.26	12.25±3.97	57.90±6.29	16.99±1.86	106.26±12.56
49.4±0.4 <sup>c</sup>	-	-	-	-	-	-	14.75±1.51	112.10±11.63
51.2±1.0 <sup>b,e</sup>	0.49±0.16	-	1.55±1.13	11.29±1.23	10.37±3.49	62.00±6.73	15.20±1.66	104.21±12.68
53.9±1.0 <sup>b,e</sup>	0.56±0.18	-	1.40±1.17	11.10±1.21	8.47±4.06	62.88±6.83	13.85±1.52	86.48±9.86
56.6±0.9 <sup>b,e</sup>	-	-	2.71±0.29	9.70±1.05	10.71±3.52	64.26±6.98	11.79±1.29	93.78±11.06
59.8±0.9 <sup>b,e</sup>	-	-	1.36±0.62	8.46±0.92	-	58.93±6.40	11.72±1.27	72.59±7.89
63.0±0.8 <sup>b,e</sup>	-	-	1.32±1.16	7.74±0.84	7.73±3.76	52.84±5.74	10.21±1.12	71.57±8.64
65.9±0.7 <sup>b,e</sup>	-	-	1.39±0.89	7.13±0.75	-	48.03±4.93	10.90±1.18	59.82±6.50

<sup>a</sup> ATOMKI

<sup>b</sup> iThemba LABS, long activation

<sup>c</sup> NIRS

<sup>d</sup> iThemba LABS, short activation II

<sup>e</sup> iThemba LABS, short activation I

**Table 3.** Cross sections of  $^{nat}\text{Zr}+p$  nuclear processes leading to the formation of Zr and Sr radionuclides.

Energy (MeV)	Cross section (mb)					
	$^{95}\text{Zr}$	$^{89(0.938m+g)}\text{Zr}$	$^{88}\text{Zr}$	$^{87(m+g)}\text{Zr}$	$^{86}\text{Zr}$	$^{85(0.87m+g)}\text{Sr}$
14.3±0.4 <sup>a</sup>	1.09±0.16	-	-	-	-	-
15.6±0.4 <sup>a</sup>	1.61±0.22	10.65±1.27	-	-	-	-
16.7±0.3 <sup>a</sup>	2.06±0.29	54.81±5.96	-	-	-	-
17.9±0.3 <sup>a</sup>	2.59±0.31	137.15±14.32	-	-	-	-
20.0±1.7 <sup>b,d</sup>	3.19±0.35	268.85±25.95	-	-	-	-
24.2±1.6 <sup>b,d</sup>	4.53±0.50	425.32±46.20	2.35±0.26	-	-	-
27.3±1.6 <sup>b,d</sup>	4.80±0.53	486.72±54.29	7.19±0.78	-	-	-
30.1±1.5 <sup>b,d</sup>	4.83±0.54	493.08±53.90	54.56±5.93	-	-	-
32.8±1.5 <sup>b,d</sup>	4.69±0.53	407.10±44.49	151.51±16.46	-	-	-
35.3±1.4 <sup>b,d</sup>	4.95±0.56	330.36±36.10	244.05±26.51	-	-	3.02±0.33
38.8±1.3 <sup>b,d</sup>	4.68±0.53	290.29±31.69	303.4±32.96	-	-	14.46±1.57
40.3±0.7 <sup>c</sup>	-	-	-	15.18±1.65	-	-
42.2±1.2 <sup>b,d</sup>	4.94±0.56	271.50±29.57	325.94±35.41	67.65±13.26	-	26.88±2.92
45.1±0.6 <sup>c</sup>	-	-	-	142.61±15.49	-	-
45.3±1.2 <sup>b,e</sup>	4.49±0.51	266.67±28.97	311.58±33.85	147.59±21.47	-	35.54±3.86
48.3±1.1 <sup>b,e</sup>	4.64±0.52	257.15±27.93	269.76±29.30	279.83±32.30	0.11±0.01	39.98±4.34
49.4±0.4 <sup>c</sup>	-	-	-	322.41±32.94	-	-
51.2±1.0 <sup>b,e</sup>	4.44±0.50	244.50±26.56	236.29±25.67	394.94±45.12	0.36±0.04	38.85±4.22
53.9±1.0 <sup>b,e</sup>	4.48±0.51	233.39±25.35	219.23±23.82	469.14±51.88	1.71±0.19	35.31±3.84
56.6±0.9 <sup>b,e</sup>	4.41±0.50	220.38±23.94	195.58±21.25	447.82±49.75	5.01±0.54	31.69±3.44
59.8±0.9 <sup>b,e</sup>	4.26±0.48	210.79±22.90	200.30±21.76	500.71±54.39	13.88±1.51	29.18±3.17
63.0±0.8 <sup>b,e</sup>	4.40±0.50	203.17±22.07	191.79±20.83	417.31±45.96	25.69±2.79	28.99±3.15
65.9±0.7 <sup>b,e</sup>	4.18±0.47	200.15±20.94	180.01±18.87	418.71±45.48	36.09±3.48	29.67±3.23

<sup>a</sup> ATOMKI

<sup>b</sup> iThemba LABS, long activation

<sup>c</sup> NIRS

<sup>d</sup> iThemba LABS, short activation II

<sup>e</sup> iThemba LABS, short activation I

**Table 4.** Cross sections of  $^{nat}\text{Zr}+p$  nuclear processes leading to the formation of Y radionuclides.

Energy (MeV)	Cross section (mb)								
	$^{91m}\text{Y}$	$^{90m}\text{Y}$	$^{88}\text{Y}$	$^{87m}\text{Y}$	$^{87(0.984m+g)}\text{Y}$	$^{86m}\text{Y}$	$^{86(0.99m+g)}\text{Y}$	$^{85m}\text{Y}$	$^{85g}\text{Y}$
12.2±1.6 <sup>c</sup>	0.25±0.13	-	-	-	-	-	-	-	-
13.0±0.5 <sup>a</sup>	-	-	-	-	-	-	-	-	-
14.3±0.4 <sup>a</sup>	-	-	0.60±0.08	-	2.01±0.58	-	-	-	-
15.6±0.4 <sup>a</sup>	-	-	0.89±0.13	-	3.26±1.01	-	-	-	-
16.7±0.3 <sup>a</sup>	-	-	1.17±0.16	1.44±0.38	4.33±0.49	-	-	-	-
17.7±1.5 <sup>c</sup>	0.39±0.18	0.30±0.08	-	-	-	-	-	-	-
17.9±0.3 <sup>a</sup>	-	-	1.61±0.20	3.01±0.45	6.24±1.62	-	-	-	-
20.0±1.7 <sup>b,d</sup>	0.37±0.13	0.95±0.20	-	3.85±0.42	8.06±0.88	-	-	-	-
22.1±1.3 <sup>c</sup>	0.57±0.21	1.34±0.20	-	-	-	-	0.39±0.02	-	-
24.2±1.6 <sup>b,d</sup>	0.49±0.16	1.40±0.29	4.71±0.51	7.88±0.86	14.37±1.56	0.90±0.19	1.01±0.11	-	-
25.9±1.2 <sup>c</sup>	0.53±0.26	1.66±0.26	-	-	-	1.69±0.17	5.28±0.57	-	-
27.3±1.6 <sup>b,d</sup>	0.50±0.12	1.14±0.25	5.12±0.56	7.58±0.82	13.03±1.42	3.80±0.47	7.07±0.77	-	-
29.3±1.1 <sup>c</sup>	0.59±0.19	1.38±0.20	-	-	-	4.98±0.50	13.74±1.49	-	-
30.1±1.5 <sup>b,d</sup>	0.89±0.21	1.14±0.20	9.95±1.08	7.38±0.80	11.51±1.25	6.65±0.77	14.12±1.53	-	-
32.8±1.5 <sup>b,d</sup>	-	1.21±0.22	17.44±1.89	7.91±0.86	13.22±1.44	7.87±0.89	17.72±1.93	-	-
35.2±0.9 <sup>c</sup>	0.87±0.17	1.14±0.18	-	-	-	10.32±0.62	20.86±2.27	-	-
35.3±1.4 <sup>b,d</sup>	0.90±0.13	1.39±0.22	24.77±2.69	9.50±1.03	14.90±1.62	10.01±1.10	21.67±2.35	-	-
38.8±1.3 <sup>b,d</sup>	1.02±0.18	1.58±0.27	34.58±3.76	10.60±1.15	18.20±2.16	8.58±0.94	17.92±1.95	-	-
40.3±0.7 <sup>c</sup>	1.38±0.25	1.23±0.17	-	-	-	8.50±1.22	15.30±1.66	-	-
42.2±1.2 <sup>b,d</sup>	-	1.66±0.26	38.88±4.24	22.50±2.44	33.20±3.82	6.83±0.76	14.04±1.53	-	7.49±1.07
45.1±0.6 <sup>c</sup>	1.24±0.27	1.42±0.16	-	-	-	6.86±0.75	12.60±1.37	-	-
45.3±1.2 <sup>b,e</sup>	1.88±0.37	1.37±0.26	45.45±4.94	64.80±7.04	82.30±8.94	6.63±0.75	12.20±1.33	15.32±2.29	9.35±1.28
48.3±1.1 <sup>b,e</sup>	1.85±0.35	1.71±0.26	45.42±4.93	120.30±13.07	148.40±16.12	6.61±0.74	12.41±1.35	15.59±4.82	8.63±1.14
49.4±0.4 <sup>c</sup>	1.61±0.26	1.72±0.16	-	-	-	6.91±0.73	12.82±1.39	-	-
51.2±1.0 <sup>b,e</sup>	1.78±0.34	2.08±0.29	43.99±4.78	168.76±18.33	203.89±22.15	6.60±0.73	12.80±1.39	12.81±2.07	8.00±1.16
53.9±1.0 <sup>b,e</sup>	2.20±0.36	2.31±0.28	44.75±4.86	198.33±21.54	239.72±26.04	7.50±0.82	14.40±1.56	13.95±2.92	7.25±0.79
56.6±0.9 <sup>b,e</sup>	2.29±0.26	2.37±0.31	-	216.69±23.54	259.13±28.15	8.71±0.95	19.60±2.13	5.77±3.19	6.48±0.91
59.8±0.9 <sup>b,e</sup>	2.56±0.29	2.46±0.27	44.94±4.88	215.82±23.44	266.47±28.95	12.89±1.40	32.73±3.56	8.24±1.90	5.17±0.56
63.0±0.8 <sup>b,e</sup>	2.73±0.28	2.23±0.28	45.73±4.97	207.17±22.51	251.59±27.33	16.62±1.82	48.51±5.27	9.30±2.44	5.62±0.75
65.9±0.7 <sup>b,e</sup>	3.15±0.32	2.85±0.31	45.52±4.95	195.06±18.81	237.34±25.78	22.71±2.47	63.67±6.14	7.15±1.98	5.09±0.55

<sup>a</sup> ATOMKI

<sup>b</sup> iThemba LABS, long activation

<sup>c</sup> NIRS

<sup>d</sup>iThemba LABS, short activation II

<sup>e</sup>iThemba LABS, short activation I